	<p>Research and Development Programme on Seismic Ground Motion</p> <p>CONFIDENTIAL <i>Restricted to SIGMA scientific partners and members of the consortium, please do not pass around</i></p>	<p>Ref : SIGMA-2013-D2-93 Version : 01</p> <p>Date : Page :</p>
--	--	---




GROUND SHAKING SCENARIOS IN THE PO PLAIN WITH SPECIAL EMPHASIS ON THE AREA AFFECTED BY THE EARTHQUAKE SEQUENCE OF MAY 2012

(Deliverable D2-93)

AUTHORS			REVIEW			APPROVAL		
NOM	DATE	VISA	NOM	DATE	VISA	NOM	DATE	VISA
R. Paolucci Research POLIMI			J. Douglas BRGM	In written review attached		M. Corigliano		
			A.Gürpınar	In written review attached				

DISSEMINATION: Authors; Steering Committee; Work Package leaders, Scientific Committee, Archiving.

	<p style="text-align: center;">Research and Development Programme on Seismic Ground Motion</p> <p style="text-align: center;">CONFIDENTIAL</p> <p style="text-align: center;"><i>Restricted to SIGMA scientific partners and members of the consortium, please do not pass around</i></p>	<p>Ref : SIGMA-2013-D2-93 Version : 02</p> <hr/> <p>Date : 7 January 2014 Page : 2</p>
--	---	--


Executive Summary

Stimulated by the advances in the computational tools for the simulation of seismic wave propagation problems in complex geological environment, this Deliverable aims at illustrating the main results of a physics-based numerical study on the prediction of earthquake ground motion in the Po Plain, with emphasis on the sites affected by the Emilia-Romagna earthquakes of May-June 2012. Such a study is intended to provide a better understanding of the seismic response at deep alluvial sites and of the variability of site response with respect to source-to-site propagation path, directivity effects coupled with complex site effects and non-linear soil response.

After the introductory discussion (Chapter 1), the main tool used throughout this work, i.e., the high-performance computer code SPEED - *Spectral Elements in Elastodynamics with Discontinuous Galerkin*: <http://mox.polimi.it/it/progetti/speed/SPEED/Home.html> -, is presented in Chapter 2. The code, based on the Discontinuous Galerkin Spectral Elements Method, allows to deal with non-conforming meshes and, thus, turns out to be particularly useful in tackling multi-scale seismic wave propagation problems in highly heterogeneous media. An overview of the strong ground motion recordings obtained during the M_W 6.1 20 and M_W 6.0 29 May 2012 earthquakes is provided in Chapter 3.

Chapter 4 illustrates the most significant results concerning the 3D numerical modelling of the seismic response of the Po Plain during the 20 and 29 May 2012 earthquakes. Special emphasis is devoted to the 29 May event because it is the best constrained in terms of strong motion records and inversion of the seismic fault mechanism. The issues related to the 3D model of the Po plain, the effect of the kinematic seismic source representation and of the the soil behaviour (linear vs non-linear visco-elastic), the spatial variability of ground motion in near-fault conditions are discussed.

Finally, in Chapter 5 various ground shaking scenarios characterized by different magnitude and focal mechanism are produced to evaluate the variability of site amplification functions associated to the inter-event variability, i.e., source-to-site propagation path, directivity effects coupled with complex site effects and non-linear soil response.

	<p>Research and Development Programme on Seismic Ground Motion</p> <p>CONFIDENTIAL</p> <p><i>Restricted to SIGMA scientific partners and members of the consortium, please do not pass around</i></p>	<p>Ref : SIGMA-2013-D2-93 Version : 02</p> <hr/> <p>Date : 7 January 2014 Page : 3</p>
--	---	--

1. Introduction

The aim of this report is to describe the research activities carried out in the framework of the SIGMA Project “Seismic Ground Motion Assessment” – Axis 2 – by means of generation of earthquake ground motion scenarios in the Po Plain. The main contribution concerned the numerical modelling of the seismic response of the sites affected by the 2012 Emilia-Romagna seismic sequence.


Taking advantage the available information on the subsurface geology of the Po Plain, 3D numerical simulations of the 20 and 29 May 2012 earthquakes were performed making use of the spectral element code SPEED (<http://mox.polimi.it/it/progetti/speed/SPEED/Home.html>), developed at Politecnico di Milano. The numerical models were created to propagate up to about 1.5 Hz, including a simplified description of the irregular submerged bedrock topography beneath the Po Plain and a proper kinematic characterization of the seismic source as well. A significant effort has been devoted to the numerical simulations of the 29th May earthquake, because the latter provides a more complete ground motion dataset than the one obtained during the 20th May and, consequently, it is the best documented as regards to the source characterization. For this case study, the validation of the numerical model against strong ground motion recordings has been a relevant phase of this work, as illustrated in Section 4.1.2.

Owing to the frequency limit of the numerical model (~ 1.5 Hz), that may be critical for nuclear applications where frequency above 5 Hz are of interest, the issue related to the generation of broadband accelerograms, apt for engineering use over a large band of vibration periods, will be discussed.

In response to the main goals of the SIGMA project, as a final result, various ground shaking scenarios characterized by different magnitude and focal mechanism are produced to give insights into the inter-event variability of site amplification functions, i.e., related to source mechanisms and including directivity, complex site effects and non-linear soil response.

With respect to the preliminary results illustrated in Deliverable D3-54, the following tasks, described in this report, were achieved in the second year of the project:


- improvement of the numerical model of the 29 May earthquake in terms of: (i) update of the velocity model of the Po Plain deposits based on the most recent findings in connection with other research projects (i.e., Seismological Project

	<p>Research and Development Programme on Seismic Ground Motion</p> <p>CONFIDENTIAL</p> <p><i>Restricted to SIGMA scientific partners and members of the consortium, please do not pass around</i></p>	<p>Ref : SIGMA-2013-D2-93 Version : 02</p> <hr/> <p>Date : 7 January 2014 Page : 4</p>
--	---	--

S2-2012, <https://sites.google.com/site/ingvdpc2012progettos2/home>); (ii) non-linear elastic soil behaviour of the soft deposits in the uppermost layers of the Po Plain.

- numerical simulations of the 20 May earthquake based on the geological model discussed at previous point as well as on the kinematic source model developed by Atzori et al. (2012).
- parametric study on the effects of the seismic source model on earthquake ground motion predictions in the near field, to clarify the reasons for the major discrepancies between observations and simulations at the close-by stations.
- generation of broadband accelerograms, combining the low frequency waveforms from 3D numerical simulations with the synthetics obtained through a stochastic approach, specifically for the case of the 29 May earthquake;
- generation of a suite of ground shaking scenarios for hypothetical fault rupture events along the two seismic faults responsible of the 29 and 20 May earthquakes characterized by various magnitude and kinematic parameters;
- based on the 3D numerical scenarios at previous point, evaluation of the Spectral Amplification Functions (SAF) at selected sites in the Po Plain with respect to outcropping bedrock;
- Evaluation of the variability of the SAFs related to the inter-event variability, as discussed previously.

This Deliverable is organized as follows. In Chapter 2 the numerical tool used throughout this work, namely SPEED, is briefly described. In Chapter 3 the most salient features of the May 2012 seismic sequence and the strong ground motion dataset are illustrated. Then, Chapter 4 focuses on the 3D numerical simulations of the two mainshocks of the 2012 Emilia seismic sequence, presenting, firstly, the comparison between recordings and synthetics along with the effect of various assumptions on the kinematic source model and, secondly, the application regarding the generation of ground shaking maps in the Po Plain during realistic earthquakes generated by various fault rupture scenarios with different magnitude, co-seismic slip distribution, hypocenter location etc. Finally, in Chapter 5 the aforementioned suite of ground shaking scenarios is used to evaluate on a numerical basis the inter-event variability of site response at selected sites in the Po Plain with respect to factors, such as the source-to-site propagation path and directivity effects, coupled with site effects induced by the complex site geometry (surface wave generation).

	<p>Research and Development Programme on Seismic Ground Motion</p> <p>CONFIDENTIAL</p> <p><i>Restricted to SIGMA scientific partners and members of the consortium, please do not pass around</i></p>	<p>Ref : SIGMA-2013-D2-93 Version : 02</p> <hr/> <p>Date : 7 January 2014 Page : 5</p>
--	---	--

2. The Spectral Element Code SPEED

Physics-based numerical modelling of the seismic response of complex earth media has gained major relevance in recent years, owing, on one side, to the ever-increasing progress in computational algorithms and resources, and, on the other side, to the growing interest towards the development of deterministic scenarios as input within seismic hazard and risk assessment studies. Especially in the last 10 years there has been an impressive progress worldwide towards the development of high-order numerical methods for the simulation of seismic wave propagation under realistic tectonic and geo-morphological conditions. Such an advancement was boosted by several international benchmarks, regarding, for instance, the 3D seismic response of the Los Angeles basin (see e.g. Day et al., 2008), of the Grenoble Valley (e.g. Chaljub et al., 2010, Stupazzini et al., 2009), and of the Euroseistest site (Cashima project, <https://www-cashima.cea.fr/>), as well as by innovative approaches to seismic hazard and risk assessment, such as in the CyberShake project (Graves et al., 2010) and in the ShakeOut Exercise in Southern California (Jones et al., 2008, Bielak et al. 2010).

Such examples testify the increasing need for certified numerical models apt to include the coupled effects of the seismic source, the propagation path through complex geological structures and localized superficial irregularities, such as alluvial basins or/and man-made infrastructures. However, accounting for all these features within a single model still poses challenging demands on computational methods in elastodynamics due to the coexistence of very different spatial scales.

The spectral element method (SEM) is a powerful, well-established, numerical technique naturally suited for three-dimensional seismic wave propagation analyses.

In this Deliverable, we adopt a new numerical code, namely SPEED (Spectral Elements in Elastodynamics with Discontinuous Galerkin), jointly developed at the Departments of Civil and Environmental Engineering and of Modeling and Scientific Computing of Politecnico di Milano (<http://mox.polimi.it/it/progetti/speed/SPEED/Home.html>).

The code is based on the Spectral Element Method, which takes its origin from a long lasting experience in this field (Faccioli et al., 1997; Stupazzini et al., 2009). SPEED is the new generation of the spectral element code GeoELSE, that was developed at the Department of Structural Engineering together with the CRS4, a research center located in Sardinia, Italy. GeoELSE, based on the spectral element method published by Faccioli et al. (1997), underwent a number of engineering applications, including the

Grenoble validation benchmark (Stupazzini et al., 2009) and the study of the seismic response of deep alluvial basins, especially in Italy (Smerzini et al., 2011; Smerzini and Villani, 2012) but in other countries as well (Pilz et al., 2011; Guidotti et al., 2011). In its present version, SPEED fully reproduces the GeoELSE results, therefore we will limit the presentation of its validation activity to a few cases.

SPEED Version 1.0 allows one to perform seismic wave propagation analyses in linear visco-elastic heterogeneous 3D media on both local and regional scale. Relying on non-conforming high-order techniques, like the Discontinuous Galerkin spectral element (DGSE) method, see e.g. Arnold et al. (2002), Rivière (2008), Hesthaven and Warburton (2008), SPEED allows us to deal with a non-uniform polynomial degree distribution (*p*-adaptivity), as well as a locally varying mesh size (*h*-adaptivity) in different sub-domains, as sketched in Figure 2.1. As it has been proven in Antonietti et al. (2012), the resulting formulation is stable, provides optimal approximation properties, and suffers from low dispersion and dissipation errors.

Further details on the theoretical framework and main features of the code along with verification tests can be found in Mazzieri et al. (2013).

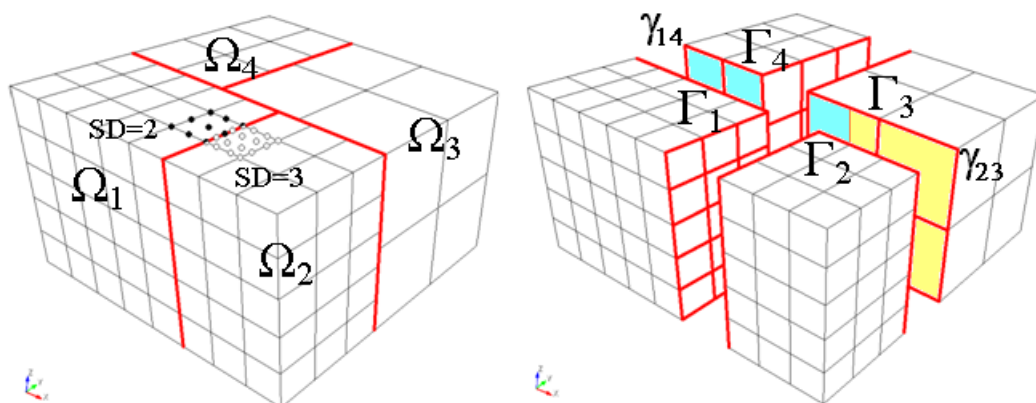


Figure 2.1 - 3D example of non-conforming domain decomposition. The whole domain is composed by different non-overlapping polygonal sub-domains, made by hexahedral elements. Non-conforming high-order techniques allow to deal with a non-uniform polynomial degree distribution (*p*-adaptivity, e.g. $N_1 = 2$ in mesh elements of sub-domain Ω_1 and $N_2 = 3$ in mesh elements of sub-domain Ω_2), as well as a locally varying mesh size (*h*-adaptivity, e.g. between sub-domains $\Omega_{1,2}$, Ω_3 and Ω_4). The surface γ between two neighbouring sub-domains Ω_k , Ω_i , then may not be a complete side of Ω_k or Ω_i (e.g. γ_{14} and γ_{23}).

Main features of the present version of the SPEED code are:

- Linear and non-linear visco-elastic soil materials, with frequency proportional

- quality factor (for further details see Stupazzini et al., 2009);
- Paraxial boundary conditions (Stacey, 1988); upgrade of these boundaries by the implementation of the Perfectly Matched Layers (PML) is planned;
- Pre-processing tools to provide input in terms of an arbitrary kinematic source models;
- Native parallel implementation with scalable approach, naturally oriented to large scale applications;
- Handling the partitioning and load balancing of the computational domain by incorporating the METIS software library (<http://glaros.dtc.umn.edu/gkhome/views/metis/>);
- Post-processing output in GID (<http://gid.cimne.upc.es/>), ArcGIS (<http://www.esri.com/software/arcgis>) and VTK (<http://www.vtk.org/>) formats.

1.1. Verification, efficiency and speed-up of the code

In addition to the tests reported in Deliverable D3-54, we illustrate in this Section some additional verification case studies carried out in the second part of the Project.

The test case LOH (Layer Over Halfspace), proposed by Day and Bradley (2001), was considered. The problem, depicted in Figure 2.2, is currently a reference benchmark for different advanced numerical codes for seismic wave propagation. The dynamic and mechanical properties of the materials are given in Table 2.1.

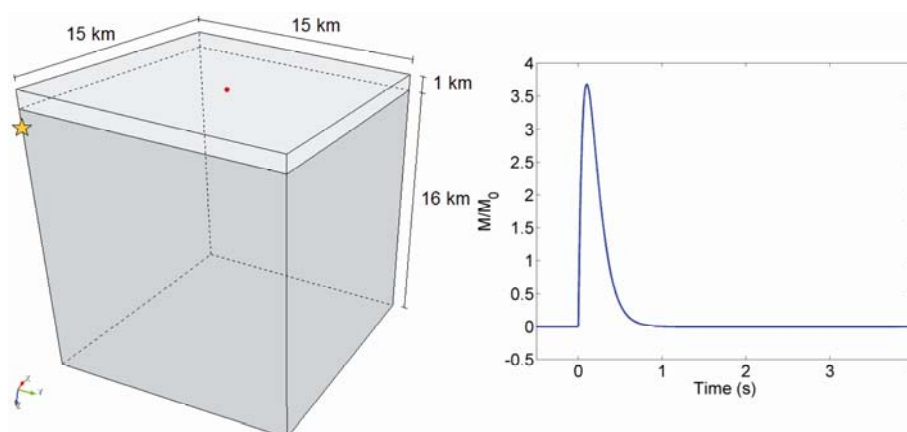


Figure 2.2 - Left hand side: LOH Benchmark test, only one of the four symmetric quadrants is shown, the source (yellow star) is located at 2 km depth and different colors mean different mechanical characteristics; in red the receiver considered. Right hand side: moment rate function for the validation-test.

Table 2.1 - LOH Benchmark test: dynamic and mechanical properties for the layer (L) and the halfspace (HS)

Layer	Depth [km]	V_P [m/s]	V_S [m/s]	ρ [kg/m ³]
L	0-1	4000	2000	2600
HS	1-17	6000	3464	2700

The seismic source is represented by a point double couple located at the centre of the model. The accuracy of the DG solutions was verified by comparing the results obtained with a conforming model and with a non-conforming model (Table 2.2). The characteristics of the numerical models and the main parameters of the analysis performed at Lagrange cluster (located at CINECA, CILEA Department, www.cilea.it) are listed in Table 2.2.

It is important to underline that, although the non-conforming model has a sensibly lower number of elements, the accuracy of the solution is preserved. We report in Figure 2.4 the time-history of the velocity field recorded at point (6, 8, 0) km on the top layer along with the reference solution and the corresponding least-square error. These results are promising, especially compared with those available in literature, see for instance Stupazzini et al. (2009).

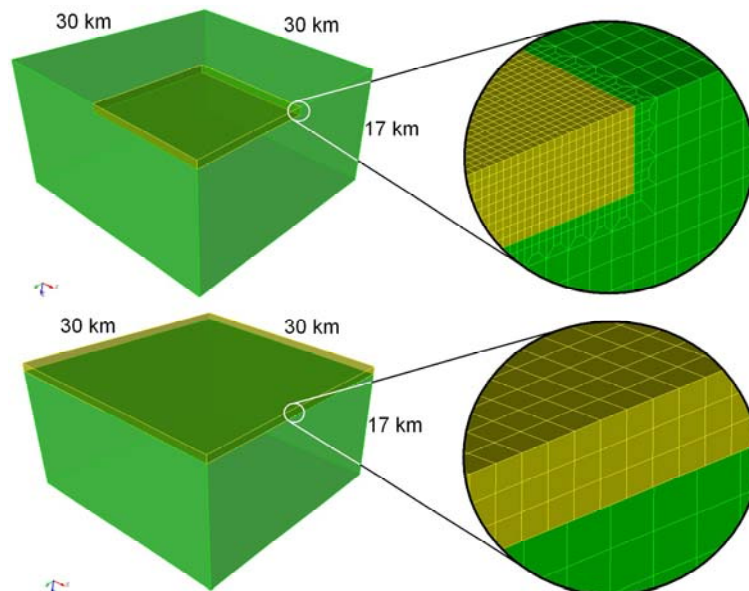


Figure 2.3 - LOH1 conforming model, having size of 30x30x17km: (top) the conforming mesh with 814,833 hexahedral elements, varying from size of 100 m, in the first quadrant, to 300 m in the remaining part of the domain; (bottom) the non-conforming model with 70,228 hexahedral elements, having size of around 400 m in the upper layer (1 km thickness) and size of around 650 m in the lower layer (16 km thickness).

Table 2.2 - Main characteristics of the conforming (C) and non-conforming (NC) numerical models of the LOH Benchmark test, with the main parameters of the analysis performed at Lagrange cluster.

Mesh	El.	SD	Nodes	Δt	Cores	Set Up [h]	Total Time[h]
C	814,833	4	52.7 10 ⁶	0.0003	128	~0.42	~3.03
NC	70,228	5	9.0 10 ⁶	0.0005	128	~0.58	~3.53

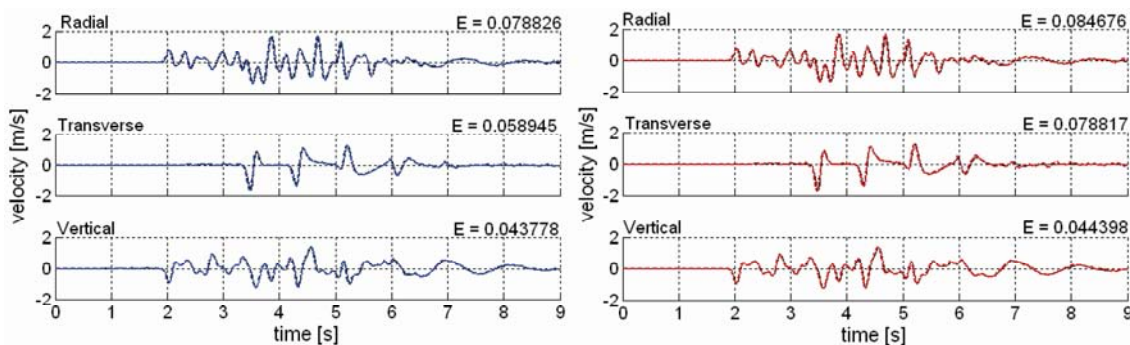


Figure 2.4 - Velocity time history recorded at (6, 8, 0) km: comparison between the semi-analytic solution (black line) and the numerical one (colored line) for both conforming (blue, left) and non-conforming (red, right) numerical models.

With reference to the two different models, represented in Figure 2.3, several tests were performed at the Lagrange cluster, to evaluate the performance of the parallel algorithm as a function of the number of cores adopted for the computation, in terms of efficiency and speed-up. The results are plotted in Figure 2.5 against the ideal behaviour, considering the total computing time.

In particular, having defined T_{seq} (resp. T_{par}) the CPU time of the sequential (parallel) code to carry out the simulation, the efficiency (E) and speed-up (SU) are computed through the following equations:

$$E = T_{seq}/T_{par} \quad \text{and} \quad SU = NE, \quad (1)$$

where N is the number of CPU used for the parallel computation. The ideal scalability of the parallel code is reached for $E = 1$ and $SU = N$.

The behaviour of the parallel kernel with 32 cores has been regarded as the reference solution. It is possible to appreciate the good performance of the code, using from 64 to 128, 256 and 512 cores. In particular, considering 512 cores, the efficiency is around 90% of the ideal efficiency for the conforming mesh and around 70% for the non-conforming mesh. Similar good performance scores can be observed also for the speed-up of the code.

We refer the reader to Mazzieri et al. (2013) for a thorough discussion on the computational features of SPEED.

CONFIDENTIAL

*Restricted to SIGMA scientific partners and members of the consortium,
please do not pass around*

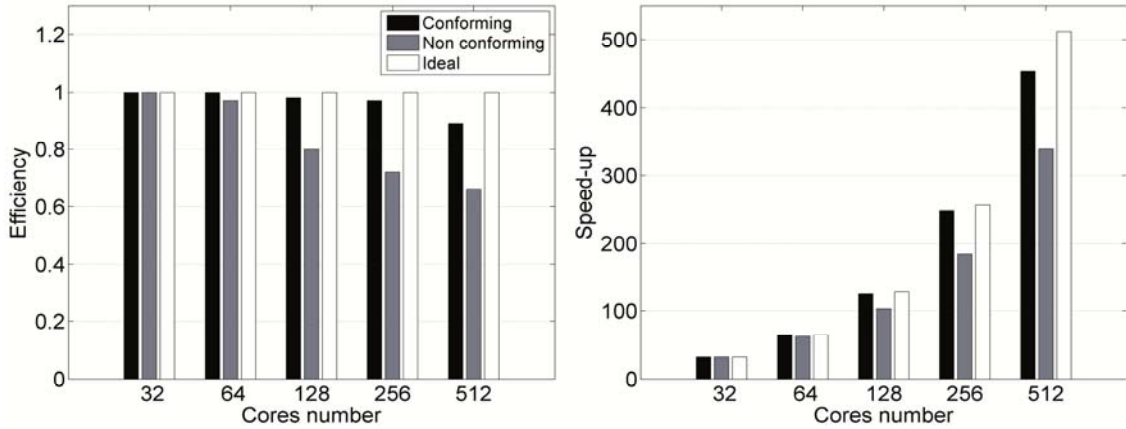



Figure 2.5 - Performance of the parallel algorithm implemented in SPEED, in terms of efficiency and speed-up (total time), with reference to the conforming and non-conforming models (see Figure 2.3).

	<p style="text-align: center;">Research and Development Programme on Seismic Ground Motion</p> <p style="text-align: center;">CONFIDENTIAL</p> <p style="text-align: center;"><i>Restricted to SIGMA scientific partners and members of the consortium, please do not pass around</i></p>	<p>Ref : SIGMA-2013-D2-93 Version : 02</p> <hr/> <p>Date : 7 January 2014 Page : 11</p>
--	---	---

3. The 2012 Emilia earthquakes

3.1. Seismo-tectonic and geologic context

The 2012 Emilia seismic sequence occurred on the southern portion of the Po Plain, a subsident EW trending basin, surrounded by the Alps to the north and the Apennines to the south, which developed in response to the collision of the African plate with the Euro-Asiatic plate. The Po Plain is filled with Plio-Quaternary alluvium deposits, whose thickness ranges from a few tens of meters on the top of buried anticlines up to about 9 kilometers in the eastern part of the basin toward the Adriatic sea.

Information on the deep structural geologic setting of the Po Plain is mostly provided by extensive hydrocarbon exploration (Bigi et al., 1992), while data regarding the superficial stratigraphic sequences come from shallow water wells performed by the Emilia-Romagna region (Regione Emilia Romagna & Eni-Agip, 1998).

Figure 3.1 reports a simplified structural map of the Po Plain illustrating the main seismotectonic features together with the epicenter of the 29 May 2012 earthquake that will be investigated in detail in this report.

Seismicity of this area is related to the presence of buried compressive structures bordering the southern and northern edge of the Po Plain along the S-verging Northern Apennine fold-and-thrust belt and the southernmost thrust sheets of the Southern Alps, respectively. No evidence of activity of these buried thrusts has been recorded due to fast sedimentation rates combined with low deformation rates (Burrato et al., 2012; Toscani et al., 2009).

The tectonic evolution of this area is marked by a progressive migration of the Tyrrhenian basin-Apenninic arc system from east to north-east, since the late Miocene, driven by the retreat of the Adriatic foreland (for further details see e.g. Castellarin et al., 2006; Fantoni and Franciosi, 2010; Scrocca et al., 2007; Selvaggi et al., 2001). As a consequence of this, extension is accommodated by the well-known normal active faults in the western sector with respect to the Apenninic chain, while the eastern areas are dominated by a compressive tectonic regime. The tectonic setting of this area is characterized by two main compressional structural units: the Pede-apenninic thrust front (PTF, as defined by Boccaletti et al., 1985) and the system of three complex folded arcs, namely, Monferrato, Emilia and Ferrara-Romagna, from west to east (see Figure 3.1). The latter is subdivided into three secondary structures: Ferrara, Romagna and

Adriatic (Bigi et al., 1990). These buried structures of the Northern Apennines thrust front were extensively imaged through seismic reflection lines and deep well logs carried out for hydrocarbon exploration (e.g., Pieri and Groppi, 1981). The 2012 Emilia seismic sequence was generated by the central portion of the Ferrara-Romagna arc. It showed pure reverse faulting and focal depths in the range between 1 and 12 km (Burrato et al., 2012).

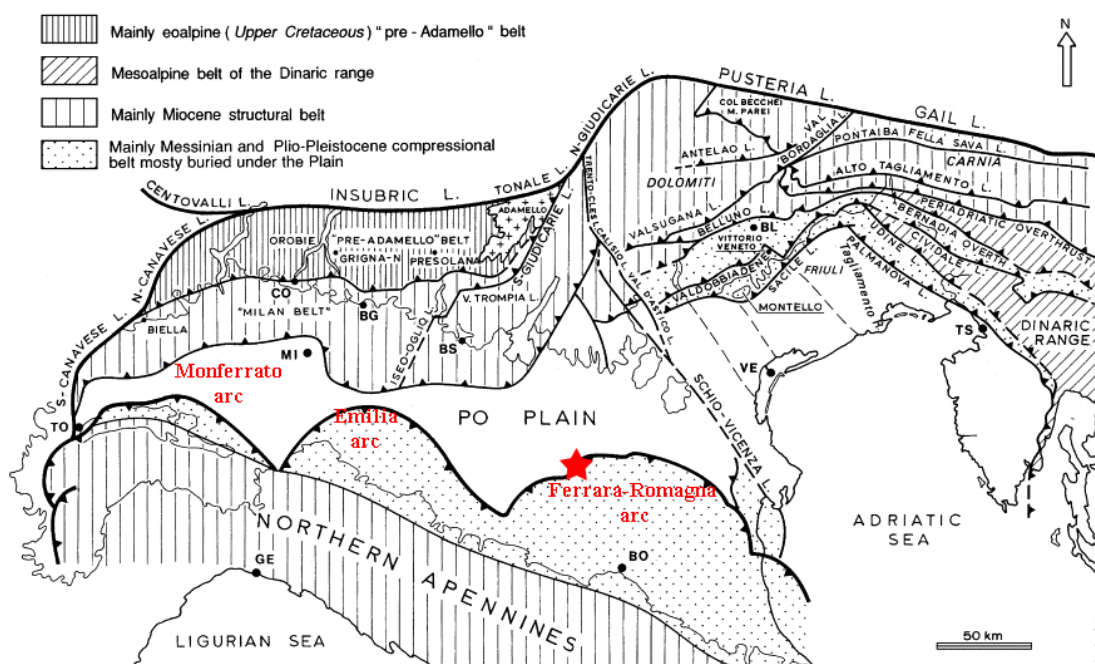



Figure 3.1 – Simplified structural setting of the Po Plain (adapted from Castellarin et al., 2006) with indication of the fold systems forming the outermost thrust front of the Northern Apennine belt. The superimposed star denotes the approximate location of the epicentre of the 29 May 2012 M_L 5.8 earthquake.

3.2. The seismic sequence

The seismic sequence initiated on 19 May with a local magnitude (M_L) 4.1 event, followed by four relevant shocks with $4.8 \leq M_L \leq 5.1$ within a few days, and culminated with a M_L 5.9 event on 20 May, at 02:03:53 (UTC), and a M_L 5.8 event 9 days later, on 29 May, at 07:00:03 (UTC). The 29 May event was followed by three relevant aftershocks with $M_L \geq 5.0$ (Mirandola Earthquake Working Group, 2012a and 2012b). Maximum Mercalli-Cancani-Seiberg (MCS) intensity values of VIII were estimated (Rovereto, Novi di Modena), as a result of the cumulative effects of the entire seismic sequence (Galli et al., 2012).

	<p>Research and Development Programme on Seismic Ground Motion</p> <p>CONFIDENTIAL</p> <p><i>Restricted to SIGMA scientific partners and members of the consortium, please do not pass around</i></p>	<p>Ref : SIGMA-2013-D2-93 Version : 02</p> <hr/> <p>Date : 7 January 2014 Page : 13</p>
--	---	---

The seismic sequence involved a relatively large area with a maximum EW extension of about 50 km. Figure 3.2 illustrates the spatial distribution of the epicenters of the seismic sequence from 20 May to 20 July 2012: the superimposed stars denote the epicenters of the most relevant earthquakes with $M_L \geq 5.0$.

The main parameters of the 20 and 29 May earthquakes are summarized in Table 3.1 together with the data regarding the geometry of the fault solutions, as derived within the INGV seismic source inversion works, based on seismological, geological and Synthetic Aperture Radar (SAR) data (Atzori, Pers. Comm., 2012; see also Atzori et al., 2012). The co-seismic slip distribution for both earthquakes, as provided by the aforementioned inversion study, is illustrated in Figure 3.3. The source model for the 20 May earthquake is poorly constrained due to a poor coverage of SAR data, so that more attention was devoted to the numerical simulations of the 29 May earthquake, even though preliminary results will be discussed also for the 20 May earthquake (see Section 4.2). It is worth remarking that the fault lengths and widths, as provided in Table 3.1, refer to the whole fault plane used for the seismic source inversion and therefore are larger than the fault area that did slip indeed during the two earthquakes, as displayed in Figure 3.3. This is the reason why the fault sizes are above the range predicted by the scaling laws of Wells and Coppersmith (1994).

The seismic sequence was recorded by the Italian strong motion network (RAN), including some temporary stations (Mirandola Earthquake Working Group, 2012a), managed by the Department of Civil Protection (DPC), and by the regional accelerometric network (RAIS), managed by the INGV Milano-Pavia. About 20 stations of the RAN are installed in the Po Plain.

The good strong motion dataset provided by the Emilia seismic sequence led us to create an accelerometric database for the Po Plain including the RAN and RAIS recordings obtained from the earthquakes from 20 May to 13 June 2012 with magnitudes larger than 4 at epicentral distances (R_e) less than 60 km (see Figure 3.4). Data from the M_W 5.4 Correggio earthquake on the 15th of October 1996 (Lat: 44.76, Lon: 10.6) and from the M_W 5.4 Parma earthquake on the 23rd of December 2008 (Lat: 44.52, Lon: 10.38), downloadable from the ITACA network (<http://itaca.mi.ingv.it>), were also included in the database owing to their relevance. At present, the Po Plain database consists of 143 three-component waveforms, in terms of acceleration, velocity and displacement waveforms, from 21 earthquakes. The raw recordings were corrected using the processing scheme proposed by Paolucci et al. (2011) in the framework of the DPC-INGV Project S4, involving the construction of the ITACA network.

A careful overview of the Emilia earthquake sequence with emphasis on the features regarding the attenuation, source function and site effects has been recently published by Castro et al. (2013).

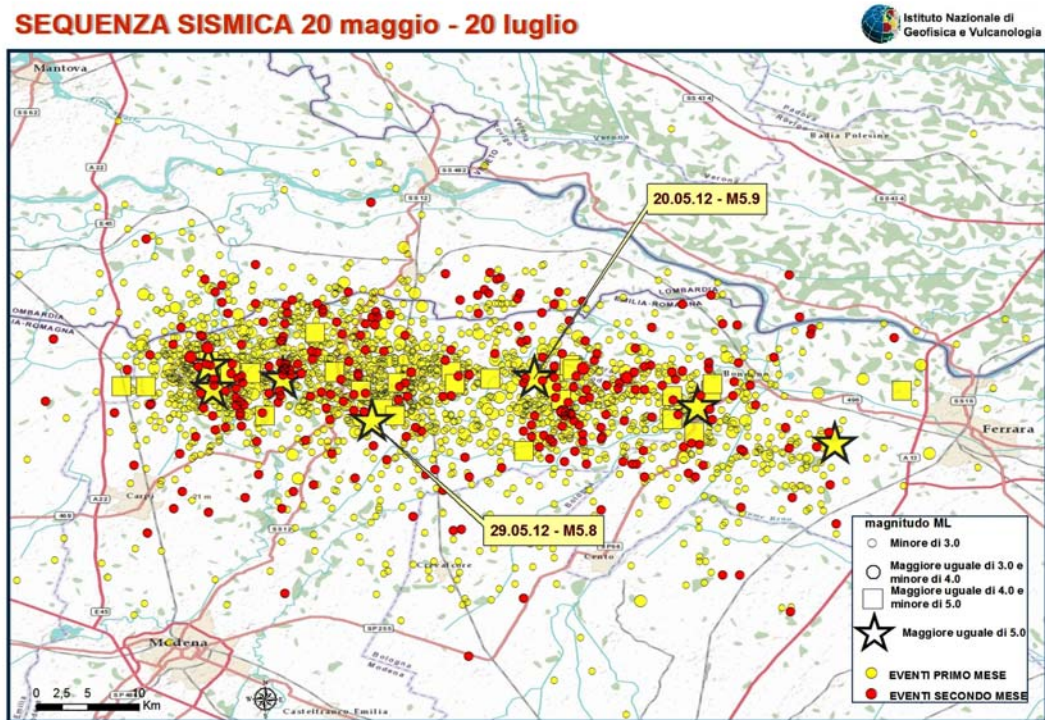


Figure 3.2 – Epicenters of the 2012 Emilia seismic sequence, from 20 May to 20 July (INGV, www.ingv.it). The yellow stars denote the seismic events with magnitude larger than 5. The mainshocks on the 20th and 29th of May are highlighted by the superimposed rectangles.

Table 3.1 - Source parameters for the 20 and 29 May 2012 earthquakes. Moment magnitude estimates come from <http://autoremt.bo.ingv.it/quicks.html>

	20 May 2012	29 May 2012
Moment magnitude M_w	6.11	5.96
Lat, Lon (°N,°E)	44.89, 11.23	44.851, 11.086
Focal Depth (km)	6.3	10.2
Length L (km)	30	32
Width W (km)	20	20
Strike ϕ (°)	114	95
Dip δ (°)	40	40
Rake λ (°)	85	90

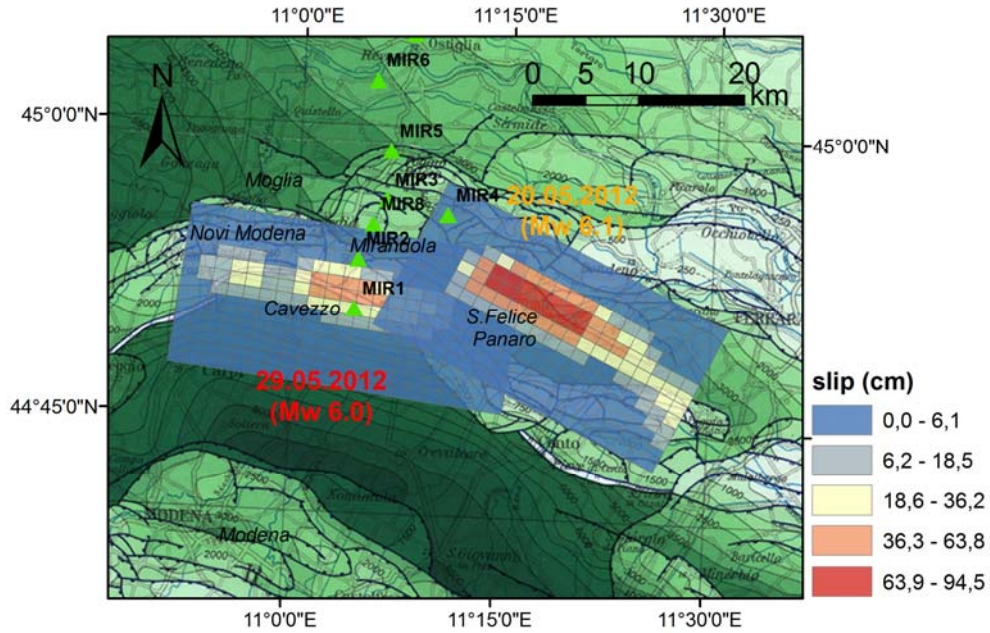


Figure 3.3 – Kinematic seismic source models for the 20 May (Ferrara fault) and 29 May (Mirandola fault) earthquakes (Atzori et al., 2012).

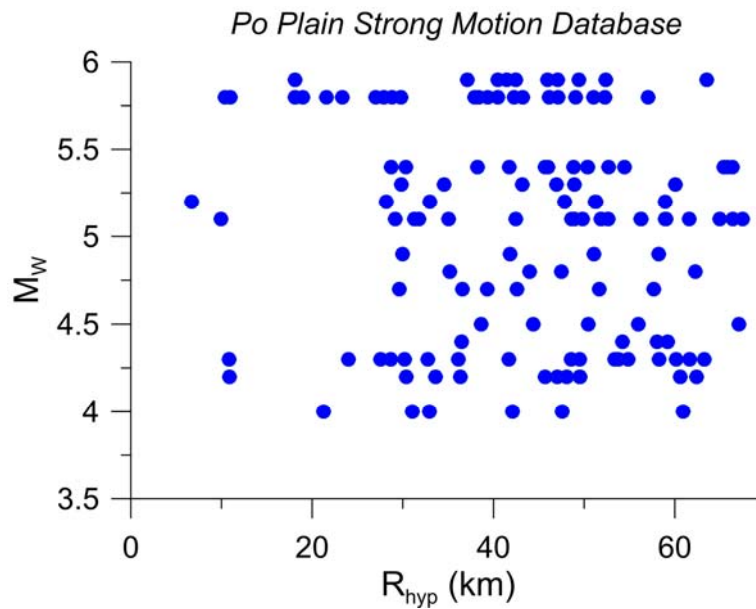



Figure 3.4 – Po Plain strong motion database: magnitude (M_w) – hypocentral distance (R_{hyp}) distribution.

	<p>Research and Development Programme on Seismic Ground Motion</p> <p>CONFIDENTIAL</p> <p><i>Restricted to SIGMA scientific partners and members of the consortium, please do not pass around</i></p>	<p>Ref : SIGMA-2013-D2-93 Version : 02</p> <hr/> <p>Date : 7 January 2014 Page : 16</p>
--	---	---

3.3. Strong motion dataset

In this section the most salient features of the strong motion recordings of the 20 and 29 May 2012 M_L 5.8 earthquake are presented.

Table 3.2 lists the main features of the strong motion stations located at distances from the epicenter of the 20 and 29 May earthquakes less than about 40 km (for further details see Chioccarelli et al., 2012). Information on the soil category according to the Italian seismic norms (CS.LL.PP., 2008), when available, is also provided. Peak ground motion values (PGA = Peak Ground Acceleration; PGV = Peak Ground Velocity, PGD = Peak Ground Displacement) obtained at these stations on the two horizontal directions and on the vertical one for both earthquakes are given in Table 3.3. Note that many more recordings are available for the 29 May shock because many temporary arrays managed by the DPC and the INGV were installed soon after the 20 May event.

During the 20 May earthquake, maximum values of horizontal PGA , PGV and PGD of 0.264 g, 46.3 cm/s and 10.4 cm, respectively, are recorded at the Mirandola station (MRN), located at about 13 km from the epicenter. At the same station vertical PGA , PGV and PGD of 0.31 g, 5.97 cm/s and 1.8 cm are observed.

Referring to the 29 May earthquake, for which a broader dataset is available, it is interesting to note that maximum horizontal PGA of about 0.3 g is recorded at the closest station from the epicenter, i.e., Mirandola (MRN), where, on the other hand, vertical accelerations reach peak values of almost 0.9 g. For the stations located at $R_e < 5$ km, horizontal PGV values, on the NS component, range from about 57 cm/s, at MRN ($R_e = 3.6$ km), to 35 cm/s, at SAN0 (San Felice sul Panaro, $R_e = 4.7$ km). Vertical PGV ranges from 26 cm/s to 8 cm/s. Recorded motion at MRN shows horizontal and vertical PGD of 15 cm and 5 cm, respectively.

In the epicentral region of both earthquakes maximum peak ground motion values are obtained on the NS component owing to source directivity effects, as illustrated in Figure 3.5 and Figure 3.6, depicting the NS velocity waveforms recorded at selected stations during the 20 and 29 May earthquakes, respectively. As regards the latter, directivity effects are clearly noted in the proximity of the seismic source, while recordings at larger distances are predominantly affected by long period surface wave trains related to the complex subsoil structure of the Po Plain. Note that, among the ones plotted in Figure 3.5, only four stations recorded the first shock on 20 May (MRN, NVL, MDN, MODE; MODE is not displayed because it is very close to MDN).

For an overview on the strong motion dataset obtained during the Emilia-Romagna seismic sequence we refer the reader to Luzi et al. (2013). In this paper, a discussion on the predominant effect of surface waves on recorded signals at periods longer than 2 s is provided. In fact, it is found that at distances larger than 30 km PGV and PGD generally occur within the surface wave phase and a strong increase of signal duration can be noted.

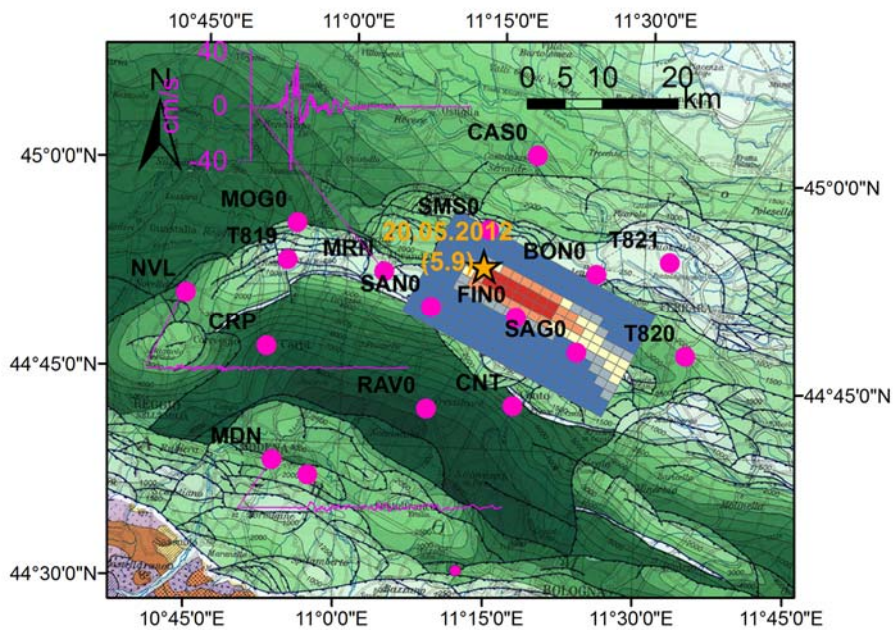


Figure 3.5 – NS velocity recordings in the epicentral area of the 20 May earthquake plotted on the structural map of the Po Plain.

CONFIDENTIAL

Restricted to SIGMA scientific partners and members of the consortium,
please do not pass around

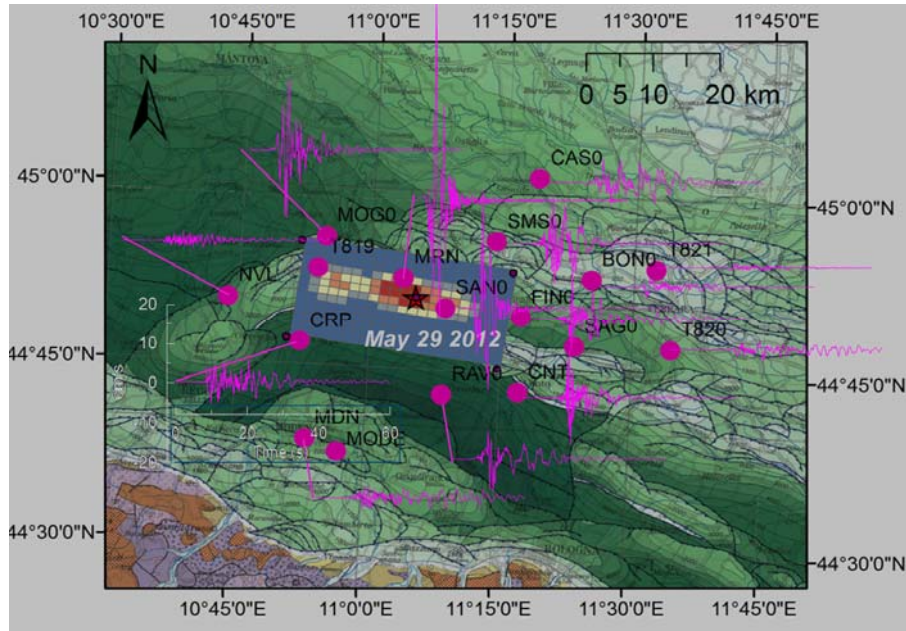


Figure 3.6 – Same as in Figure 3.5 but for the 29 May earthquake

Table 3.2 - RAN (DPC) and RAIS (INGV) strong motion stations in the epicentral region of the M_L 5.8 earthquake on the 29th of May 2012. The soil class according to the Italian seismic norms (CS.LL.PP., 2008), when available, is also provided.

Station Name	Station Code	Lat (°N)	Lon (°E)	Elev. (m)	Soil Class	Owner
Mirandola	MRN	44.8782	11.0617	15	C	DPC
San Felice Panaro*	SAN0	44.8380	11.1430	71	-	DPC
San Martino Spino*	SMS0	44.9340	11.2350	55	-	DPC
Ravarino*	RAV0	44.7157	11.1428	87	-	DPC
Finale Emilia*	FIN0	44.8297	11.2867	61	-	DPC
Moglia*	MOG0	44.9320	10.9120	79	-	DPC
Carpi*	CRP	44.7823	10.8703	89	-	DPC
Cento*	CNT	44.7230	11.2870	71	-	DPC
Sant Agostino*	SAG0	44.7910	11.3904	66	-	DPC
Castelmassa*	CAS0	45.0250	11.3110	65	-	DPC
Bondeno*	BON0	44.8860	11.4180	65	-	DPC
Modena	MODE	44.6300	10.9500	41	-	INGV
Modena	MDN	44.6460	10.8890	37	C	DPC
Novellara	NVL	44.8419	10.7306	23	C	INGV
Casaglia	T821	44.9035	11.5406	3	C	INGV
Chiesuol del Fosso	T820	44.7912	11.5732	8	-	INGV

* DPC temporary stations.



	Research and Development Programme on Seismic Ground Motion	Ref : SIGMA-2013-D2-93 Version : 02
	CONFIDENTIAL <i>Restricted to SIGMA scientific partners and members of the consortium, please do not pass around</i>	Date : 7 January 2014 Page : 19

Table 3.3 - Horizontal and vertical Peak Ground Acceleration (*PGA*), Velocity (*PGV*) and Displacement (*PGD*) obtained at the stations of Table 3.2 during the 20 (top) and 29 (bottom) May 2012 earthquakes. R_{hyp} and R_{epi} denote the hypocentral and epicentral distance.

Station Code	R_{hyp} km	R_{epi} km	PGA_{EW} cm/s ²	PGA_{NS} cm/s ²	PGA_{UP} cm/s ²	PGV_{EW} cm/s	PGV_{NS} cm/s	PGV_{UP} cm/s	PGD_{EW} cm	PGD_{NS} cm	PGD_{UP} cm
20 May 2012											
<i>MRN</i>	15	13	257.70	259.56	303.66	29.99	46.32	5.97	8.16	10.39	1.80
<i>NVL</i>	40	40	47.83	50.95	29.02	2.80	2.03	0.86	0.47	0.41	0.12
<i>MDN</i>	39	38	36.00	32.44	28.81	6.11	3.65	1.47	1.43	1.28	0.73
<i>MODE</i>	37	36	26.92	41.71	32.61	4.37	6.25	2.4	2.2	2.16	0.98
29 May 2012											
<i>MRN</i>	11	4	222.99	289.00	863.19	28.05	57.04	25.93	8.51	14.80	5.22
<i>SANO</i>	11	5	171.15	217.37	308.03	19.36	34.72	8.39	7.11	10.40	2.86
<i>SMSO</i>	18	15	174.80	175.07	106.84	13.55	14.27	3.03	4.49	4.24	1.02
<i>RAVO</i>	19	16	57.72	82.38	64.30	6.15	9.77	1.64	1.22	4.50	1.20
<i>FINO</i>	19	16	207.76	234.32	208.44	17.50	16.83	2.98	2.68	2.48	0.87
<i>MOGO</i>	19	16	235.79	167.74	125.16	26.67	20.47	4.96	3.65	6.14	1.59
<i>CRP</i>	21	19	117.69	173.76	83.91	9.06	6.64	2.21	1.93	1.60	0.70
<i>CNT</i>	24	21	219.78	295.18	64.58	17.05	13.81	2.59	3.38	3.10	0.68
<i>SAGO</i>	27	25	79.20	66.42	66.46	7.74	6.11	2.24	1.49	1.65	0.60
<i>CASO</i>	28	26	66.16	42.06	29.82	7.51	6.87	1.30	2.26	3.74	0.51
<i>BONO</i>	28	27	35.56	25.52	30.34	2.24	2.89	1.22	1.04	1.57	0.28
<i>MODE</i>	29	27	43.85	21.81	42.46	3.44	2.94	2.04	1.37	1.32	0.53
<i>MDN</i>	29	28	29.75	50.55	35.24	2.65	3.48	2.09	0.98	1.41	0.53
<i>NVL</i>	30	28	53.62	48.66	46.80	2.59	3.04	1.11	0.52	0.60	0.20
T821	40	39	19.77	18.30	8.17	2.11	1.34	0.48	0.58	0.58	0.24
T820	38	36	23.73	29.75	16.30	2.39	3.53	1.20	0.74	1.07	0.31


	<p style="text-align: center;">Research and Development Programme on Seismic Ground Motion</p> <p style="text-align: center;">CONFIDENTIAL</p> <p style="text-align: center;"><i>Restricted to SIGMA scientific partners and members of the consortium, please do not pass around</i></p>	<p>Ref : SIGMA-2013-D2-93 Version : 02</p> <hr/> <p>Date : 7 January 2014 Page : 20</p>
--	---	---

4. Numerical simulations of the 29 and 20 May 2012 Emilia earthquakes

The aim of this section is to describe the most relevant results regarding the 3D numerical simulations of the seismic response of the Po Plain during the 20 and 29 May 2012 earthquakes making use of the SE code SPEED (see Section 2). Compared to standard approaches based on plane wave propagation analyses through horizontally layered media, the distinctive features of these numerical simulations include:

- a kinematic seismic fault model based on the available seismic source inversion studies (see Figure 3.3);
- the inclusion of the buried topography of the base of Pliocene formation beneath the Po Plain, as provided by the structural map of Italy (Bigi et al., 1992).

As mentioned in the introduction, in this research activity numerical modelling focused on the 29 May earthquake due to the availability of numerous recordings as well as of well constrained source inversion studies. For this reason, we will start discussing the results on the 29 May earthquake (Section 4.1) to switch then to the description of numerical modelling of the 20 May event (Section 4.2). Referring to the former, which is investigated in more details in this report, the following issues will be discussed: (i) verification of the simulations against other independent solutions (Section 4.1.1); (ii) validation of the simulations by comparison with the earthquake recordings both in the near- and far- field (Section 4.1.2); (iii) dependence of numerical results on the seismic source model (Section 4.1.4); (iv) application to produce broadband accelerograms, usable over a large frequency band of interest for engineering applications (Section 4.1.7); and (v) generation of ground shaking maps. As regards the 20 May earthquake, a brief discussion will be given focusing on the comparison between the simulations and the available recording (Section 4.2.1) and on the predicted spatial variability of seismic motion (Section 4.2.2). Finally, ground shaking maps for future earthquakes, generated by various fault rupture sources and characterized by different magnitude and kinematic parameters, are illustrated to shed light on the spatial variability of earthquake ground motions associated to source-related effects combined with a complex geologic environment such as the Po Plain (Section 5).

	<p>Research and Development Programme on Seismic Ground Motion</p> <p>CONFIDENTIAL</p> <p><i>Restricted to SIGMA scientific partners and members of the consortium, please do not pass around</i></p>	<p>Ref : SIGMA-2013-D2-93 Version : 02 Date : 7 January 2014 Page : 21</p>
--	---	--

4.1. 3D numerical simulations of the 29 May 2012 earthquake

As depicted in Figure 4.1, the model extends over a volume of about $74 \times 51 \times 20 \text{ km}^3$ and is discretized using an unstructured hexahedra mesh with characteristic element size ranging from $\sim 150 \text{ m}$ at the surface to $\sim 1400 \text{ m}$ at the bottom of the model. The mesh was generated using the software CUBIT (<http://cubit.sandia.gov/>). Due to the small topographic variations of the investigated area, a flat free surface was taken into consideration.

The mesh includes the kinematic source model described in section 3.2 (Mirandola fault in Figure 3.3). We specify herein that the top depth of the seismic fault is assumed to be equal to 5 km . The source time function is given by an approximate Heaviside function, as follows:

$$M_0(t) = \frac{1}{2} \left[1 + \operatorname{erf} \left(4 \frac{t - 2\tau}{\tau} \right) \right] \quad (2)$$

where M_0 is the scalar seismic moment, $\operatorname{erf}(\cdot)$ is the error function and $\tau = 0.7 \text{ s}$ is the rise time, assumed to be constant across the fault plane. A constant value of rupture velocity $V_R = 2.8 \text{ km/s}$ is considered.

Referring to the 3D subsoil model, a homogenous average soil profile was defined for the Po Plain sediments (see Table 4.1), while a horizontally layered model was assumed in the rock Miocene formations (see Table 4.2). The V_S profile for both the Po Plain sediments (red) and the underlying rock formations is displayed in Figure 4.3. The 3D velocity model was calibrated merging the information coming from the available V_S profiles and published works (e.g. Cocco et al., 2001; Lai et al., 2012; Margheriti et al., 2000, Martelli and Molinari, 2008; Vuan et al., 2011). Note that the subsoil model has been slightly changed with respect to the one adopted for the previous set of numerical simulations (see D3-54, Section 4.4) to include the most recent indications on the features of the uppermost layers (Martelli, Pers. Comm., 2013), mainly as regards Mirandola and Casaglia stations. Both a linear visco-elastic and non-linear elastic soil behaviour has been adopted for the numerical simulations, as discussed in further details in the sequel. Note that the subsoil model is in reasonable agreement with the results recently published by Milana et al. (2013).

The model consists of 1.852.651 spectral elements, yielding 50.850.136 Legendre-Gauss-Lobatto (LGL) nodes, for spectral degree equal to 3. The model can propagate frequencies up to about 1.5 Hz . The numerical simulations were carried out on the

supercomputer FERMI at CINECA (<http://www.cineca.it/en/content/fermi-bgg>). The total computer time using 512 cores and 16 threads (exploiting a hybrid MPI-OpenMPI programming) for a duration of synthetics equal to 50 s and time step $\Delta t = 0.001$ s (~16% of the well-known Courant-Friedrichs-Levy, CFL, stability limit for 1D wave propagation) is about 4.55 hours.

Table 4.1 - Mechanical properties within the Po Plain sediments. Q_s is the quality factor at a representative frequency of 0.67 Hz.

Depth (m)	V_S (m/s)	V_P (m/s)	ρ (kg/m ³)	Q_s (-)
0 – 120	300	1500	1800	30
120 – 500	800	1800	2000	80
> 500	$800 + 15\sqrt{z - 500}$	$1800 + 20\sqrt{z - 500}$	$2000 + 0.0725 \cdot (z - 500)$	$800 + 0.03 \cdot (z - 500)$

Table 4.2 - Mechanical properties for the rock Miocene formations.

Depth (m)	V_S (m/s)	V_P (m/s)	ρ (kg/m ³)	Q_s (-)
< 1000	1200	2300	2100	150
1000 – 3000	2100	3500	2200	200
3000 – 6000	2750	4750	2400	250
> 6000	3670	6340	2800	350

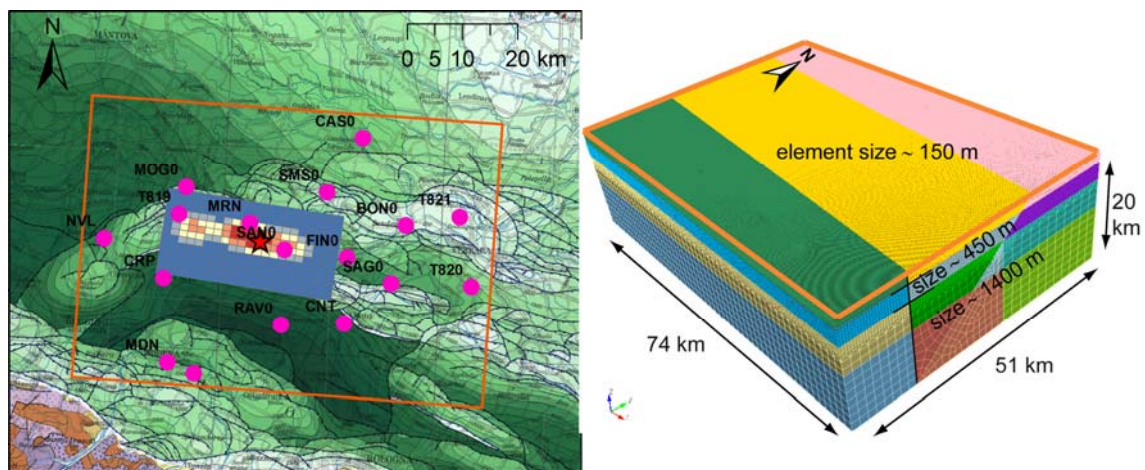


Figure 4.1 – Left: kinematic rupture model of the 29 May 2012 Emilia earthquake plotted on the structural map of Italy (Bigi et al., 1992). The dots denote the location of the strong motion stations operated by the RAN and the RAIS, while the superimposed rectangle indicates the extension of the numerical model. Right: numerical model pointing out the variable element size adopted to correctly sample the shear wave velocity (300 m/s) of the shallowest layers of the Po Plain up to frequencies of about 1.5 Hz.

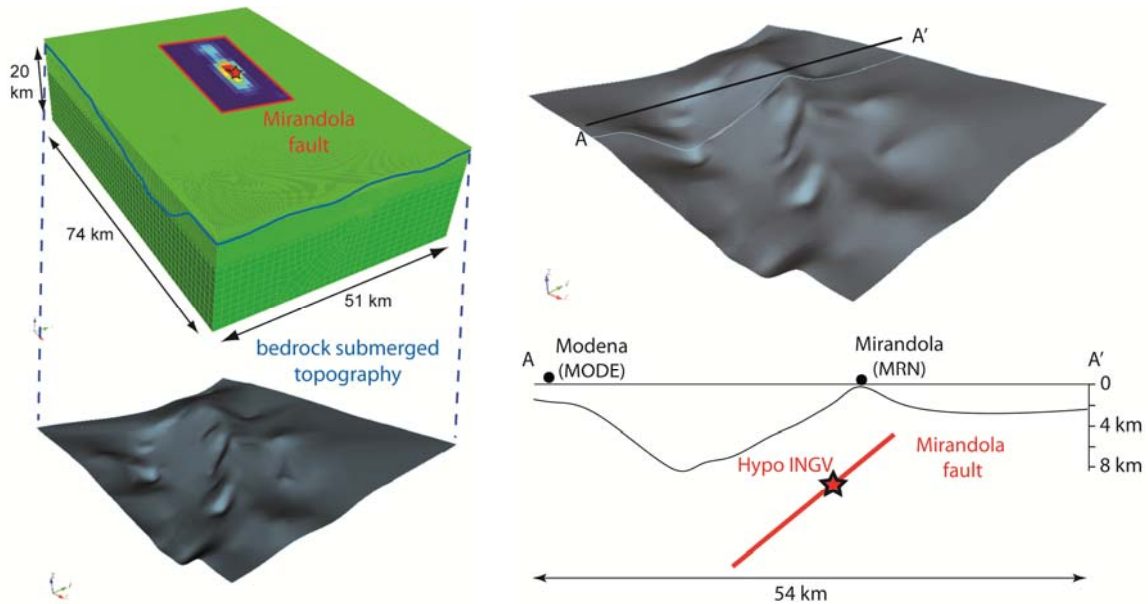


Figure 4.2 – Left panel: sketch of the numerical model including the kinematic seismic source model for the Mirandola fault and the 3D shape of the bedrock-sediment interface. Right panel: representative ~NS cross-section passing through the Mirandola site, as adopted in the numerical model.

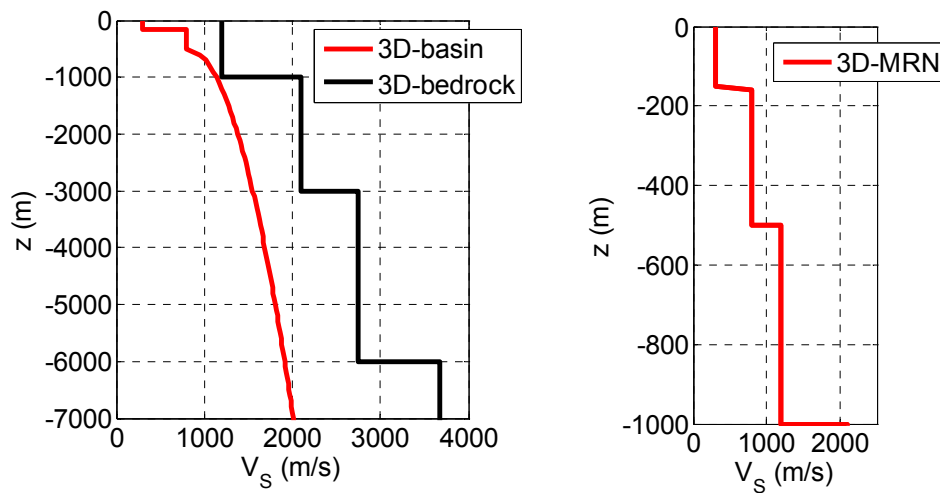


Figure 4.3 – Left panel: V_S profile adopted for the 3D numerical simulations (red: Po Plain sediments; black: Miocene formations). Right panel: V_S profile beneath the Mirandola (MRN) station in the uppermost 1000 meters from ground surface.

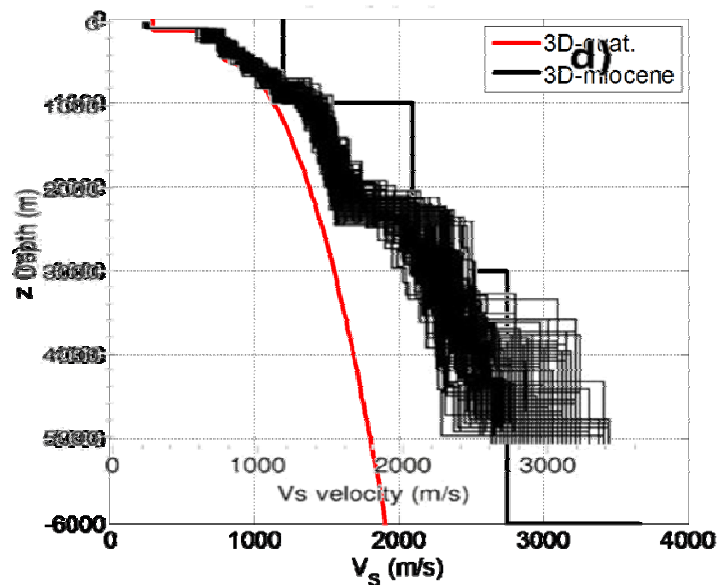


Figure 4.4 – Comparison between the 3D velocity profile and the one published by Milana et al. (2013).

4.1.1. Verification: comparison with independent solutions

Before discussing the results for the 29 May earthquake, we briefly introduce in this Section some verification tests that were carried out to check the accuracy of the numerical computations. To this end, the numerical results obtained through SPEED are compared with those computed through the Discrete Wavenumber Method implemented in the Hisada code (Hisada, 1994). For verification purposes, for the soil model, a homogeneous halfspace with $V_S = 3500$ m/s, $V_P = 6000$ m/s, $\rho = 2800$ kg/m³, and $Q_S = 350$, is assumed. Regarding the seismic source, the kinematic fault model by Atzori is adopted.

Figure 4.5 shows the comparison between the displacement time histories (filtered between 0.1-1.5 Hz) obtained through SPEED and Hisada at two selected stations, namely, MRN (left) and SAN0 (right). A reasonable agreement is found, confirming the accuracy of the SE model.

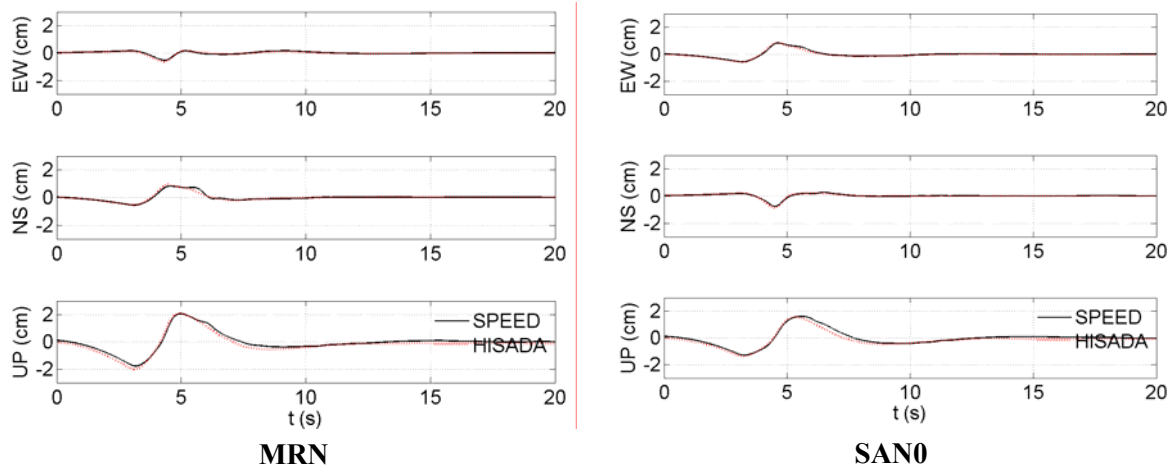



Figure 4.5 – Verification: comparison between the results obtained through SPEED (black) and Hisada (red) in terms of displacement time histories (0.1-1.5 Hz) at MRN (left) and SAN0 (right) stations.

4.1.2. Comparison with strong motion observations

Figure 4.6 shows the comparison between synthetics (blue) and recordings (black) in terms of three-component displacement waveforms at 12 representative strong motion stations. The latter were chosen fairly uniformly based on their geographical distribution. Both recorded and simulated waveforms were band-passed filtered with an acausal Butterworth 3rd order filter between 0.1 and 1.5 Hz, the latter being the frequency limit of the numerical model. Note that for this set of results, a linear visco-elastic soil behaviour has been assumed (Q_S values are given in Table 4.1).

On the whole, it turns out that the agreement between synthetics and recordings is satisfactory, especially for stations distant from the near-field region (see e.g. T821 station). On the other hand, at stations close to the epicenter, such as MRN and SAN0, the numerical model tends to underestimate significantly the observed horizontal ground motion amplitudes, while a good agreement is found for the vertical component. In spite of these discrepancies, first arrivals and waveforms are well captured by the numerical simulations with the exception of the EW component for the MRN record. Parametric analyses performed with the analytical method of Hisada (1994), reported in the following Section 4.1.4, have pointed out that the directivity effects associated to the relative position of the hypocenter with respect to the slip asperity may have a predominant role.

At NVL, the numerical model predicts larger values than the observed ones for all components of ground motion, leading to a poor fit. Instead, for T821 a satisfactory

	<p>Research and Development Programme on Seismic Ground Motion</p> <p>CONFIDENTIAL</p> <p><i>Restricted to SIGMA scientific partners and members of the consortium, please do not pass around</i></p>	<p>Ref : SIGMA-2013-D2-93 Version : 02</p> <hr/> <p>Date : 7 January 2014 Page : 26</p>
--	---	---

agreement is obtained. It is underlined herein that the coda of the synthetics at NVL and T821 may be affected by spurious reflections since they are located close to the lateral absorbing boundaries of the computational domain.

In general, ground response close to the fault, such as at MRN station, is predominantly affected by the features of the kinematic source models, while away from the source, such as at T821, the 3D model seems to better explain the onset of prominent surface wave trains propagating within the Po Plain.

The performance of the numerical simulations was evaluated in a quantitative way using the Goodness of Fit (GoF) criteria proposed by Anderson (2004). For the frequency band of interest (i.e., 0.1-1.5 Hz) a GoF score from 0 to 10 (<4, poor fit; 4–6, fair fit; 6–8, good fit; >8, excellent fit) is estimated on 5 metrics of interest for engineering purposes, namely: energy duration (ED), peak ground velocity (PGV), peak ground displacement (PGD), response spectral acceleration (RS), and Fourier Amplitude Spectrum (FAS). The GoF scores, computed as the average value over the three ground motion components over the 5 metrics (the vertical bars denote the maximum and minimum value of the misfit) for the 12 stations under consideration, are reported in Figure 4.8. These results confirm that overall the numerical model provides predictions that in reasonable agreement (fair-good) with the strong motion observations.


4.1.3. Update of the Po Plain model: comparison with the preliminary set of results

Within the second year research activities, the numerical model has been revised by introducing slight changes in the velocity model of both the uppermost deposits in the Po Plain and the deep crustal model, based the most recent findings emerged within other research projects (i.e., the Seismological Project S2-2012, <https://sites.google.com/site/ingvdpc2012projetto2/home>).

Further details on the preliminary velocity model can be found in Section 4.4. of D3-54). However, for clarity, we report herein the main features of the preliminary model:

Po Plain sediments

- $V_S = 300$ m/s, $V_P = 1500$ m/s, $\rho = 1800$ kg/m³, $Q = 30$ for $z \leq 150$ m
- $V_S = 600$ m/s, $V_P = 1500$ m/s, $\rho = 2000$ kg/m³, $Q = 60$ for $150 < z \leq 500$ m
- $V_S = 600 + 20(z-500)^{1/2}$ m/s, $V_P = 2.4 V_S$ m/s, $\rho = 2000 + 0.08(z-500)$ kg/m³,
 $Q = 60 + 0.025(z-500)$ for $z > 500$ m (3a)

	<p>Research and Development Programme on Seismic Ground Motion</p> <p>CONFIDENTIAL</p> <p><i>Restricted to SIGMA scientific partners and members of the consortium, please do not pass around</i></p>	<p>Ref : SIGMA-2013-D2-93 Version : 02</p> <hr/> <p>Date : 7 January 2014 Page : 27</p>
--	---	---

Bedrock Miocene formations

$$V_S = 3500 \text{ m/s}, V_P = 6000 \text{ m/s}, \rho = 2800 \text{ kg/m}^3, \text{ and } Q = 350 \quad (2b)$$

Figure 4.7 and Figure 4.9 illustrate the comparison between these results (blue lines) and the ones obtained in the preliminary numerical analyses (red lines) in terms of displacement waveforms and GoF scores, respectively. It is noted that these modifications do not produce significant changes in simulated waveforms. At some stations, such as MRN, SAN0, and T821, a better agreement is found, while at other stations, such as FIN0, SAG0, and MDN, a worse fit is obtained.

In the following discussion, reference to the revised basin model will be made.

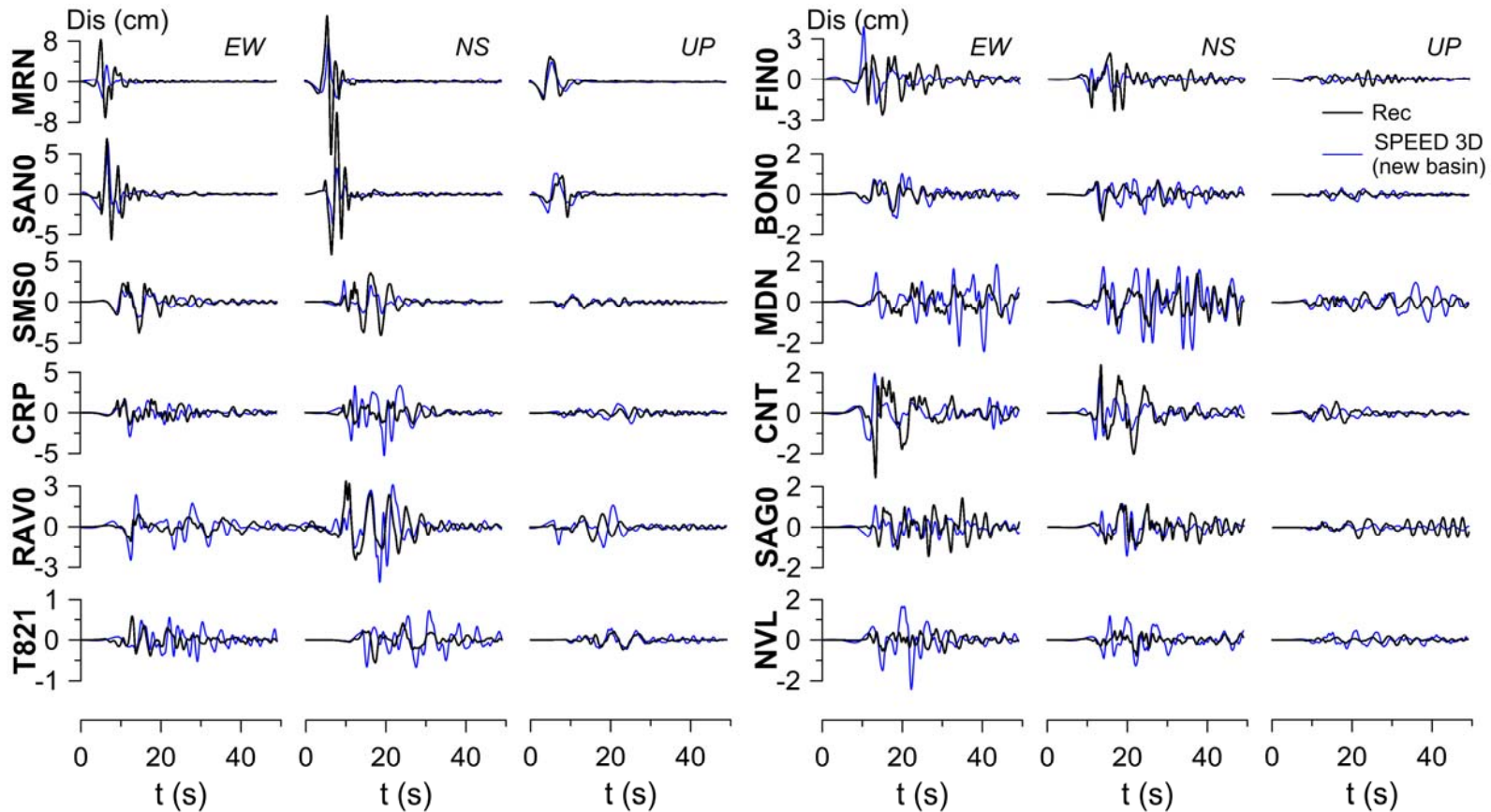


Figure 4.6 – Comparison between strong motion observations (black) and 3D synthetics (blue) in terms of displacement time histories band-passed filtered between 0.1 and 1.5 Hz.

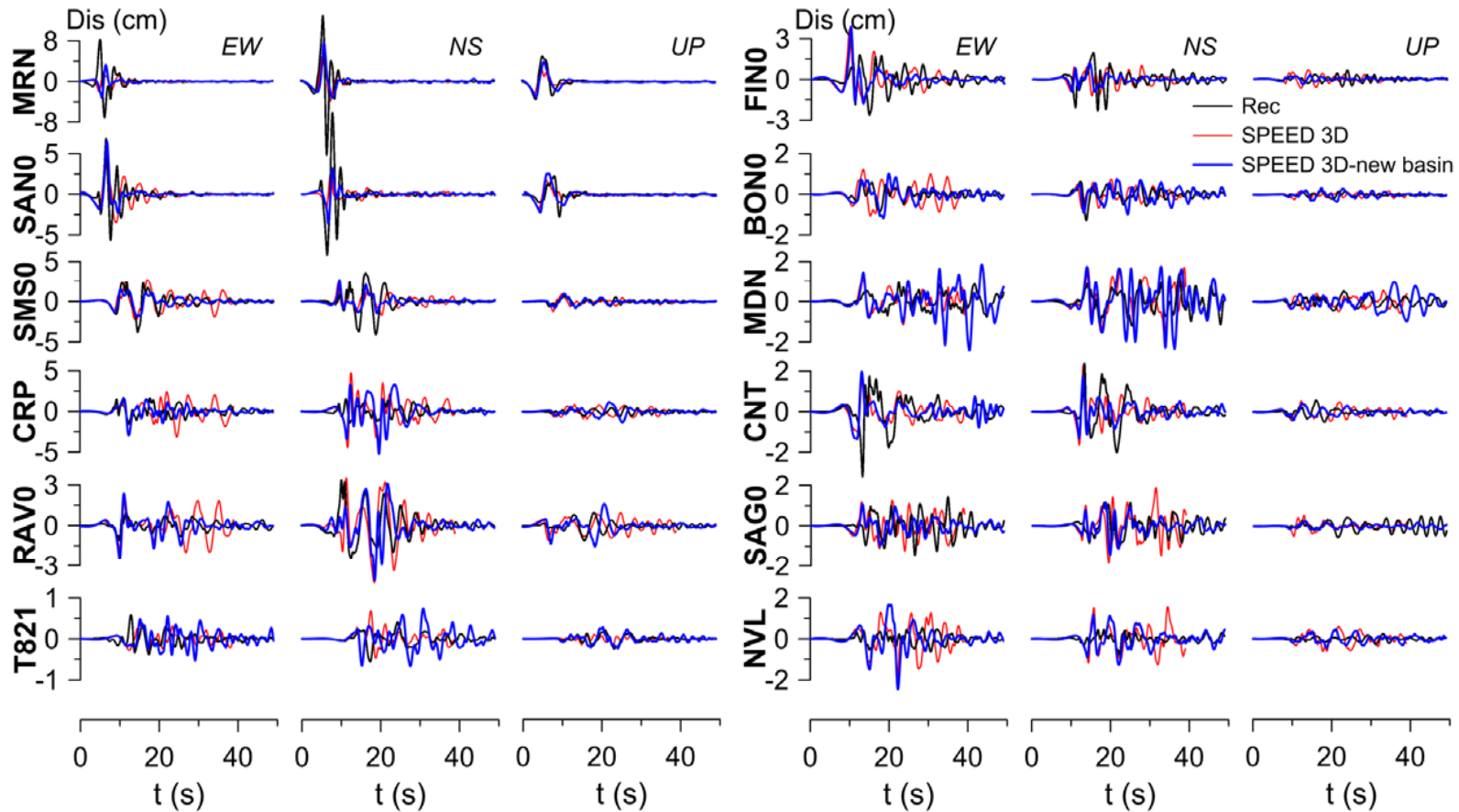


Figure 4.7 – Comparison between strong motion observations (black) and 3D synthetics (blue) in terms of displacement time histories (0.1-1.5 Hz). The results of the preliminary numerical model, as reported in Deliverable D3.54, are also shown (red).

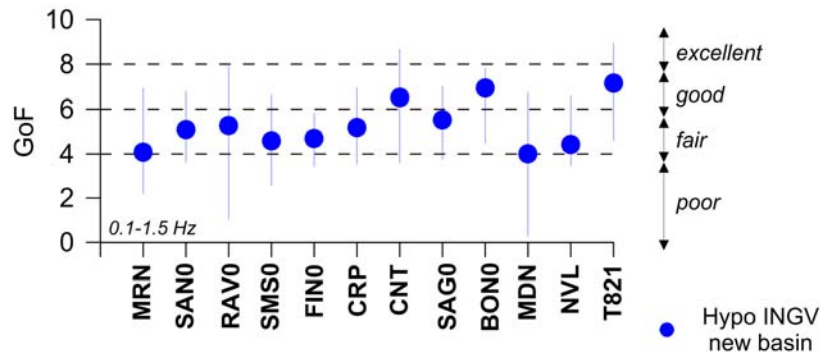


Figure 4.8 – Average Goodness-of-Fit (GoF) scores according to Anderson (2004) over the 5 metrics under consideration (Energy Duration, Peak Ground Displacement, Peak Ground Velocity, Response Spectra, Fourier Spectra), for 12 strong motion stations.

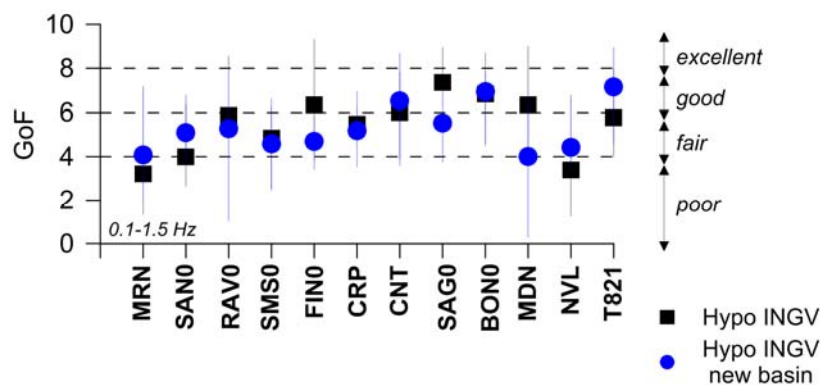



Figure 4.9 – Same as in Figure 4.8: comparison with the preliminary results illustrated in the Deliverable D3-54 (denoted by squares).

4.1.4. Effect of seismic source model

As discussed previously, the major drawback of the numerical simulations is the strong underestimation of ground motion amplitudes at sites located in the proximity of the seismic source, at distances $R_e < 5$ km, in particular at MRN and SAN0. Some parametric analyses were performed by making use of the Hisada code (Hisada, 1994) to investigate whether some changes in the seismic source model may provide a better fit between observations and synthetics and to guide the calibration of selected source parameters as well. We underline that the Hisada code allows one to account for 3D kinematic seismic source representation but under the assumption of 1D horizontally layered soil media.

A set of parametric analyses were carried out to study the influence of:

	<p>Research and Development Programme on Seismic Ground Motion</p> <p>CONFIDENTIAL</p> <p><i>Restricted to SIGMA scientific partners and members of the consortium, please do not pass around</i></p>	<p>Ref : SIGMA-2013-D2-93 Version : 02</p> <hr/> <p>Date : 7 January 2014 Page : 31</p>
--	---	---

- (a) the position of the nucleation point;
- (b) the location of the seismic fault;
- (c) the rake angle,;
- (d) the rupture velocity.

The effects of these parameters are evaluated only at the station MRN, where the hypotheses on the kinematic source model have the greatest impact.

In all these simulations, as base kinematic parameters, the slip pattern plotted in Figure 3.3, rupture velocity $V_R = 2800$ m/s and rake angle $\lambda = 90^\circ$, are assumed. As regards the rise time, $\tau = 0.4$ s is assumed for the parametric analyses in terms of nucleation point and location of seismic fault, while $\tau = 0.6$ s for the ones concerning rupture velocity and rake angle. These discrepancies are due to the fact the such analyses were performed in different phases of the work. However, it has been verified that rise time variations have minor effect in this frequency range. Furthermore, a simplified 1D soil profile is assumed (see Table 4.3).

It is worth underlining that the fault dip was not considered in these preliminary analyses because we decided to keep constant the geometry of the seismic source model, since this feature cannot be changed once the SE model is constructed. However, provided that Cesca et al. (2013) found values of dip angles for both earthquakes of about $25-27^\circ$, in apparent disagreement with our model (40°), it would be interesting to further investigate this point.

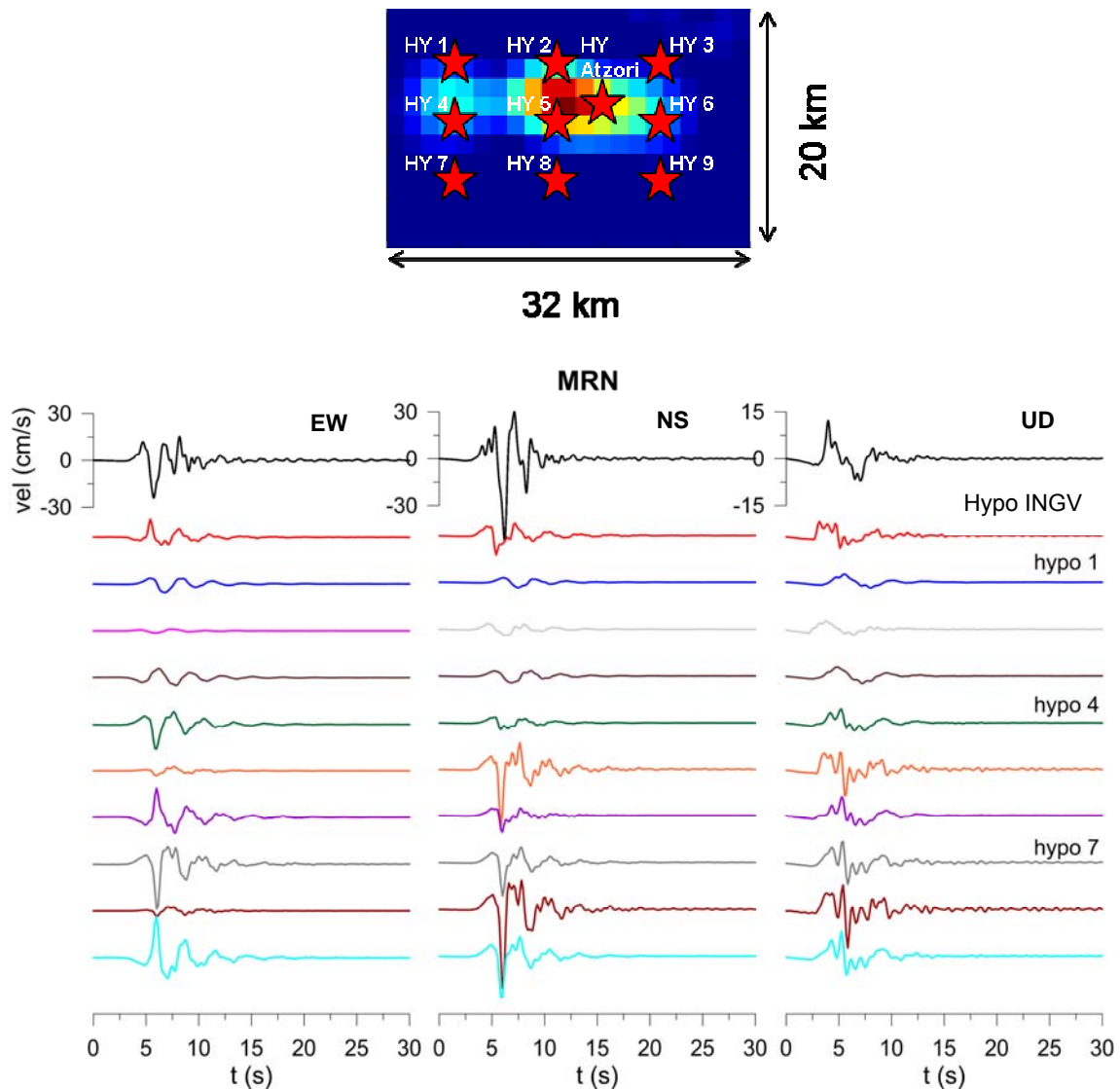
Nucleation point

As a first set of analyses, we study the effect of various positions of the nucleation point, by keeping unchanged the position of the seismic fault and all other kinematic parameters. Figure 4.10 illustrates the comparison between the recordings (black) and the simulations obtained with Hisada for the station MRN by considering the ten hypocenter locations sketched in the top panel of the figure in terms of velocity time histories. Both recorded and simulated time histories are filtered with an acausal Butterworth 3rd order filter between 0.1 and 2.0 Hz, the latter being the frequency limit of the computations provided by Hisada.

Two major effects are found, i.e.:

- hypocenters 5,7,8 and 9 produce a strong velocity pulse on the NS component in satisfactory agreement with the observed recording, clarifying that shifting the hypocenter downward along the fault, below the region of maximum asperity, induces strong directivity effects along the NS component;

- for hypocenters 1, 4, and 7 a better agreement is found on the EW motion in terms of polarity and amplitude (especially for hypo 4 and 7), thus pointing out that placement of the hypocenter on the west side of the seismic fault has a strong positive effect on the predicted polarity on ground motion.
- Hypocenters 1, 2 and 3 tend to underestimate significantly the observations, also for the vertical component. In all other cases, vertical motion are simulated with reasonable accuracy.




	<p>Research and Development Programme on Seismic Ground Motion</p> <p>CONFIDENTIAL</p> <p><i>Restricted to SIGMA scientific partners and members of the consortium, please do not pass around</i></p>	<p>Ref : SIGMA-2013-D2-93 Version : 02</p> <hr/> <p>Date : 7 January 2014 Page : 33</p>
--	---	---

Figure 4.10 – Effect of hypocenter location: comparison between observations (black) and simulations obtained with the Hisada code at MRN considering the different hypocenters (Hypo INGV, hypo from 1 to 9) sketched on the top panel. Velocity time histories filtered between 0.1 and 2 Hz.

Location of the seismic fault

In this Section, the effect of varying the position of the seismic fault, by keeping unchanged the coordinate of the hypocenter (i.e., Hypo INGV) all other kinematic parameters, is presented. In particular, the original fault (referred to as “atzori”) is moved about 3 km northward (fault N), southwest (fault S), eastward (fault E) and westward (fault W), as sketched in Figure 4.11 on the top panel. In this figure the observed and simulated velocity time histories at MRN are compared (0.1-2 Hz).

It is noted that:

- changing the position of the fault does not affect positively the prediction on the EW component (a poor fit in terms of polarity is still found);
- faults N and E produce a better agreement especially on the NS component owing to directivity effects. As discussed previously, in this case the hypocenter is located exactly below the region of maximum slip, therefore inducing a strong NS pulse at the stations located above at ground surface.
- the model with Fault S underestimates significantly the observed motion on all three components.

Rake angle

As a further analysis, we study herein the influence on the rake angle on predicted ground motion at MRN. The seismic fault and the hypocenter are the same as considered in the original model (i.e. fault atzori and hypo INGV).

Figure 4.12 illustrates the comparison between recorded and simulated velocity waveforms (0.1-2 Hz), the latter being obtained with six different values of rake angle (λ), from a minimum of 50° to a maximum of 150° .

This comparison shows that:

- slip angles of 130° and 150° , i.e. the presence of right-lateral strike-slip components in the focal mechanism, allow us to reproduce the polarity of observed EW motion, while no major effects are found on the NS component with respect to the original model with $\lambda = 90^\circ$.

- Slip angles of 50° and 70° produce a strong velocity pulse on the EW component but with opposite polarity with respect to the recording.

Rupture velocity

As a final test, the effect of rupture velocity (V_R) is investigated. The seismic fault and the hypocenter are the same as considered in the original model (i.e. fault atzori and hypo INGV). A rake angle $\lambda = 90^\circ$ (pure reverse faulting) is considered.

Three values of V_R , i.e. 2.8 km/s, 3.2 km/s, and 3.5 km/s (super-shear rupture), are taken into account for the simulation. The comparison between recorded and simulated velocity time histories (Figure 4.13) shows that the effect of rupture velocity is minimal and limited to a narrow frequency range, between 0.7 – 1.5 Hz.

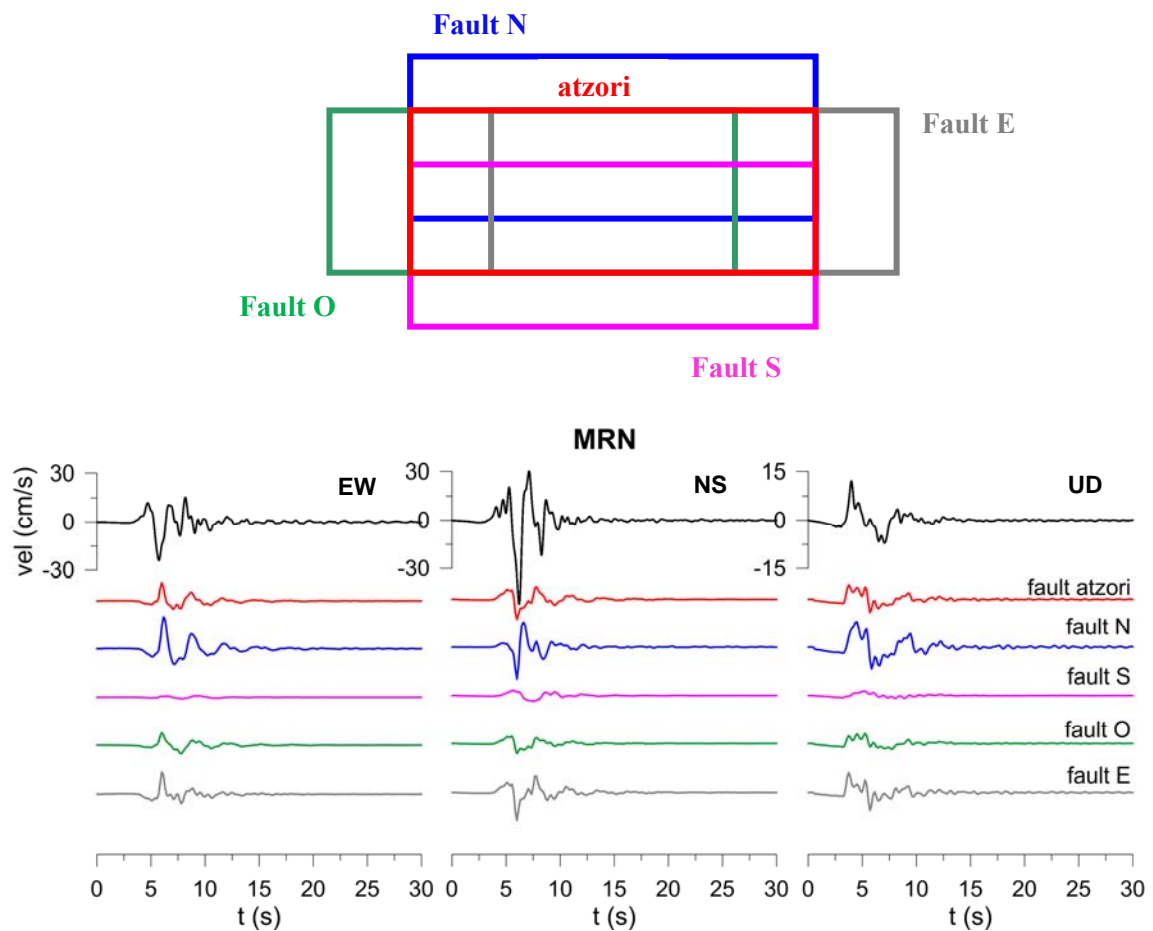


Figure 4.11 – Effect of location of the seismic fault: comparison between observations (black) and simulations obtained with the Hisada code at MRN considering the different faults (original atzori model, fault N, S, O and E) sketched on the top panel.

CONFIDENTIAL

Restricted to SIGMA scientific partners and members of the consortium,
please do not pass around

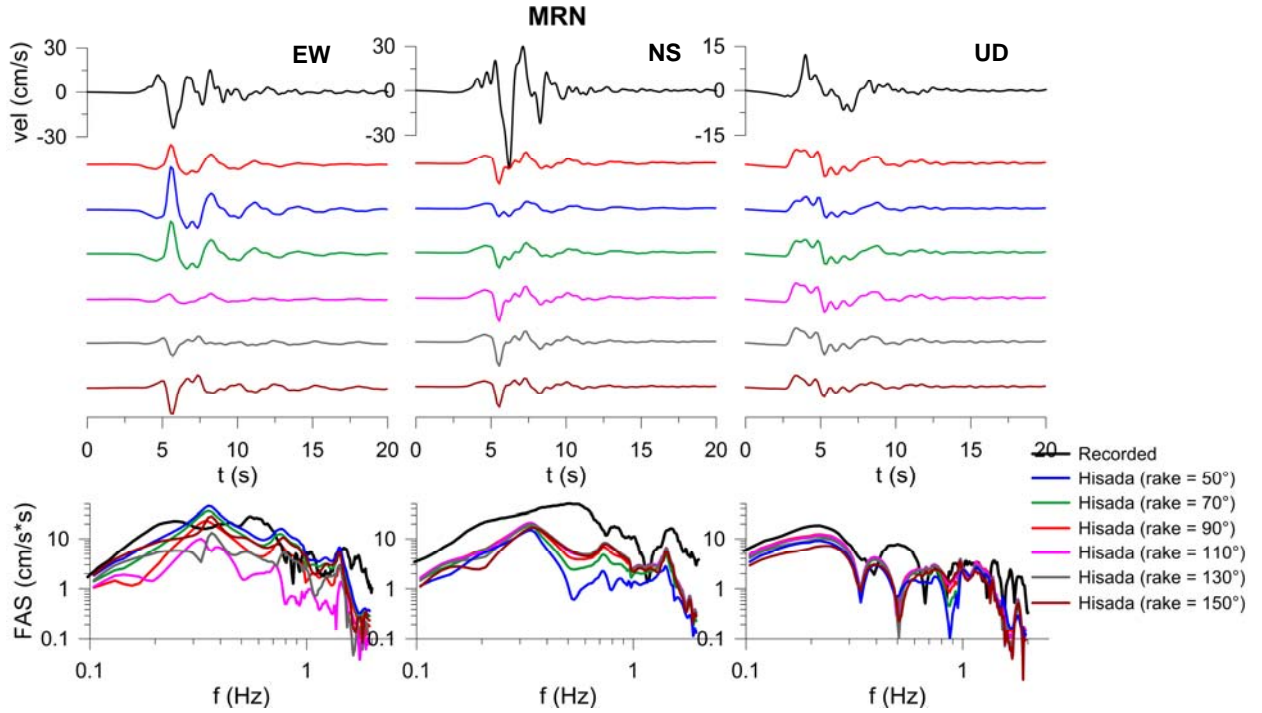


Figure 4.12 –Effect of rake angle: comparison between observations (black) and simulations obtained with the Hisada code at MRN considering different values of rake angle ($\lambda = 50^\circ, 70^\circ, 110^\circ, 130^\circ, \text{ and } 150^\circ$).

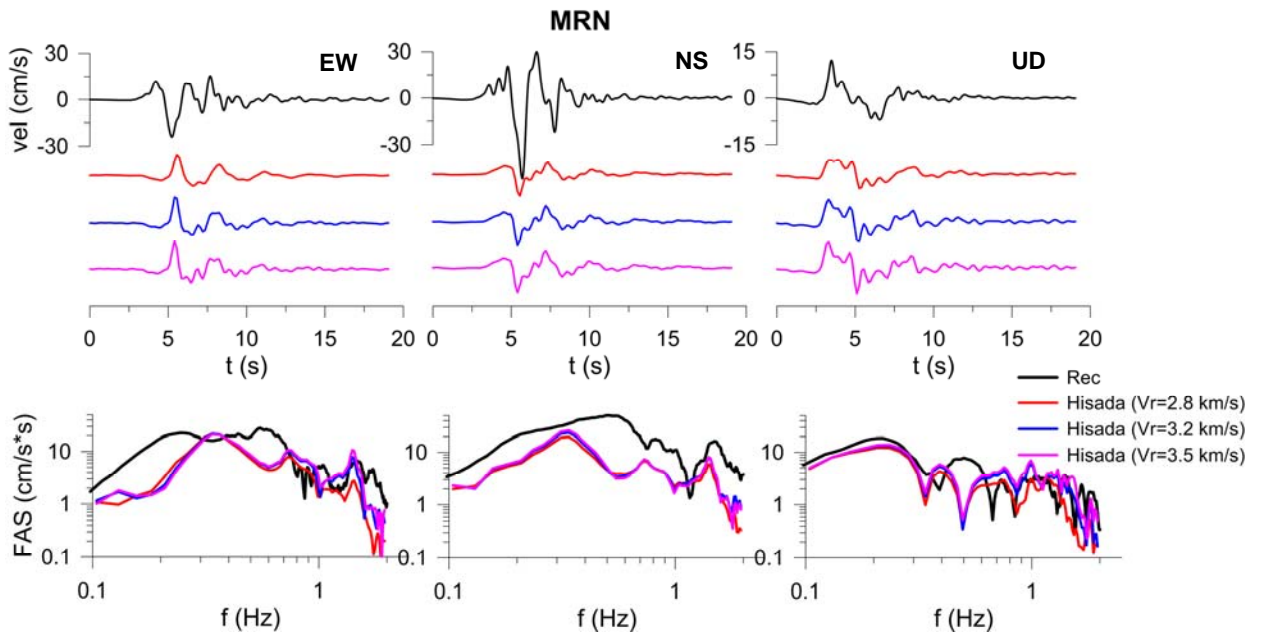


Figure 4.13 – Effect of rupture velocity: comparison between observations (black) and simulations obtained with the Hisada code at MRN considering different values of rake angle ($\lambda = 50^\circ, 70^\circ, 110^\circ, 130^\circ, \text{ and } 150^\circ$).

Table 4.3 – 1D soil model adopted for the simulations with the Hisada code.

H (m)	ρ (kg/m ³)	V_P (m/s)	Q_P	V_S (m/s)	Q_S
160	1800	1500	100	300	30
200	2200	1500	150	600	60
2940	2500	4400	400	2000	200
-	2700	6000	600	3400	350

Based on the these parametric analyses, in the following we will present the results obtained with SPEED (3D source model + 3D soil model), by varying the location of the nucleation point. The original hypocenter (INGV solution, referred to as “Hypo INGV”) was indeed shifted westward and downward, as illustrated in Figure 4.14.

The geographic coordinates of the new hypocentre, referred to as “Hypo SW” hereafter, are 44.8357 °N latitude, 11.0174 °E Longitude and the focal depth is 12.1 km. Note the Hypo SW corresponds to the macroseismic epicenter (Galli et al. 2012; see the superimposed yellow star in **Errore. L'origine riferimento non è stata trovata.**).

Figure 4.15 shows the comparison between the recorded and simulated displacement waveforms, as obtained with the two hypocenters (Hypo INGV vs Hypo SW), at three representative stations, namely, MRN, SAN0 and MDN. On the other side, Figure 4.16 reports the comparison between the two source models in terms of average GoF scores for a larger suite of strong motion stations. It is found that the hypocenter location predominantly affects the predictions at the closest stations (MRN and SAN0), while results at the farther stations (except for some peculiar cases) are similar to those shown in the previous section. It is interesting to note that, for MRN and SAN0, the fit with the observations is largely improved, as pointed out by the GoF scores in Figure 4.16 (the scores increase of nearly 2 points). At these stations a better agreement is found in terms of ground motion amplitudes, and, at MRN, the polarity of the EW displacement waveform is well reproduced with the new hypocenter. Nevertheless, at other sites, such as RAV0, SAG0, BON0, located at larger epicentral distances, the agreement tends to deteriorate, probably due to an exaggeration of source directivity coupled with complex site effects.

Furthermore, to highlight the effect of the hypocenter location on the spatial variability of seismic motion, we compare in Figure 4.17 the ground shaking maps in terms of horizontal (geometric mean) PGD as obtained with the Hypo INGV (top panel) and the Hypo SW (bottom).

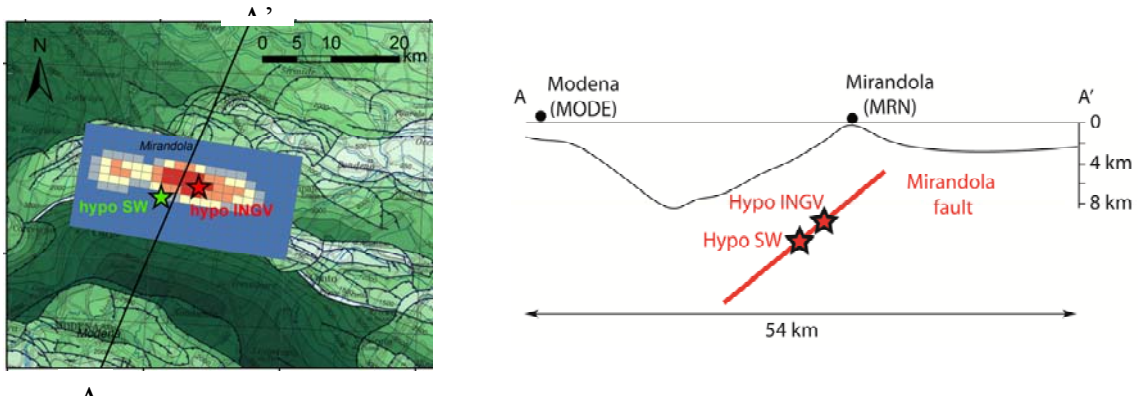


Figure 4.14 - Parameter study on the seismic source model: the red star denotes the instrumental epicenter (INGV hypocenter) while the green one indicates the new hypocenter (“hypo SW”) shifted SW with respect to the original position.

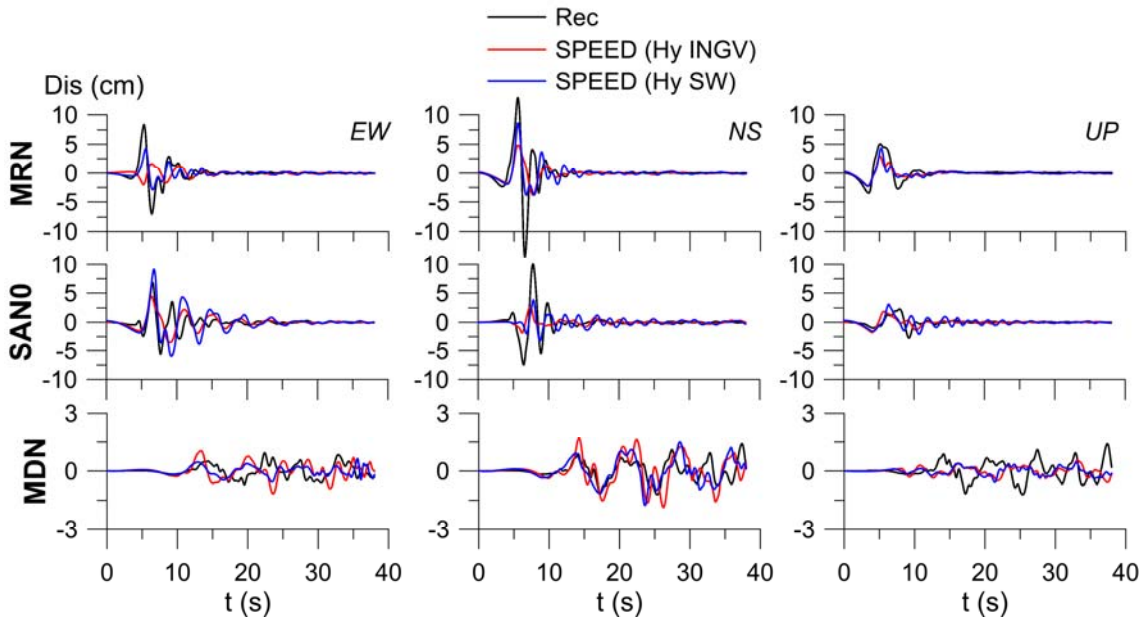


Figure 4.15 –Recorded (black) vs synthetic displacement time histories (0.1-1.5 Hz) at MRN (top panel), SAN0 (centre), and MDN (bottom), as obtained with the two hypocenters (red = INGV hypocenter; blue, new hypocenter SW).

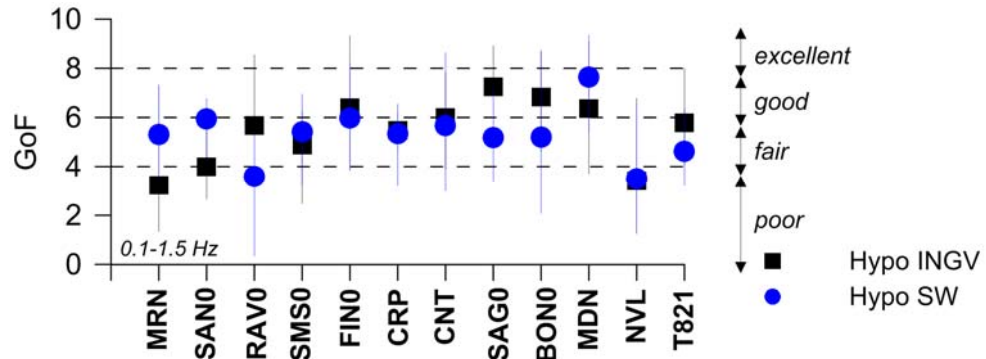


Figure 4.16 – Average GoF scores (0.1-1.5 Hz) as obtained with the two hypocenters.

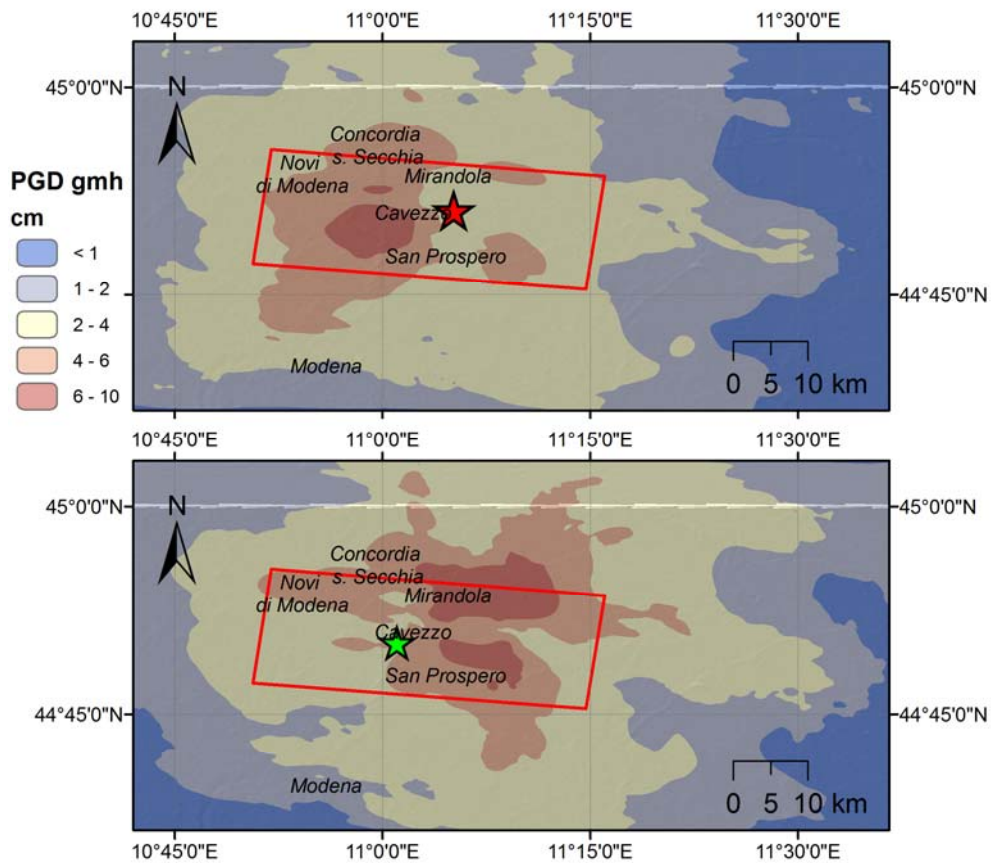



Figure 4.17 – Simulated ground shaking map of horizontal (geometric mean) *PGD* as a function of the hypocenter location (top, hypo INGV; bottom, hypo SW).

	<p>Research and Development Programme on Seismic Ground Motion</p> <p>CONFIDENTIAL</p> <p><i>Restricted to SIGMA scientific partners and members of the consortium, please do not pass around</i></p>	<p>Ref : SIGMA-2013-D2-93 Version : 02</p> <hr/> <p>Date : 7 January 2014 Page : 39</p>
--	---	---

4.1.5. Effect of non-linear elastic soil behaviour

As a further improvement of the numerical model, a non-linear visco-elastic (referred to as NLE hereafter) soil behaviour has been assumed for the uppermost sediments in the Po Plain.

NLE soil model is implemented in SPEED as a generalization to 3D load conditions of the classical modulus reduction ($G-\gamma$) and damping ($D-\gamma$) curves used within 1D linear-equivalent approaches (e.g. Kramer, 1996; SHAKE91 and EERA computer codes), where G , D and γ are shear modulus, damping ratio and 1D shear strain, respectively. Namely, to extend those curves to the 3D case, a scalar measure of shear strain amplitude was considered as:

$$\gamma_{max}(\mathbf{x},t) = \max\left[|\varepsilon_I(\mathbf{x},t) - \varepsilon_{II}(\mathbf{x},t)|, |\varepsilon_I(\mathbf{x},t) - \varepsilon_{III}(\mathbf{x},t)|, |\varepsilon_{II}(\mathbf{x},t) - \varepsilon_{III}(\mathbf{x},t)|\right] \quad (4)$$

where ε_I , ε_{II} and ε_{III} are the principal values of the strain tensor. Once the value of γ_{max} is calculated at the generic position x and generic instant of time t , this value is introduced in the $G-\gamma$ and $D-\gamma$ curves and the corresponding parameters are updated for the following time step. Therefore, unlike the classical linear-equivalent approach, the initial values of the dynamic soil properties are recovered at the end of the excitation.

Concerning the $G-\gamma$ and $D-\gamma$ used in the 3D numerical simulations, the curves defined by Fioravante & Giretti (2012) from RC tests on the Po river embankment area (see Figure 4.18). Such curves were applied only for the most superficial layers of the Po plain down to a depth of about 150 m.

The simulated displacement waveforms, as obtained with the NLE soil model, are reported in Figure 4.19 and compared with the ones produced under the hypothesis of linear visco-elastic soil behaviour. The most significant effects are found at those stations where the thickness of soft sediments reaches considerable values of a few thousands of kilometres (see e.g. MDN station). Given the low frequency propagated by the model (< 1.5 Hz), the overall impact of soil nonlinearity is small especially for the stations in the near-fault region.

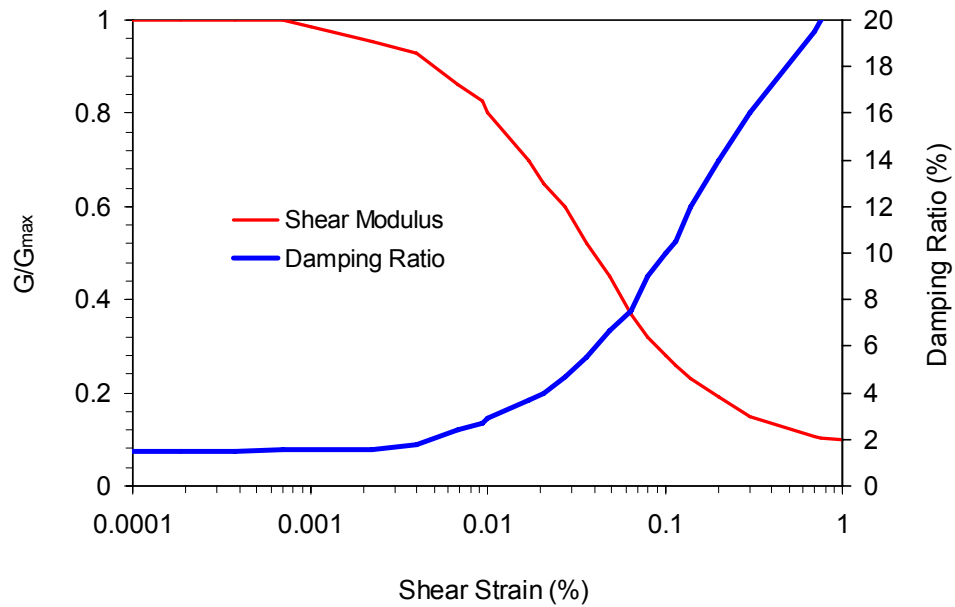


Figure 4.18 – $G-\gamma$ and $D-\gamma$ curves adopted for the 3D non-linear visco-elastic numerical simulations. From Fioravante & Giretti (2012).

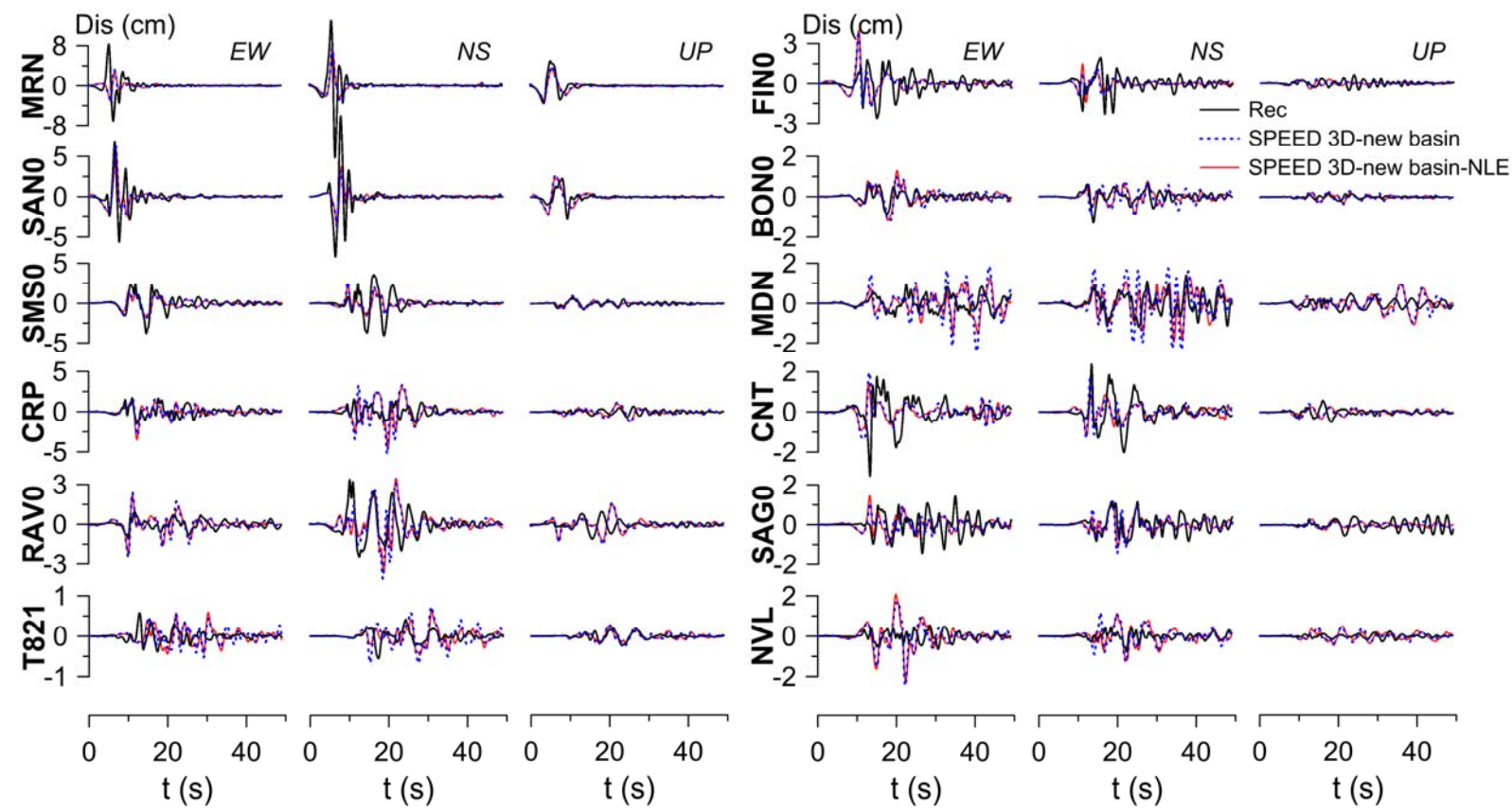



Figure 4.19 – Recorded (black) and simulated displacement waveforms (0.1-1.5 Hz). Results for both linear (blue dotted) and non-linear (red) visco-elastic soil behavior are shown.

	<p style="text-align: center;">Research and Development Programme on Seismic Ground Motion</p> <p style="text-align: center;">CONFIDENTIAL</p> <p style="text-align: center;"><i>Restricted to SIGMA scientific partners and members of the consortium, please do not pass around</i></p>	<p>Ref : SIGMA-2013-D2-93 Version : 02</p> <hr/> <p>Date : 7 January 2014 Page : 42</p>
--	---	---

4.1.6. Ground shaking maps

To provide more through insights into the spatial variability of ground motion, as predicted by 3D numerical simulations, Figure 4.22 illustrates the spatial distribution of PGD (top) and PGV (bottom) as predicted by 3D numerical modelling for the area under study. In both case, the geometric mean of horizontal components is plotted.

The simulated shaking map shows a fairly complex pattern: maximum ground motion amplitudes turn out to be concentrated in a NNE-SSW region, west of the epicenter, with maximum *PGD* and *PGV* values, of about 8.5 cm and 24 cm/s, respectively. This pattern turns out to be fairly realistic if compared with the spatial distribution of MCS intensity, as computed by the DPC (Department of Civil Protection) working group Galli et al., 2012 (see **Errore. L'origine riferimento non è stata trovata.**), showing concentration of damage in a NS-elongated region from Mirandola to Cavezzo approximately. Note that the MCS map shows the combined effects due to the entire seismic sequence from 20 May to 15 June 2012. The superimposed ellipse denotes the MCS pattern which most likely can be attributed to the 29 May 2012 mainshock.

Finally, Figure 4.20 shows the comparison of the *PGD* values computed from the numerical simulations at a regular grid of receivers at ground surface, with the GMPE by Cauzzi & Faccioli (2008), referred to as CF2008, for magnitude $M_w = 6$, site class C and reverse focal mechanism. It turns out that the agreement is satisfactory, even though some discrepancies are found in the attenuation with distance. Nevertheless, as regards the latter point, comparison with the observed *PGD* values at strong motion stations (superimposed dots) is more positive. In the near-fault region the peak displacement amplitudes are consistent with the CF2008, even if their spatial variability is clearly more complex than the one predicted by standard empirical approaches.

To further investigate this point, we discuss herein the comparison between the ground shaking map as obtained through 3D physics-based numerical simulations and the ShakeMaps produced by the INGV (<http://shakemap.rm.ingv.it/shake/index.html>). The latter are produced by using both observed strong motion data, GMPEs and local site amplification functions when available (for further details see Lauciani et al., 2012). In Figure 4.23 the comparison is shown in terms of *PGV* (top) and Pseudo-Acceleration Response Spectra, *PSA*; at 3 s (bottom). In both cases the geometric mean of horizontal components is displayed.

It is observed that:

- 3D numerical simulations underestimate significantly the maximum *PGV* values owing to the drawbacks associated to the kinematic source model, as discussed in Section 4.1.4;
- the range of *PSA*(3s) values from both methods are in reasonable agreement;
- strong differences are found in terms of spatial variability of ground motion in the epicentral area for both ground motion measures (*PGV* and *PSA*);
- ground motion pattern from the ShakeMaps is much smoother than the one from SPEED.

This example highlights that, provided a sufficiently detailed knowledge on the geologic model and the seismic source, the major advantage of using physics-based numerical simulations is related to their ability to estimate the spatial variability of near-source ground motion over an extended territory with a resolution that cannot be given by observed data even when strong motion networks are relatively dense, as in the case of the 29.05 earthquake (that is an exceptional case for the Italian context). Furthermore, it should be considered that strong motion data in near-field conditions are still very scarce and, hence, these numerical simulations offer an interesting tool to study ground motion spatial variability as well as to investigate its dependence on the features of the kinematic source model (slip distribution, location of nucleation point, fault location, etc).

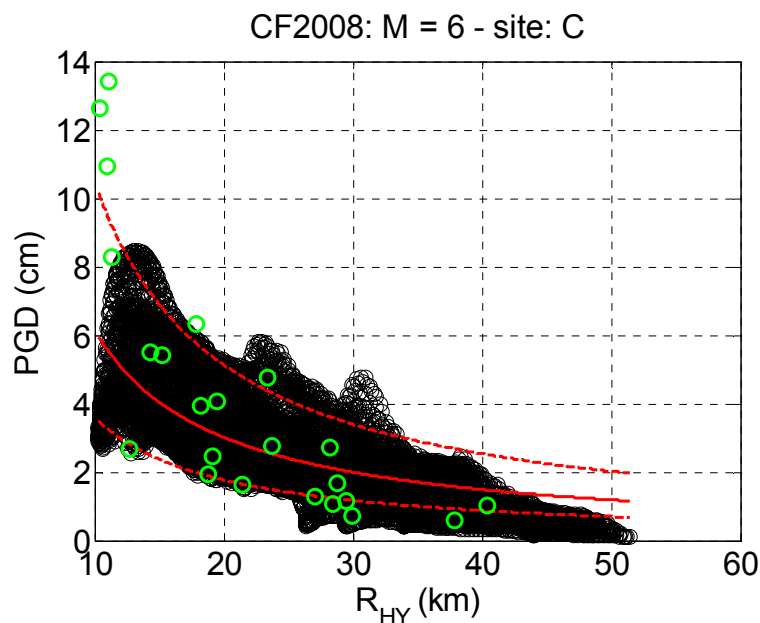


Figure 4.20 – Comparison with the GMPE by Cauzzi & Faccioli (2008), median $\pm \sigma$ in red, for site class C and $M_W = 6$ with the numerical predictions (black dots). The green dots denote the recorded values of *PGD* at the strong motion stations.

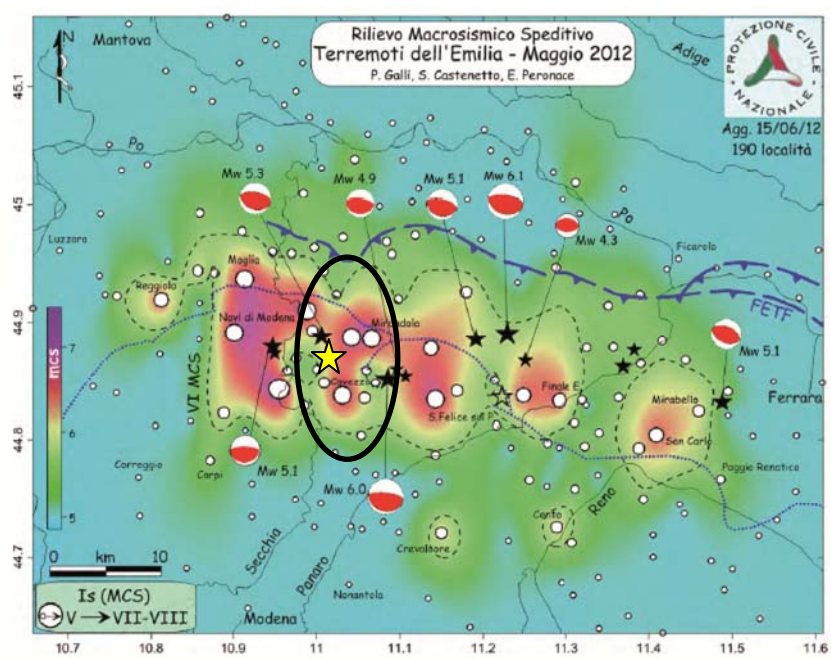


Figure 4.21 – *MCS* intensity map (from Galli et al., 2012) related to the May-June 2012 seismic sequence. The superimposed ellipse denotes the region that is most likely associated to the 29 May earthquake, while the yellow star indicates the macroseismic epicenter.

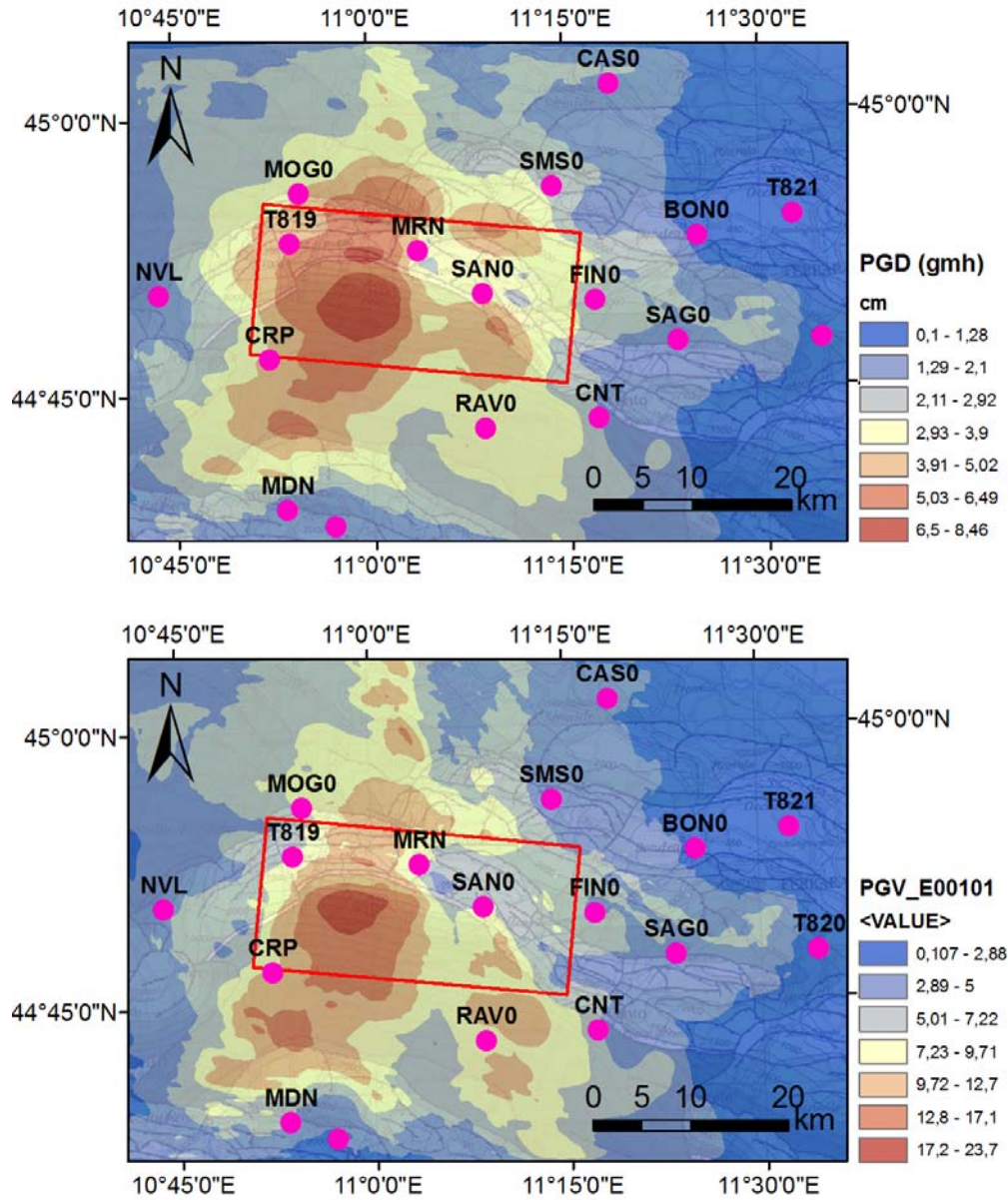


Figure 4.22 – Ground shaking maps computed through SPEED for the 29 May earthquake. Top: horizontal (geometric mean) *PGD* (top) and *PGV* (bottom) wavefield.

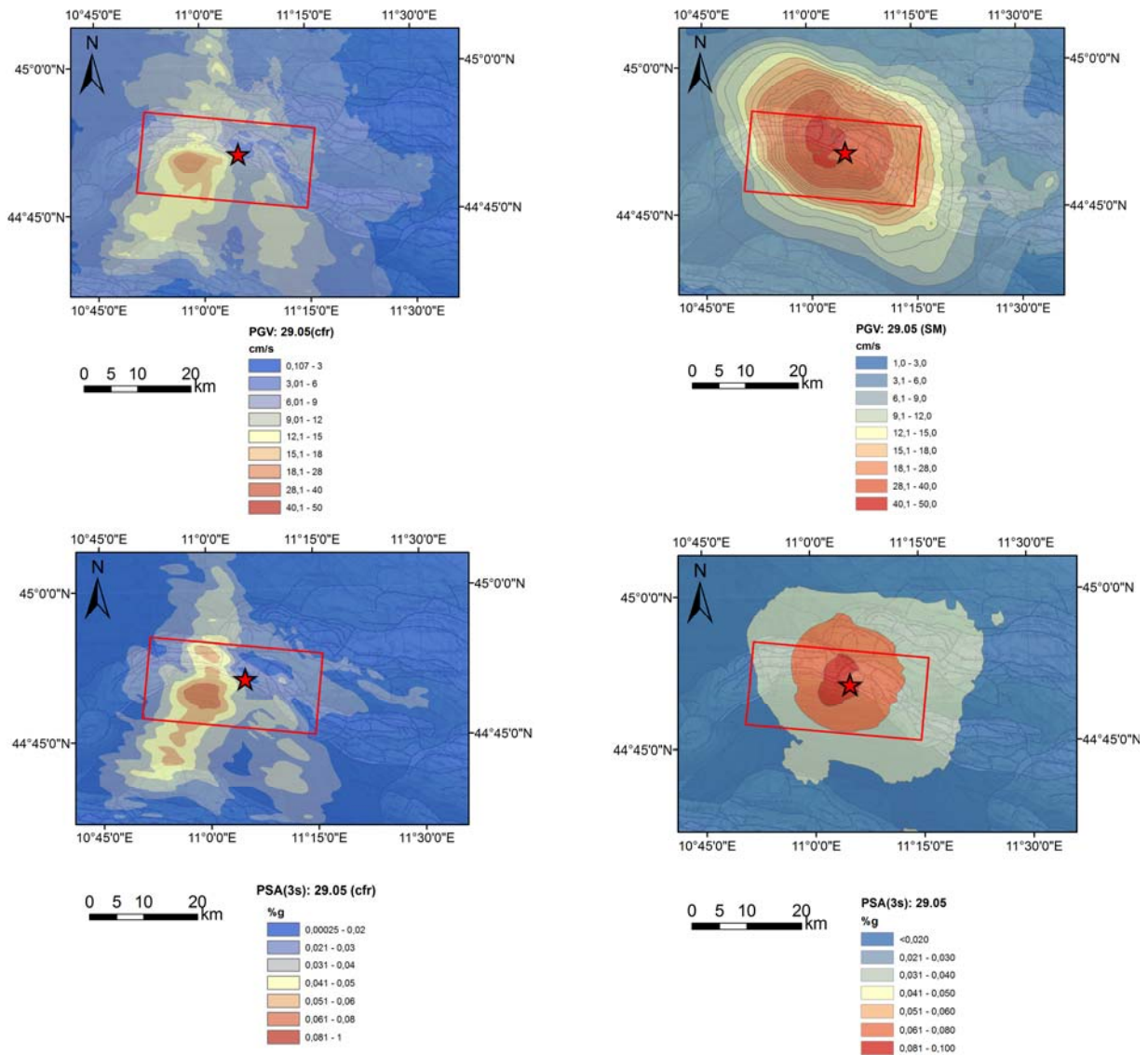



Figure 4.23 – Comparison between the ground shaking maps produced through SPEED and the Shake Maps based on GMPEs coupled with observed data (developed by the INGV: <http://shakemap.rm.ingv.it/shake/index.html>) in terms of PGV (top) as well as PSA at 3 s (bottom).


4.1.7. Generation of broadband accelerograms and shaking maps

As a further application, in this Section we show how the 3D numerical simulations can be used in conjunction with other methods to generate broadband (BB) ground motions. The 29 May 2012 earthquake (simulation with hypocenter INGV) will be taken as a representative case study for this application.

	<p style="text-align: center;">Research and Development Programme on Seismic Ground Motion</p> <p style="text-align: center;">CONFIDENTIAL</p> <p style="text-align: center;"><i>Restricted to SIGMA scientific partners and members of the consortium, please do not pass around</i></p>	<p>Ref : SIGMA-2013-D2-93 Version : 02</p> <hr/> <p>Date : 7 January 2014 Page : 47</p>
--	---	---

Earthquake engineering applications need realistic ground motion time histories with reliable features in the entire frequency range of interest. The 3D numerical results shown in the previous sections are still restricted to relatively low frequencies, up to about 1.5 Hz, mainly due to computational limitations as well as insufficient resolution in our knowledge of the geologic and source model rather than inherent drawbacks of the method. Referring in particular to the structural setting of historical Italian towns, dominated by masonry low rising (2-3 storeys) buildings with relatively short fundamental periods (~ 0.3 s), increasing the frequency limit of predicted ground motion time histories is therefore compulsory for engineering applications. Nevertheless, it should be considered that a frequency resolution of 1.5 Hz represents a good achievement in the field of computation seismology. For the majority of complex 3D numerical models the frequency resolution is typically up to about 0.5 Hz. Furthermore, it should be remarked that the relatively low frequency limit of our models is due to the fact the mesh has to be designed to account for low velocity sediments up to thousands of meters (the maximum SE size should be at least $\sim V_s/f_{max}$ for spectral degree equal to 4), leading to an increase of computation burden to model the Po Plain. A hybrid scheme is applied to produce broadband ground motions at selected stations of in the Po Plain during the 29 May earthquake. Low Frequency (LF) waveforms from SPEED are combined with the High Frequency (HF) synthetics computed through other independent approaches (e.g., stochastic methods) by means of matching filters. In this study, we adopt for the HF part the non-stationary synthetic accelerograms computed through the method of Sabetta and Pugliese (1996), referred to as SP96.

The main advantages of using SP96 are the following: (i) it is fast and easy due to the limited number of input parameters (moment magnitude, epicentral distance, and site class = deep alluvium site according to the GMPE by SP96); (ii) the prediction of ground motion intensity measures is consistent with the GMPEs (that were proved to provide in most cases estimates in agreement with the observations for different recent earthquakes even in near-fault conditions). On the contrary, this method does not allow accounting neither for the same extended kinematic fault rupture model as adopted in the LF computations nor for specific 1D site amplification functions. Instead of SP96, the exsim code (Motazedian and Atkinson, 2005) can be used for the generation of HF synthetics. The major advantages of this method are related to the possibility to model heterogeneous slip patterns as well as to include 1D local site amplification functions to account for specific site effects. The combination of 3D numerical simulations with

	<p>Research and Development Programme on Seismic Ground Motion</p> <p>CONFIDENTIAL</p> <p><i>Restricted to SIGMA scientific partners and members of the consortium, please do not pass around</i></p>	<p>Ref : SIGMA-2013-D2-93 Version : 02</p> <hr/> <p>Date : 7 January 2014 Page : 48</p>
--	---	---

EXSIM to construct BB signals has been recently explored in the work by Smerzini and Villani (2013), for the case of the L'Aquila earthquake.

It was only during the review process of this work that we became acquainted with the procedure proposed by Pousse et al. (2013) for the generation of non-stationary stochastic accelerograms. This method modifies and improves the model developed by Sabetta & Pugliese (1996), mainly in terms of: (a) frequency content of synthetic signals that follow a ω -square model, overcoming, hence, the deficit of energy in the low frequency range; (b) advanced envelope time function for P-, S- and coda waves represented by the so-called average instantaneous power; (c) ground motion variability by including the uncertainties of model parameters. For our purposes, point (c) represents the most relevant advancement, as it allows one to account for the ground motion variability as observed in real data. This feature is substantially lacking in the original method of Sabetta & Pugliese (1996), where variability of simulated ground motion is due only to the random phase. Therefore, provided this progress, future work will involve the implementation of the method developed by Pousse et al. (2006) instead of SP96, to produce the stochastic HF part of BB synthetics.


The procedure adopted to generate BB acceleration time histories at a given site can be summarized as follows (see example in Figure 4.24):

- compute $N=20$ stochastic realizations with SP96 for each ground-motion component (EW and NS);
- for each stochastic realization, synchronize the LF and HF time histories in the time domain, based on the value of normalized Arias intensity $I_a = 5\%$;
- for each stochastic realization, combine HF and LF waveforms in the frequency domain by applying a match filter, defined as follows:

$$BB(f) = w_{LF} \cdot A_{LF}(f) + w_{HF} \cdot A_{HF}(f) \quad (5)$$

where $A_{LF}(f)$ and $A_{HF}(f)$ denote the Fourier transform of the LF and HF acceleration time histories, respectively; w_{LF} and w_{HF} are the corresponding weighting cosine-shape functions; and $BB(f)$ is the Fourier transform of the output BB signal.

For the application presented herein, the low-pass and high-pass frequencies $f_l = 0.5$ Hz and $f_h = 0.7$ Hz have been assumed. Even though waveforms generated by SPEED are usable up to about 1.5 Hz, a low cross-over frequency is adopted to make the Fourier spectrum of the BB signal more realistic by avoiding the presence of unphysical spectral holes.

	<p>Research and Development Programme on Seismic Ground Motion</p> <p>CONFIDENTIAL</p> <p><i>Restricted to SIGMA scientific partners and members of the consortium, please do not pass around</i></p>	<p>Ref : SIGMA-2013-D2-93 Version : 02</p> <hr/> <p>Date : 7 January 2014 Page : 49</p>
--	---	---

In Figure 4.25 we report the comparison between the pseudo-acceleration response spectra of recorded (horizontal EW, NS and GM components), HF (SP96) and BB (SPEED+SP96) accelerograms at two sites in the Po Plain: MRN (left) and NVL (right). It turns out that broadband spectra are in satisfactory agreement with the observed ones, especially in the low period range ($T < \sim 0.5$ s) both for near- and far- field stations. On the other hand, at long periods numerical simulations do not reproduce properly the recorded motion. In particular, at MRN simulations underestimate significantly the recorded spectral ordinates, whereas at NVL simulations are larger than the observations. As discussed in the previous section the large misfit of numerical simulations at MRN is due to the inadequacy of some features of the kinematic source model. Referring to NVL, instead, it is interesting to note that LF component, coming from SPEED, are slightly closer to the observations.

As a further application, we present in Figure 4.26 the ground shaking map (PGV, left; PGA, right - geometric mean of horizontal components for both maps) as obtained by using the method presented in this section (SPEED+SP96). For comparison purposes, the map computed through SPEED, usable only in the LF range, is also displayed. Although it is too simplistic, particularly regarding the spatial coherence of HF ground motion, the method offers a simple tool to predict realistic ground shaking maps over the entire frequency range. Note that the spatial variability of BB ground motion is fairly similar to the INGV ShakeMap, that is constrained on ground motion observations (see Figure 4.23). However, as commented previously, the major drawback of this model is the strong underprediction of *PGV* values.

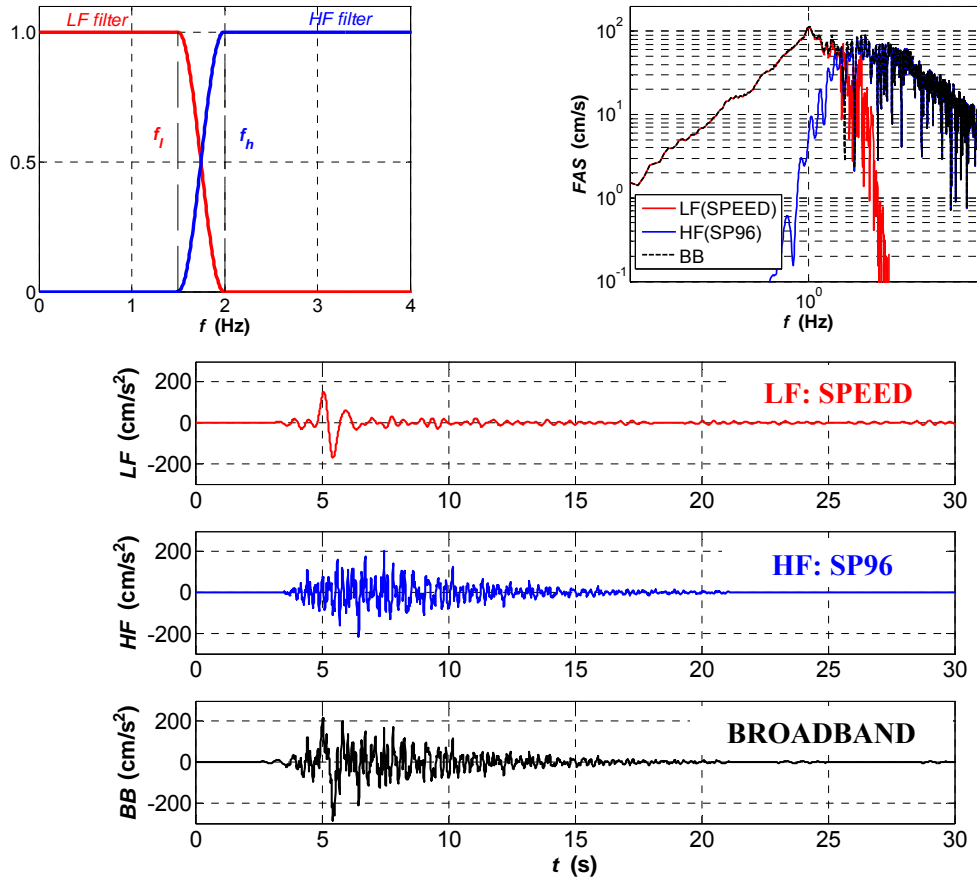


Figure 4.24 – Procedure implemented for the generation of broadband ground motions (black) combining the LF waveforms from SPEED (red) with the HF synthetic accelerograms of Sabetta and Pugliese (1996), SP96 (blue), through suitable matching filters.

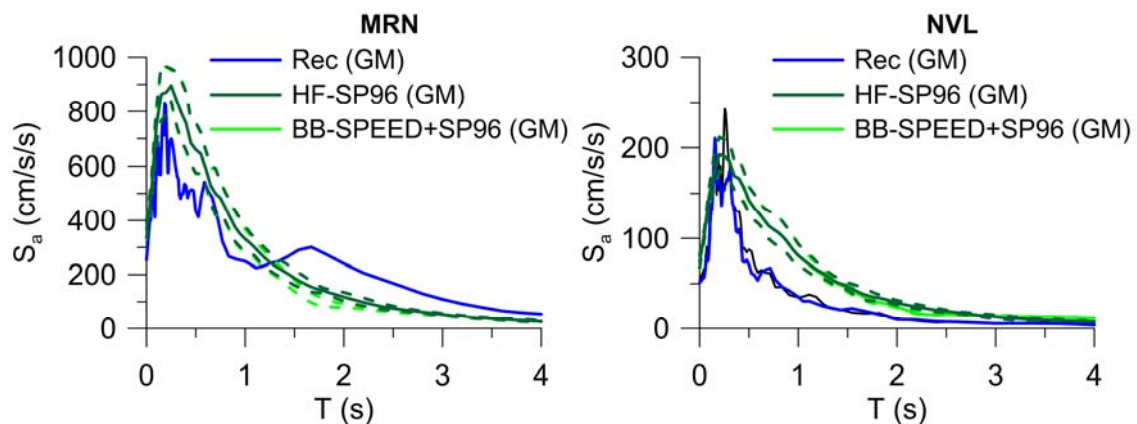


Figure 4.25 – Pseudo-acceleration response spectra of recorded (EW, NS, and GM component), HF (SP96) and broadband accelerograms (SPEED+SP96) at two sites: MRN (left) and NVL (right).

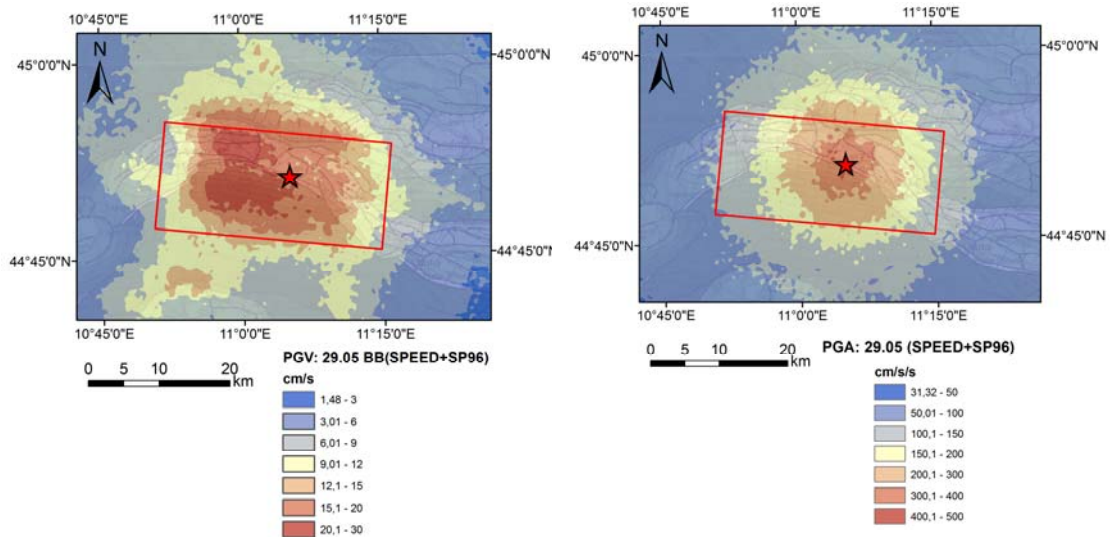


Figure 4.26 – BB (SPEED+SP96) shaking maps in terms of PGV (left) and PGA (right). The geometric mean of horizontal components is shown.

4.2. 3D numerical simulations of the 20 May 2012 earthquake

As mentioned in the introduction, in addition to the numerical simulations of the 29 May earthquake, in the second year activity a numerical model for the 20 May earthquake was also created.

As depicted in Figure 4.1, the model extends over a volume of about $89 \times 62 \times 20 \text{ km}^3$ and is discretized using an unstructured hexahedra mesh with characteristic element size ranging from $\sim 150 \text{ m}$ at the surface to $\sim 1500 \text{ m}$ at the bottom of the model.

Similarly to the model for the 29 May, the mesh, generated using CUBIT, is characterized by:

- (i) the kinematic source model described in Section 3.2 (Ferrara fault in Figure 3.3) and developed by Atzori et al. (2012), see map in Figure 4.27 on the left hand side; the source time function is the same as in Eq. (1), with rise time $\tau = 0.8 \text{ s}$ and rupture velocity $V_R = 2.8 \text{ km/s}$.
- (ii) the 3D model of the deep Po Plain sediments, as described in Section 4.1 and sketched in Figure 4.2 and Figure 4.3;
- (iii) non-linear visco-elastic soil behaviour for the top 150 m of soft deposits, as discussed in Section 4.1.5;
- (iv) flat topography;
- (v) maximum frequency of about 1.5 Hz.

The computational model consists of 2.328.544 SEs, for a total of 62.126.294 LGL nodes, assuming spectral degree equal to 3. The numerical simulations were carried out on the supercomputer FERMI at CINECA (<http://www.cineca.it/en/content/fermi-bgq>). The total computer time with 512 cores and 16 threads for a duration of synthetics equal to 50 s and time step $\Delta t = 0.001$ s ($\sim 24\%$ of Δt_{CFL}) is about 4.3 hours.

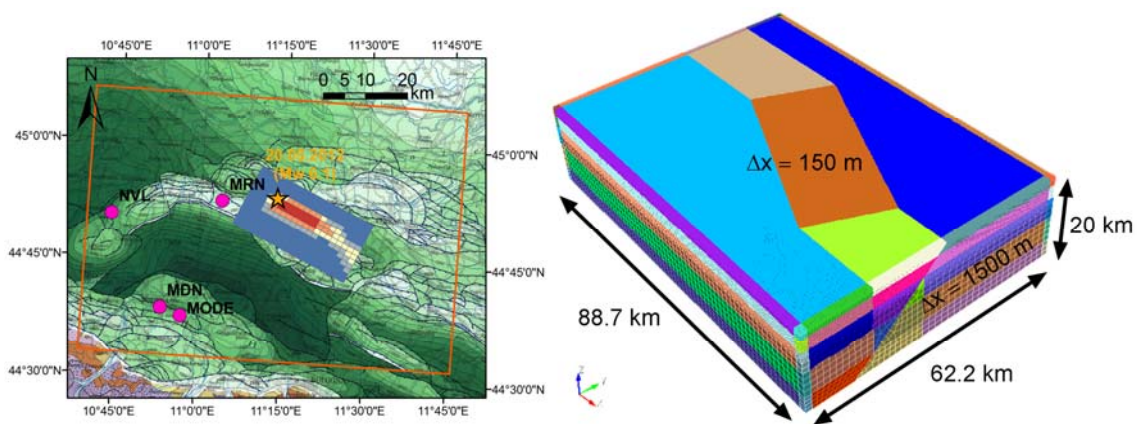


Figure 4.27 – Left: kinematic rupture model of the 20 May 2012 Emilia earthquake plotted on the structural map of Italy (Bigi et al., 1992). The superimposed rectangle indicates the extension of the numerical model. Right: numerical model discretized by SEs.

4.2.1. Comparison with strong motion observations

The record set available for the 20 May earthquake is much limited that the one for the 29 May earthquake. Figure 4.28 displays the comparison between the strong ground motion observations, at the stations MRN, located at about 13 km from the epicenter, NVL and MDN, located at larger distances of about 38-39 km, and the numerical simulations in terms of displacement waveforms. Both recorded and simulated waveforms are processed with an acausal Butterworth 3rd order filter between 0.1 and 1.5 Hz.

As noted for the 29 May earthquake, computations underestimate significantly the peak ground motion amplitudes recorded in the near field region most likely due to some limitations of the source model (see e.g. MRN). Nonetheless, polarity of first arrivals and vertical motion are reproduced well by the numerical simulations. At larger distances, simulated and recorded displacement ground motion amplitudes show a better agreement, even though some discrepancies are still found.

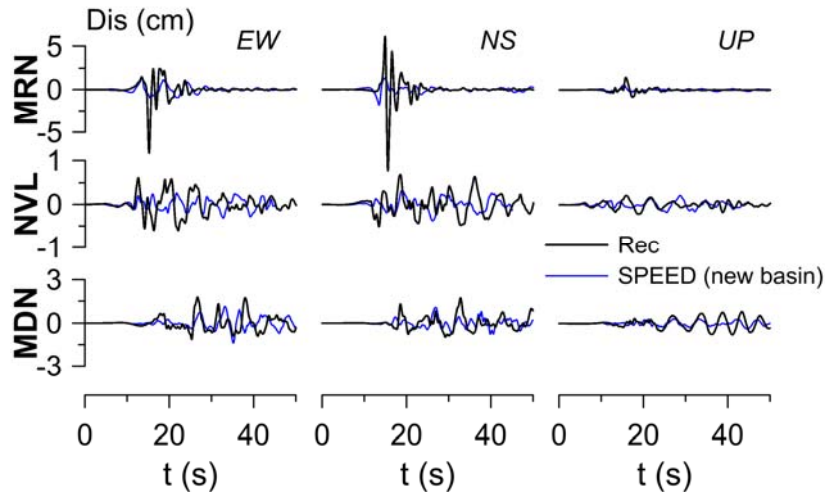


Figure 4.28 – Comparison between observations (black) and numerical simulations (blue) in terms of displacement waveforms filtered in the frequency range 0.1-1.5 Hz for the 20 May earthquake.

4.2.2. Ground shaking map

Figure 4.29 depicts the spatial variability of PGV (geometric mean of horizontal components) as predicted by 3D numerical modelling of the 20 May 2012 earthquake. Maximum PGV values of about 80 cm/s are found in the region east of the epicenter, in the proximity of the *comuni* of Sant’Agostino and Finale Emilia.

The complexity of the spatial pattern of peak ground motion values points out the role of the combined effects of a heterogeneous extended seismic fault model and site effects induced by the complex site geometry.

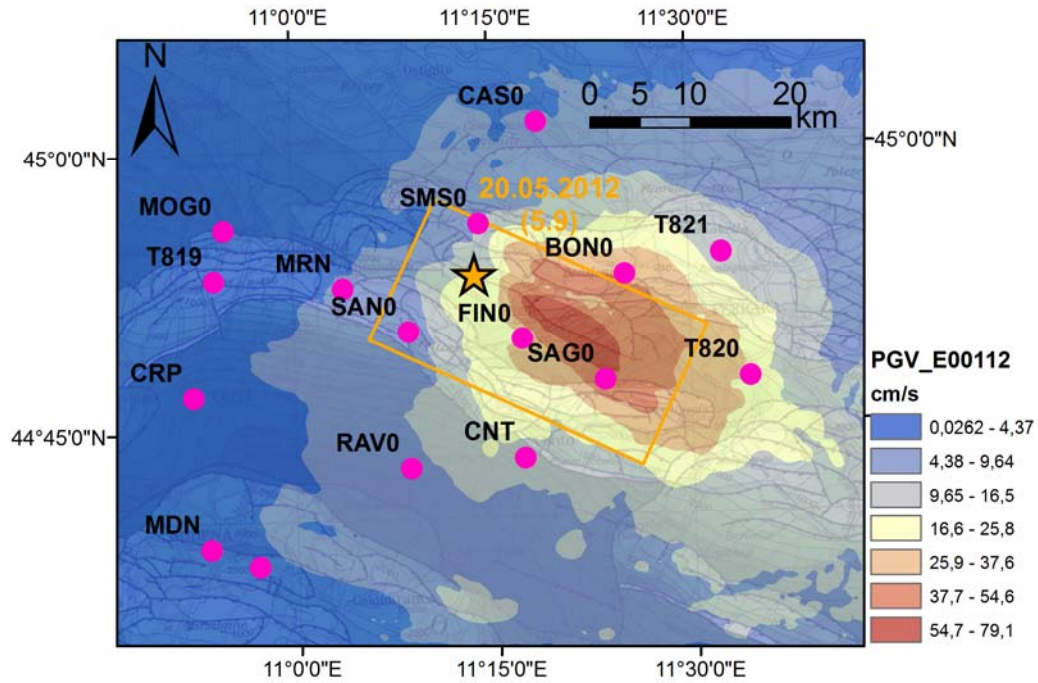



Figure 4.29 – *PGV* (geometric mean of horizontal components) wavefield computed through SPEED for the 20 May 2012 earthquake.

	<p style="text-align: center;">Research and Development Programme on Seismic Ground Motion</p> <p style="text-align: center;">CONFIDENTIAL</p> <p style="text-align: center;"><i>Restricted to SIGMA scientific partners and members of the consortium, please do not pass around</i></p>	<p>Ref : SIGMA-2013-D2-93 Version : 02</p> <hr/> <p>Date : 7 January 2014 Page : 55</p>
--	---	---

5. On the evaluation of Site Amplification Functions (SAF) from 3D seismic scenarios

The general objective of the WP3 of the SIGMA project is the development of tools and approaches for site-specific PSHAs together with the study of the different sources of variability in the evaluation of site amplification function, with emphasis on the response of deep soft alluvial sites. An introduction on the approaches to account for site effects in site-specific PSHA is included in Deliverable D3-96 “Approaches to account for site effects in the PSHA of selected sites in the Po area” and they will not be further discussed herein.


In this context, the goals of this Section can be summarized as follows:

- generation of various 3D ground motion scenarios making use of the SE models described in the previous section. Such scenarios are produced by different fault rupture events along the two Ferrara and Mirandola faults, i.e. the seismogenic structures responsible of the 20 and 29 May earthquakes, respectively, and are characterized by different magnitudes, rupture lengths and widths, slip distributions and nucleation points;
- Evaluation of the spectral amplification function at selected sites in the Po Plain for the different 3D seismic scenarios and of its variability related to 3D effects, i.e., source-to-site azimuth and directivity effects coupled with site effects induced by the complex site geometry.

5.1.1. 3D seismic scenarios for SAF assessment

With the aim of evaluating the effect of the source-to-site propagation path coupled with complex site effects on site amplification response, a suite of 3D numerical simulations is carried out by considering different seismic rupture scenarios occurring on selected portions of the Mirandola and Ferrara faults. These scenarios are characterized by different magnitude, from 5.5 to 6.5, co-seismic slip distribution, focal mechanism, rupture velocity and rise time (the source time function is the same as in Eq. (1)). Four rupture scenarios are produced along the Ferrara fault (20 May 2012) and four are activated along the Mirandola fault (29 May 2012), for a total of eight scenarios.

To compute the SAFs, the following procedure has been devised:

	<p>Research and Development Programme on Seismic Ground Motion</p> <p>CONFIDENTIAL</p> <p><i>Restricted to SIGMA scientific partners and members of the consortium, please do not pass around</i></p>	<p>Ref : SIGMA-2013-D2-93 Version : 02</p> <hr/> <p>Date : 7 January 2014 Page : 56</p>
--	---	---

- for each seismic scenario under consideration, two numerical simulations are carried out: (1) one including the irregular submerged bedrock topography of the Po plain, and (2) a second one having the same features as in model (1) but neglecting the 3D subsoil structure and with the bedrock at $V_S = 800$ m/s outcropping at ground surface. This means that for each site (take for instance Mirandola, MRN) prediction at soft site and at an ideal outcropping bedrock reference site with $V_S = 800$ m/s are available.
- For a given site (e.g., MRN) and for the eight scenarios under consideration, the SAF is computed as the Fourier spectral ratio, referred to as FSR, i.e., the ratio between the Fourier spectrum of the waveform at the surface of the soft site with respect to the one at outcropping bedrock, in correspondence of the same site.

Before presenting the results in terms of SAFs (Section 5.1.2), an overview of the 3D scenarios under consideration is reported herein. Table 5.1 lists the main parameters of the seismic scenarios taken into account in this numerical study. For each scenarios (identified by one code), the following data are provided: target magnitude, length and width of fault rupture, coordinates (lat, lon) of nucleation point, focal depth, rupture velocity V_R , rise time τ , and rake angle.

Figures 5.1~5.8 present an overview of the ground shaking map in terms of spatial distribution of PGV (geometric mean of horizontal components), for the eight scenarios under study. For each scenario, the surface projection of the seismic fault is superimposed on the PGV map and the corresponding kinematic source model is displayed on the right hand side. It is interesting to note that seismic response at the sites of the Po Plain is strongly affected by directivity/focal mechanism effects, related to the specific features of the adopted kinematic source model combined with complex site effects due to the irregular submerged topography.

The co-seismic slip distributions adopted for the numerical simulations come from either source inversion studies for real earthquakes or are computed using a self-similar k -square model (Hybrid-Integral-Composite, see Gallovič Brokešová, 2007). We remark herein that SPEED features a number of options for the kinematic modelling of an arbitrarily complex seismic source, by assigning realistic distributions of co-seismic slip along an extended fault plane through *ad hoc* pre-processing tools. Such tools allow one to reproduce in a semi-automatic way the fault rupture models as catalogued in the on-line Finite Source Rupture Models Database (<http://www.seismo.ethz.ch/srcmod/>, M. Mai, ETH, Zurich) or computed by other methods using a specific format. Furthermore, these tools can be used also to define stochastically correlated random

source parameters, in terms of slip pattern, rise time, rupture velocity and rupture velocity distribution along the fault plane, which may have a key role in deterministic simulations in exciting high frequency components of ground motion (see Smerzini and Villani, 2012).

Table 5.1 – Parameters of the 3D seismic scenarios simulated through SPEED for the evaluation of SAFs.

Scenario id	M_w	L [km]	W [km]	Hy Lon [°E]	Hy Lat [°N]	Depth [km]	V_R [km/s]	τ [s]	Rake [°]
E00101 (29.05)	6.0	32	20	44.851	11.086	10.2	2.8	0.7	90
E00103	5.5	7	6	44.8226	11.0942	12.77	2.5	0.6	90
E00106	6.0	12	7	44.8532	11.0583	10.2	2.8	0.7	100
E00109	6.5	25	12.5	44.8193	11.1344	12.77	2.7	0.7	90
E00112 (20.05)	6.1	30	20	44.88998	11.2282	6.3	2.8	0.8	80
E00117	5.5	6	5	44.9515	11.1325	3.857	2.5	0.6	80
E00119	6.0	12	7	44.8618	11.2616	7.71	2.8	0.7	110
E00123	6.5	25	12.5	44.807	11.2878	11.57	2.8	0.8	70

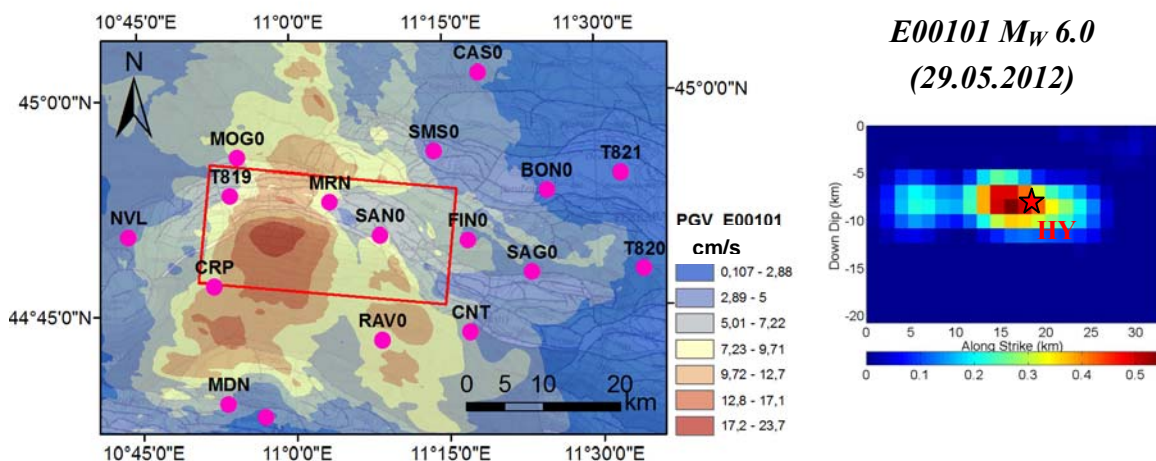
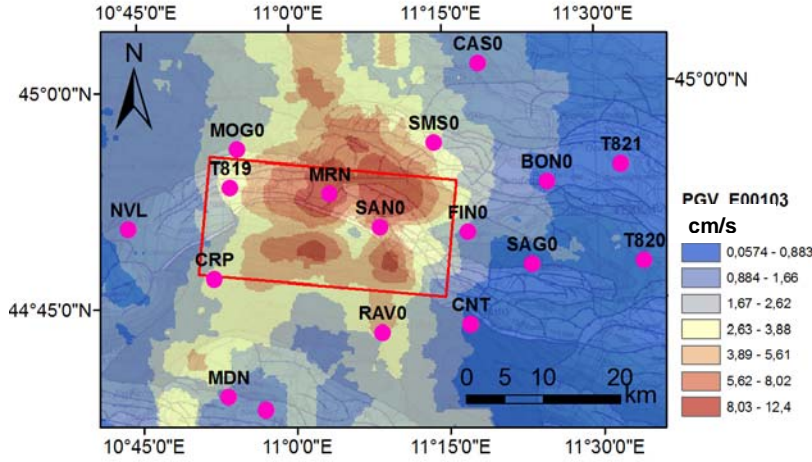


Figure 5.1 – PGV (geometric mean of horizontal components) map for scenario E00101 (corresponding to the 29.05.2012 earthquake) shown in Table 5.1. For each scenario the corresponding kinematic fault model (see projection of the seismic fault superimposed on the map) is displayed on the bottom.

CONFIDENTIAL

Restricted to SIGMA scientific partners and members of the consortium,
please do not pass around



E00103
M_w 5.5

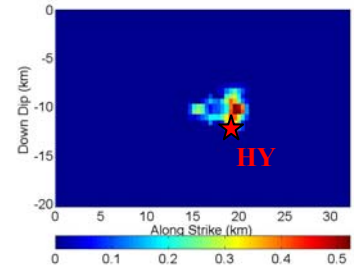
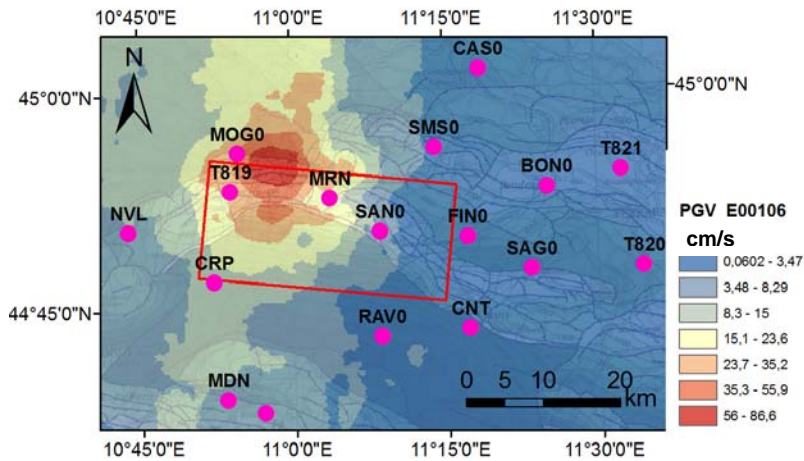


Figure 5.2 – Same as in Figure 5.1 but for scenario E00103 (see Table 5.1).



E00106
M_w 6.0

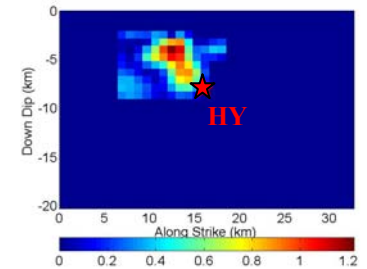


Figure 5.3 – Same as in Figure 5.1 but for scenario E00106 (see Table 5.1).

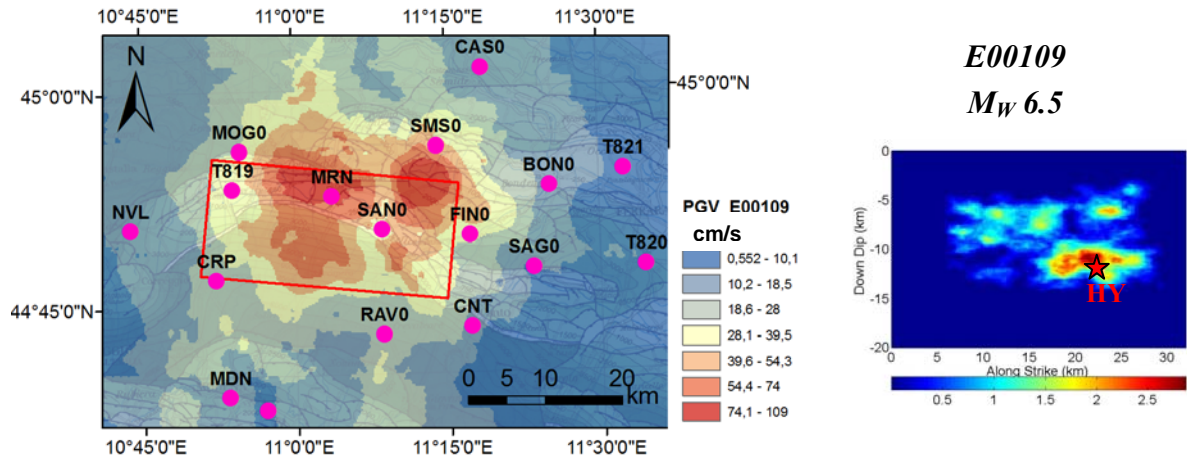


Figure 5.4 – Same as in Figure 5.1 but for scenario E00109 (see Table 5.1).

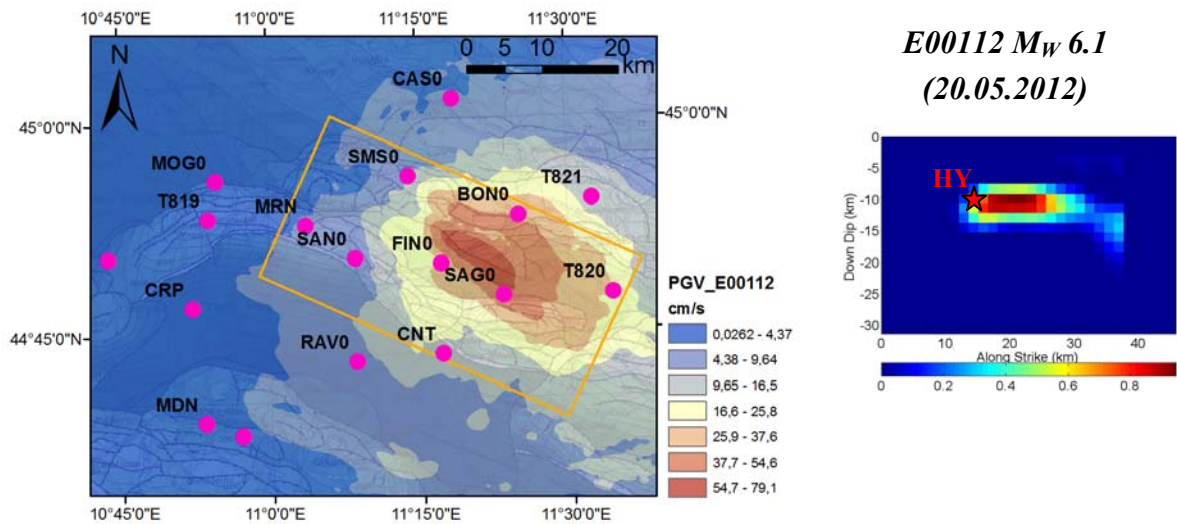


Figure 5.5 – Same as in Figure 5.1 but for scenario E00112, corresponding to the 20 May 2012 earthquake (see Table 5.1).

CONFIDENTIAL

Restricted to SIGMA scientific partners and members of the consortium,
please do not pass around

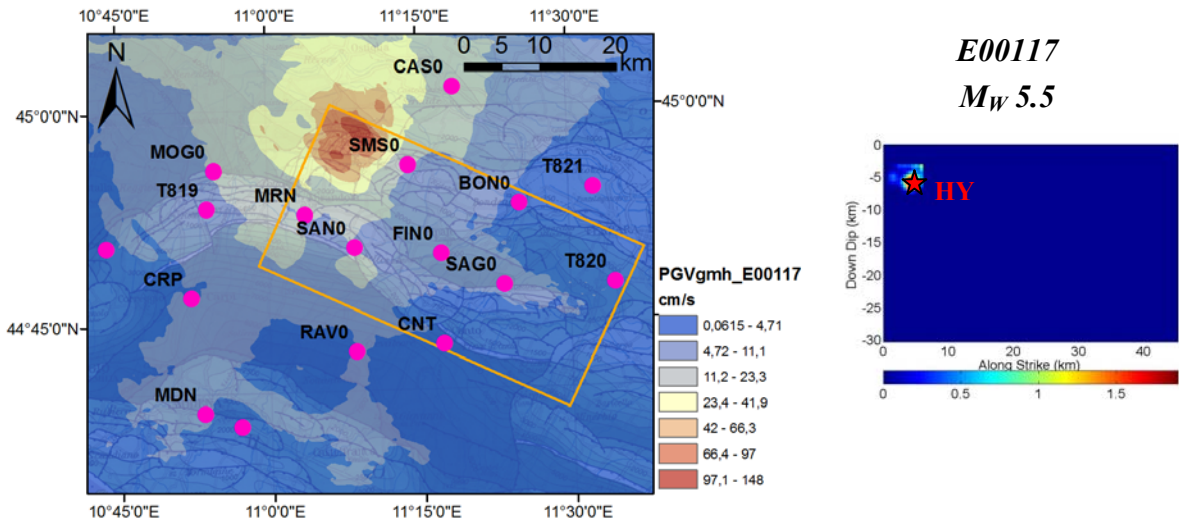


Figure 5.6 – Same as in Figure 5.1 but for scenario E00117 (see Table 5.1).

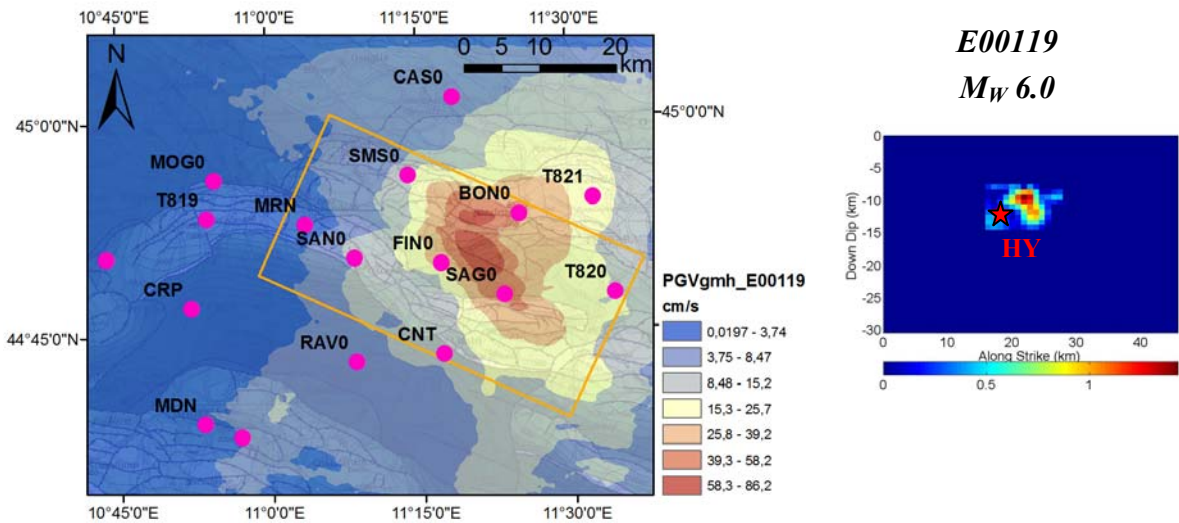


Figure 5.7 – Same as in Figure 5.1 but for scenario E00119 (see Table 5.1).

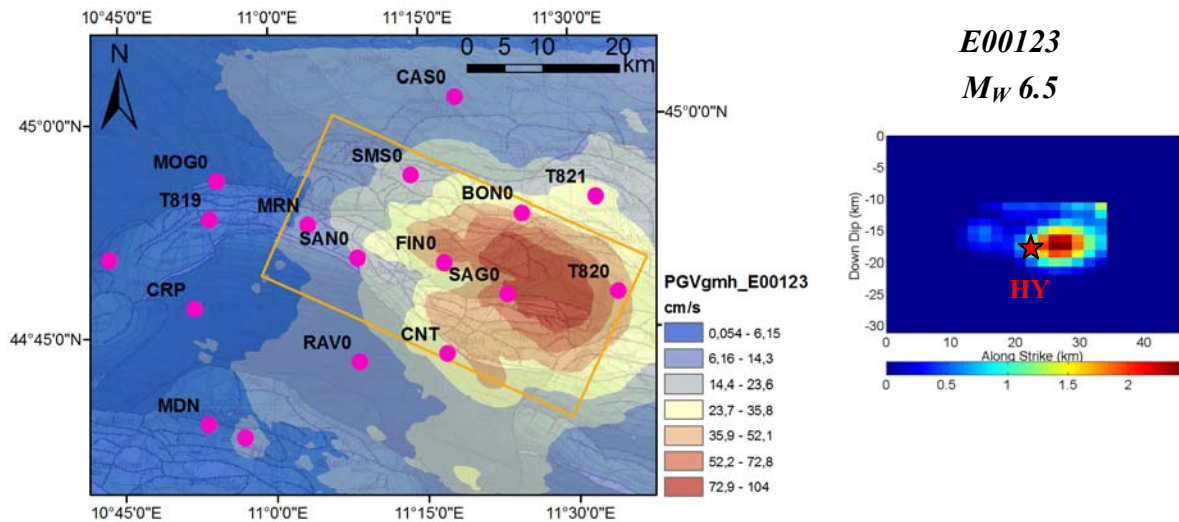



Figure 5.8 – Same as in Figure 5.1 but for scenario E00123 (see Table 5.1).

5.1.1.2. Variability of 3D SAFs at selected sites

Figure 5.9 presents the SAFs at selected sites, namely, MRN, SAN0, SMS0, BON0, FIN0 and MOG0, computed as the FSR with respect to the ideal outcropping bedrock (800 m/s) at the same position as the soil itself. The median FSR for the eight scenarios under consideration along with the corresponding standard deviation ($\pm\sigma$) are illustrated. Since numerical simulations were bounded to around 1.5 Hz, as the maximum propagated frequency, no results are provided for larger frequencies. For comparison purposes, the 1D theoretical amplification function for outcropping reference bedrock is also plotted. The latter is computed by considering a soft layer with $V_S = 300$ m/s, $\rho = 1800$ kg/m³ over bedrock with $V_S = 800$ m/s and $\rho = 2000$ kg/m³ under vertical incidence of plane S waves; the depth to bedrock assumed for the 1D model is the same as the one implemented in the 3D subsoil (see Table 4.1).

The following observations can be made:

- a reasonable agreement is found between the median 3D and 1D results: peak amplifications occur at frequencies $f \sim 0.5$ Hz and $f \sim 1.5$ Hz;
- the variability of site amplification functions may be significant due the combination of factors related to source-to-site path and complex site effects;
- the variability of SAFs for stations located at the top of thicker soft sediments turns out to be larger than the one computed for shallower soft sediments. Such effect is more pronounced at relatively large epicentral distances. As an

	<p>Research and Development Programme on Seismic Ground Motion</p> <p>CONFIDENTIAL</p> <p><i>Restricted to SIGMA scientific partners and members of the consortium, please do not pass around</i></p>	<p>Ref : SIGMA-2013-D2-93 Version : 02</p> <hr/> <p>Date : 7 January 2014 Page : 62</p>
--	---	---

illustrative example of this effect, we illustrate in Figure 5.10 the individual FSRs at two sites, namely, MIR1 and MIR8, roughly located on a NS alignment (see map in the aforementioned figure), as computed for the four scenarios along the Mirandola fault. The variability of FSRs at MIR8 is larger than the one obtained at MIR1 due to the increasing thickness of soft deposits, as we move further from the epicenter along the NS alignment (thickness of sediments increases by ~ 400 m), along with the increasing source-to-site distance (keeping almost unchanged the source-to-site azimuth).

- variability of SAFs tends to increase when accounting for seismic events breaking different faults. When single fault scenarios are considered, a smaller variability is found. An example is provided in Figure 5.11 illustrating the mean $\pm\sigma$ SAFs as obtained at BON0 considering the whole set of rupture scenarios breaking the two faults under study or the subsets of rupture scenarios breaking either the Mirandola or Ferrara fault.

Note that no results are shown herein for stations located at large distances from the epicenter because spectral ratios turn out to be affected by numerical errors related both to the spurious reflections from the close-by absorbing boundary conditions, and to an insufficient duration of signal.

Further investigations are needed for a better understanding of the factors that contribute to the variability of numerically-based SAFs. However, a quantitative evaluation of the inter-event variability of SAF related to 3D effects can be found in Deliverable D3-96 (Section 5.3).

CONFIDENTIAL

Restricted to SIGMA scientific partners and members of the consortium,
please do not pass around

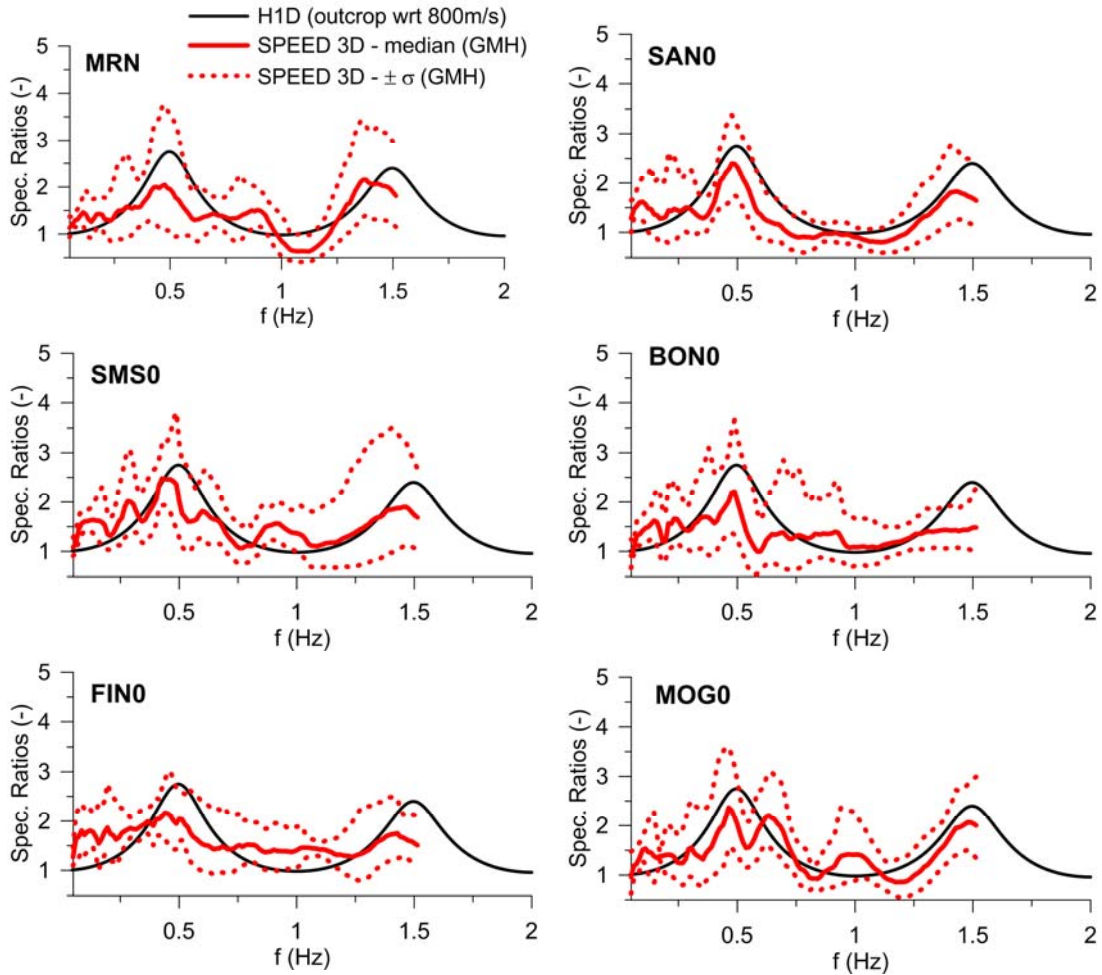


Figure 5.9 –SAFs at selected sites (MRN, SAN0, SMS0, BON0, FIN0 and MOG0), computed as Fourier spectral ratios with respect to outcropping bedrock. The theoretical 1D amplification function (one layer over halfspace) is also plotted for comparison purposes.

CONFIDENTIAL

Restricted to SIGMA scientific partners and members of the consortium,
please do not pass around

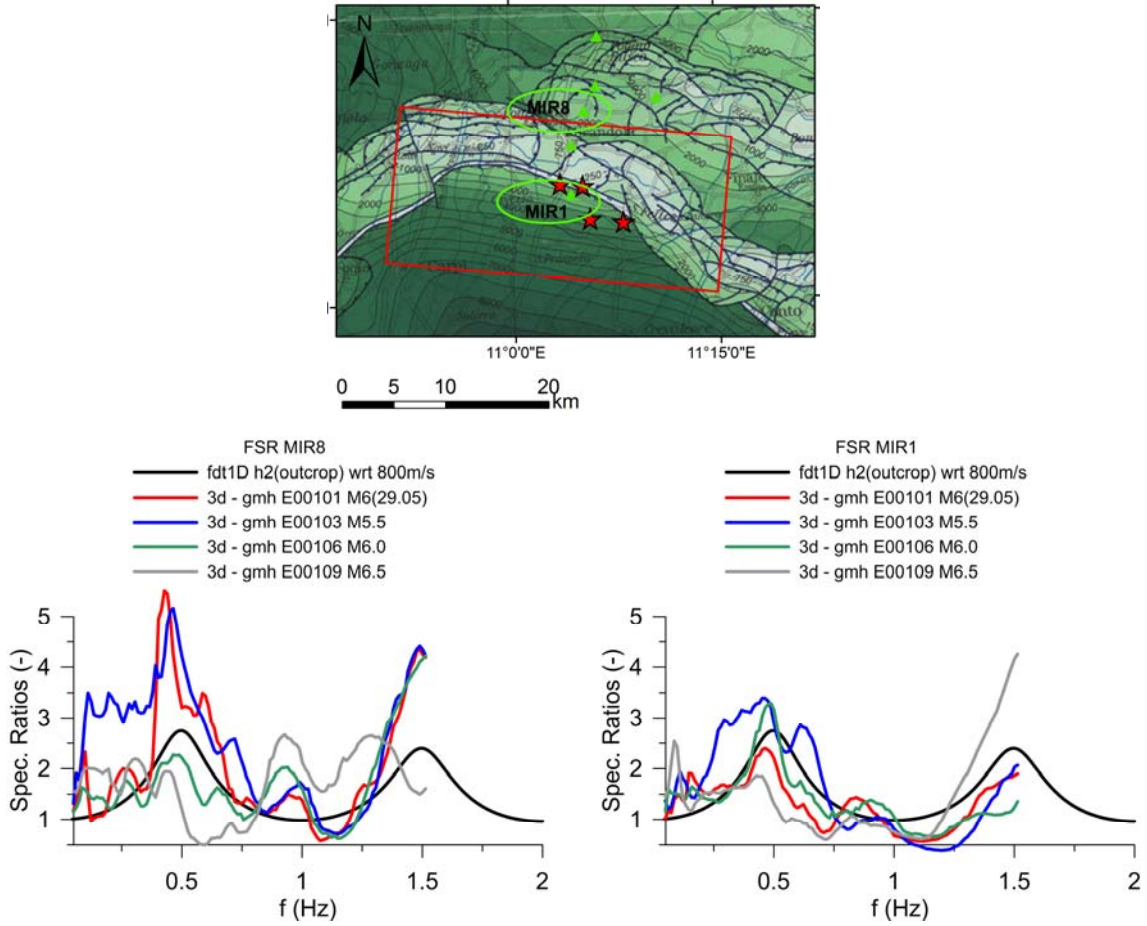


Figure 5.10 –SAFs at two sites (referred to as MIR1 and MIR8, see map on the top panel) for the same subset of scenarios on the Mirandola fault (E00101, E00103, E00106, E00109).

CONFIDENTIAL

Restricted to SIGMA scientific partners and members of the consortium,
please do not pass around

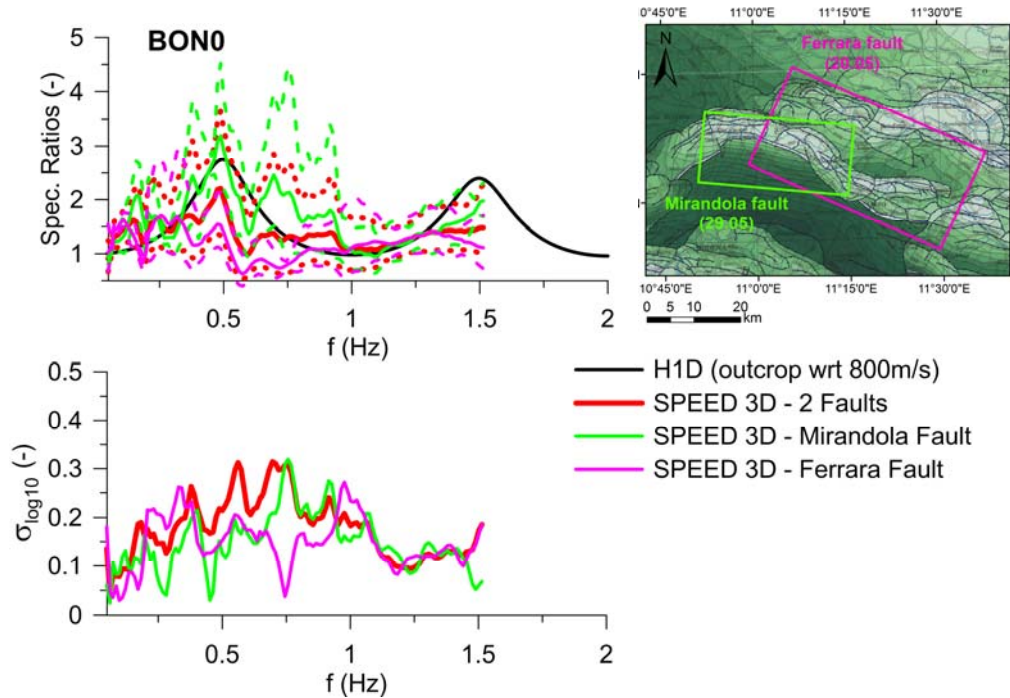



Figure 5.11 –Top: variability of SAFs at BON0 as computed considering: (i) the whole set of scenarios breaking the two faults under study (Mirandola and Ferrara); (ii) a subset of scenarios breaking only the Mirandola fault (E00101, E00103, E00106, E00109); (iii) as subset of scenarios breaking only the Ferrara fault (E00112, E00117, E00119, E00123). Bottom: $\sigma_{\log 10}$ of the SAFs plotted on the top panel as a function of frequency.

	<p style="text-align: center;">Research and Development Programme on Seismic Ground Motion</p> <p style="text-align: center;">CONFIDENTIAL</p> <p style="text-align: center;"><i>Restricted to SIGMA scientific partners and members of the consortium, please do not pass around</i></p>	<p>Ref : SIGMA-2013-D2-93 Version : 02</p> <hr/> <p>Date : 7 January 2014 Page : 66</p>
--	---	---


6. Conclusions

The Emilia-Romagna earthquake sequence of May-June 2012 provided a unique opportunity to study the seismic response in the near and far field of small to moderate earthquakes (up to M6) in the Po-Plain, which is one of the major objectives of the Italian contribution to the SIGMA Project.

3D numerical simulations of both the 29 and 20 May 2012 earthquakes were carried out making use of the Spectral Element code SPEED (<http://mox.polimi.it/it/progetti/speed/SPEED/Home.html>). To perform these simulations, usable up to frequency of about 1.5 Hz, we used quantitative data on the soil profile, both shallow and at depth, and the available kinematic models of the Mirandola and Ferrara faults. Starting from the preliminary simulations illustrated in Deliverable D3-54 (Chapter 4), the following advancements were achieved during the second year: (i) improvement of the numerical model of the 29 May earthquake by adopting a new 3D velocity model of the Po Plain deposits based on the most recent findings as well as non-linear elastic soil behaviour of the uppermost soft layers; (ii) numerical simulations of the 20 May earthquake, based on the geological model calibrated for the 29 May event and on the kinematic source model developed by Atzori et al. (2012).

Discussion of results, including *verification* and *validation* of the numerical simulations, mainly focused on the 29 May event, because for this one a good amount of information is available. The agreement of numerical simulations with observations turns out to be satisfactory in the low frequency range, especially for stations away from the source, where 3D model with submerged topography seems to better explain the onset of prominent surface wave trains propagating throughout the Po-Plain. On the other hand, a rather poor fit is noted at sites in the proximity of the fault, such as at Mirandola, where predictions are strongly affected by the details of the kinematic source model, in particular by the relative position of the nucleation point with respect to the region of maximum co-seismic slip along the fault. These considerations are clearly confirmed by the parametric analyses carried out with an independent code based on the discrete wavenumber method.

After the validation phase, various 3D ground shaking scenarios, characterized by different magnitude, geometric features of the fault rupture, co-seismic slip distribution and other kinematic parameters, are generated by making use of the aforementioned SE

	<p>Research and Development Programme on Seismic Ground Motion</p> <p>CONFIDENTIAL</p> <p><i>Restricted to SIGMA scientific partners and members of the consortium, please do not pass around</i></p>	<p>Ref : SIGMA-2013-D2-93 Version : 02</p> <hr/> <p>Date : 7 January 2014 Page : 67</p>
--	---	---


models for the 29 and 20 May earthquakes. Site Amplification Function (SAF) computed at selected sites in the Po Plain, based on the aforementioned 3D scenarios, show that the scatter of these functions strongly depends on a complex combination of the seismic source features, the source-to-site propagation path and the 3D geological configuration. However, the mean values are in reasonable agreement with the 1D theoretical transfer function for visco-elastic media. For a preliminary quantitative evaluation of the contribution to σ of the event-to-event variability from 3D seismic scenarios we refer the reader to Deliverable D3-96.

Finally, based on the experience gained during this work of numerical simulation of the earthquake ground motions occurred in the Po Plain in May 2012, it is worth to underline some considerations on the potential use of results of physics-based numerical simulations to improve seismic hazard assessment, specifically in the Po Plain.


As a matter of fact, the ultimate objective of this approach is to provide an engine to construct possible and realistic realizations of earthquake ground shaking scenarios, with the obvious positive outcome to improve the available tools for ground motion prediction in well controlled source and site conditions. The experience of the numerical simulations of the Emilia earthquakes has clearly shown that the major limitation towards this objective is, on one side, the availability of realistic fault slip distributions, sufficiently complex to excite a broad range of frequencies, up to at least 3-4 Hz, thus exploiting the ever increasing computational power as well as the advanced approaches to optimize grid size and numerical accuracy.

On the other hand, the limitation in terms of insufficiently detailed knowledge of the underground geology, which is often advocated against this type of approaches, may not be so important if we consider that tools for ground motion prediction typically refer to generic site conditions, defined in terms of average dynamic soil properties. However, location, size and type of the seismic source as well as a reliable 3D model of the depth of the engineering bedrock are the key elements for the numerical simulation and their determination should be as accurate as possible.

As regards specifically the Po Plain, use of physics-based numerical simulations of earthquake ground motion may have a key relevance as regards several further issues: (i) to provide predictions at outcropping bedrock sites, not available in the Po Plain, with potential application to non-ergodic approaches for PSHA and to reduction of uncertainty; (ii) to clarify the role of surface waves that, as shown by records of May


	<p style="text-align: center;">Research and Development Programme on Seismic Ground Motion</p> <p style="text-align: center;">CONFIDENTIAL</p> <p style="text-align: center;"><i>Restricted to SIGMA scientific partners and members of the consortium, please do not pass around</i></p>	<p>Ref : SIGMA-2013-D2-93 Version : 02</p> <hr/> <p>Date : 7 January 2014 Page : 68</p>
--	---	---

2012, dominate ground motion at distances larger than about 30 km (Luzi et al., 2013), also regarding the quantification of site effects, in near field and far field conditions.


	<p>Research and Development Programme on Seismic Ground Motion</p> <p>CONFIDENTIAL</p> <p><i>Restricted to SIGMA scientific partners and members of the consortium, please do not pass around</i></p>	<p>Ref : SIGMA-2013-D2-93 Version : 02 Date : 7 January 2014 Page : 69</p>
--	---	--

7. References


- Anderson, J. G. (2004). Quantitative measure of the goodness-of-fit of synthetic seismograms, in Proc. of the 13th World Conf. on Earthquake Engineering, Vancouver, British Columbia, Canada, 1–6 August 2004, paper 243.
- Antonietti P.F., Mazzieri I., Quarteroni A. and Rapetti F. (2012). Non-conforming high order approximations of elastodynamics equation. *Comput. Meth. Appl. Mech. Eng.*, 209-212:212-238.
- Arnold D.N., Brezzi F., Cockburn B. and Marini L.D. (2002). Unified analysis of discontinuous Galerkin methods for elliptic problems. *SIAM J. Numer. Anal.*, 39(5):1749-1779.
- Atzori S., Merryman Boncori J., Pezzo G., Tolomeri C., Salvi S. (2012). Secondo Report analisi dati SAR e modellazione della sorgente del terremoto dell'Emilia. INGV (in Italian).
- Bielak, J., R.W. Graves, K.B. Olsen, R. Taborda, L. Ramirez-Guzman, S.M. Day, G.P. Ely, D. Roten, T.H. Jordan, P.J. Maechling, J. Urbanic, Y. Cui and G. Juve (2010) 'The ShakeOut earthquake scenario: Verification of three simulation sets.' *Geophys. J. Int.*, Vol. 180 pp. 375–404.
- Bigi G., Cosentino D., Parotto M., Sartori R, Scandone P. (1990) Structural model of Italy and gravity map (1:500.000). CNR, CNR Progetto Finalizzato Geodinamica, Quad. Ric. Sci., 114 (3), 6 sheets, S.E.L.C.A., Firenze.
- Bigi, G., G. Bonardi, R. Catalano, D. Cosentino, F. Lentini, M. Parotto, R. Sartori, P. Scandone and E. Turco (Eds.) (1992). Structural Model of Italy 1:500,000, CNR Progetto Finalizzato Geodinamica.
- Boccaletti M., Coli M., Eva C., Ferrari G., Giglia G., Lazzarotto A., Merlanti F., Nicolich R., Papani G., Postpischl D. (1985) Considerations on the seismotectonics of the Northern Apennines, Volume 117, Issues 1–2, Pages 7–9, 11, 13–22, 33–38
- Burrato P., P. Vannoli, U. Fracassi, R. Basili, G. Valensise (2012). Is blind faulting truly invisible? Tectonic-controlled drainage evolution in the epicentral area of the May 2012, Emilia-Romagna earthquake sequence (northern Italy). *Annals of Geophysics*, Special Issue "The Emilia seismic sequence of May-June, 2012: preliminary data and results", in press.
- Castellarin A., Vai G., Cantelli L. (2006) The Alpine evolution of the Southern Alps around the Giudicarie faults: A Late Cretaceous to Early Eocene transfer zone, *Tectonophysics* Volume 414, Issues 1–4, 23 February 2006, Pages 203–223
- Castro R., Pacor F., Puglia R., Ameri G., Letort J., Massa M. and Luzi L. (2013). The 20 and 29 May, 2012, Emilia Earthquakes (Northern Italy) and the Main Aftershocks: S-wave Attenuation, Acceleration Source Functions and Site Effects. *Geophysical Journal International*, accepted.
- Cauzzi C., Faccioli E., 2008. Broadband (0.05 s to 20 s) prediction of displacement response spectra calibrated on worldwide digital records. *Journal of Seismology* 12,453-475
- Chaljub E, Moczo P, Tsuno S, Bard PY, Kristek J, Käser M, Stupazzini M, Kristekova M. (2010) Quantitative comparison of four numerical predictions of 3D ground motion in the Grenoble valley, France. *Bulletin of the Seismological Society of America*; 100(4):1427–1455.
- Chioccarelli E., De Luca F. and I. Iervolino (2012). Preliminary study of Emilia (May 29) earthquake ground motion records V1.0. Available at <http://www.reluis.it>

	<p>Research and Development Programme on Seismic Ground Motion</p> <p>CONFIDENTIAL</p> <p><i>Restricted to SIGMA scientific partners and members of the consortium, please do not pass around</i></p>	<p>Ref : SIGMA-2013-D2-93 Version : 02</p> <hr/> <p>Date : 7 January 2014 Page : 70</p>
--	---	---

- Cocco, M., Ardizzoni, F., Azzara, R.M., Dall'Illo, L., Delladio, A., Di Bona, M., Malagnini, L., Margheriti, L., Nardi, A. (2001). Broadband waveforms and site effects at a borehole seismometer in the Po alluvial basin (Italy). *Annali di Geofisica*, 44, 1, 137-154.
- CS.LL.PP., 2008. DM 14 Gennaio 2008. Norme tecniche per le costruzioni, Gazzetta Ufficiale della Repubblica Italiana, 29. (in Italian)
- Day SM, Graves R, Bielak J, Dreger D, Larsen S, Olsen KB, Pitarka A, Ramirez-Guzman L. (2008) Model for basin effects on long-period response spectra in Southern California. *Earthquake Spectra*; 24(1):257–277.
- Day, S. M. and C. R. Bradley (2001) Memory-efficient simulation of anelastic wave propagation. *Bulletin of the Seismological Society of America*, Vol. 91, no. 3, pp. 520-531.
- Faccioli, E., Maggio F., Paolucci R. and Quarteroni A. (1997). 2D and 3D elastic wave propagation by a pseudo-spectral domain decomposition method. *J. Seismol.*, 1(3):237-251.
- Fantoni R. and Franciosi R. (2010), Tectono-sedimentary setting of the Po Plain and Adriatic foreland, Volume 21, Supplement 1, 197-209, DOI: 10.1007/s12210-010-0102-4
- Fioravante, V., and Giretti D. (2012). Amplificazione sismica locale e prove dinamiche in centrifuga. Parma, 11 aprile 2012.
- Galli P., Castenetto S., Peronace E. (2012) Rilievo Macrosismico MCS speditivo, Terremoti dell'Emilia-Maggio 2012., Dipartimento della Protezione Civile, Rapporto finale, 15 Giugno 2012.
- Galovič, F., and J. Brokešová (2007). Hybrid k-squared source model for strong ground motion simulations: introduction, *Phys. Earth Planet. Int.* 160, 34–50, doi 10.1016/j.pepi.2006.09.002.
- Graves, R., T. Jordan, S. Callaghan, E. Deelman, E. Field, G. Juve, C. Kesselman, P. Maechling, G. Mehta, K. Milner, D. Okaya, P. Small and K. Vahi (2010). 'CyberShake: A physics-based seismic hazard model for Southern California.' *Pure Appl. Geophys.*
- Guidotti, R., Stupazzini M., Smerzini C., Paolucci R. and Ramieri P. (2011). Numerical Study on the Role of Basin Geometry and Kinematic Seismic Source in 3D Ground Motion Simulation of the 22 February 2011 Mw 6.2 Christchurch Earthquake. *Seismological Research Letters*, Vol. 82, Num. 6, pp. 767-782. DOI: 10.1785/gssrl.82.6.767.
- Hesthaven J.S. and Warburton T. (2008). Nodal discontinuous Galerkin methods, volume 54 of *Texts in Applied Mathematics*. Springer, Berlin.
- Hisada, Y. (1994). An efficient method for computing Green's function for a layered half-space with sources and receivers at close depths, *Bull. Seismol. Soc. Am.* 84, 1456–1472.
- Jones, L.M., R. Bernknopf, D. Cox, J. Goltz, K. Hudnut, D. Mileti, S. Perry, D. Ponti, K. Porter, M. Reichle, H. Seligson, K. Shoaf, J. Treiman and A. Wein (2008) 'The ShakeOut scenario.' Tech. Rep. USGS-R1150, U.S. Geological Survey and California Geological Survey.
- Kramer S. L. (1996) *Geotechnical Earthquake Engineering*, Prentice-Hall, Upper Saddle River, New Jersey.
- Lai C. G., Bozzoni F., Mangriotis M-D., Martinelli M. (2012) Geotechnical aspects of May 20, 2012 M5.9 Emilia earthquake, Italy, Technical Report, Eucentre, Pavia, Italy.

	<p>Research and Development Programme on Seismic Ground Motion</p> <p>CONFIDENTIAL</p> <p><i>Restricted to SIGMA scientific partners and members of the consortium, please do not pass around</i></p>	<p>Ref : SIGMA-2013-D2-93 Version : 02</p> <hr/> <p>Date : 7 January 2014 Page : 71</p>
--	---	---

- Lauciani V., Faenza L., Michelini A. (2012), ShakeMaps during the Emilia sequence, *Annals of Geophysics*, Vol. 55, No. 4.
- Luzi L., Pacor F., Ameri G., Puglia R., Burrato P., Massa M., Augliera P., Franceschina G., Lovati S, and Castro R. (2013) Overview on the Strong-Motion Data Recorded during the May–June 2012 Emilia Seismic Sequence, *Seismological Research Letters*, 84:4, doi: 10.1785/0220120154
- Margheriti L., Azzara R.M., Cocco M., Delladio A., Nardi A. (2000) Analysis of borehole broadband recordings: test site in the Po Basin, northern Italy, *Bulletin of the Seismological Society of America*, vol. 90, issue 6, pp. 1454-1463
- Martelli L. and Molinari F. C. (2008) Studio geologico finalizzato alla ricerca di potenziali serbatoi geotermici nel sottosuolo del comune di mirandola. Technical Report, Regione Emilia-Romagna, Servizio geologico sismico e dei suoli (in italian).
- Mazzieri I., Stupazzini M., Guidotti R., and Smerzini C. (2013). SPEED-Spectral Elements in Elastodynamics with Discontinuous Galerkin: a non-conforming approach for 3D multi-scale problems. *International Journal for Numerical Methods in Engineering*, 95 (12), DOI:10.1002/nme.4532
- Milana G., Bordoni P., Cara F., Di Giulio G., Hailemikaël S., Rovelli A. (2013) 1D velocity structure of the Po River plain (Northern Italy) assessed by combining strong motion and ambient noise data, *Bulletin of Earthquake Engineering*, 10.1007/s10518-013-9483-y.
- Mirandola earthquake working group (2012a) The Emilia thrust earthquake of 20 May 2012 (Northern Italy): strong motion and geological observations, Report 1 -, DPC, GEOSIS-LAB Uni Chieti, Uni Trieste, Regione Umbria,
- Mirandola earthquake working group (2012b) The Ferrara arc thrust earthquakes of May-June 2012 (Northern Italy): strong motion and geological observations - Report 2 -, DPC, GEOSIS-LAB UNICHJETI, Uni Trieste, Regione Umbria.
- Motazedian, D., and G. M. Atkinson (2005). Stochastic finite-fault modeling based on a dynamic corner frequency, *Bull. Seismol. Soc. Am.* 95, 995–1010.
- Paolucci R, Pacor F, Puglia R, Ameri G, Cauzzi C, Massa M, 2011. Record Processing in ITACA, the New Italian Strong-Motion Database. In Akkar S, Gülkan P, van Eck T (Eds.) *Earthquake Data in Engineering Seismology. Geotechnical, Geological, and Earthquake Engineering* 14 (2), 99-113.
- Pieri M, Groppi G (1981) Subsurface geological structure of the Po Plain, Italy: CNR, Progetto Finalizzato Geodinamica, 414, 13 p.
- Pilz, M., Parolai, S., Stupazzini, M., Paolucci, R. and Zschau, J. (2011), Modelling basin effects on earthquake ground motion in the Santiago de Chile basin by a spectral element code. *Geophysical Journal International*, 187: 929–945. doi: 10.1111/j.1365-246X.2011.05183.x
- Pousse G., Bonilla L.F., Cotton F., Margerin L. (2006), Nonstationary stochastic simulation of strong ground motion time histories including natural variability: application to the K-Net Japanese database, *Bull. Seism. Soc. Am., Viol.* 96, No. 6, 21093-2117.
- Regione Emilia Romagna & ENI-AGIP (1998) Riserve idriche sotterranee della Regione Emilia-Romagna. By G. Di Dio. S.EL.CA., Florence, pp 120

	<p>Research and Development Programme on Seismic Ground Motion</p> <p>CONFIDENTIAL</p> <p><i>Restricted to SIGMA scientific partners and members of the consortium, please do not pass around</i></p>	<p>Ref : SIGMA-2013-D2-93 Version : 02</p> <hr/> <p>Date : 7 January 2014 Page : 72</p>
--	---	---

- Rivière B. (2008). Discontinuous {G}alerkin methods for solving elliptic and parabolic equations - Theory and implementation}, volume 35 of Frontiers in Applied Mathematics. Society for Industrial and Applied Mathematics (SIAM), Philadelphia, PA.
- Sabetta, F. Pugliese, A. (1996) Estimation of Response Spectra and Simulation of Nonstationary Earthquake Ground Motions, Bull. Seism. Soc. Am., Vol. 86, No. 2, 337-352.
- Scrocca, D., E. Carminati, C. Doglioni, and D. Marcantoni (2007), Slab retreat and active shortening along the central-northern Apennines, in: Thrust belts and foreland basins: from fold kinematics to hydrocarbon systems (O. Lacombe, J. Lave', F. Roure and J. Verges, eds). Frontiers in Earth Sciences, Springer, 471-487, doi: 10.1007/978-3-540-69426-7_25.
- Selvaggi, G., F. Ferulano, M. Di Bona, A. Frepoli, R. Azzara, A. Basili, C. Chiarabba, M. G. Ciaccio, F. Di Luccio, F. P. Lucente, L. Margheriti, C. Nostro, 2001. The Mw 5.4 Reggio Emilia 1996 earthquake: active compressional tectonics in the Po Plain, Italy, Geophysical Journal International 144, 1-13.
- Smerzini C., Villani M. (2012) Broadband numerical simulations in complex near field geological configurations: the case of the MW 6.3 2009 L'Aquila earthquake, Bulletin of Seismological Society of America, 102 (6),doi: 10.1785/0120120002.
- Smerzini C., Paolucci R. and Stupazzini M. (2011) Comparison of 3D, 2D and 1D approaches to predict long period earthquake ground motion in the Gubbio plain, Central Italy, Bulletin of Earthquake Engineering, 9 (6), 2007-2029,DOI 10.1007/s10518-011-9289-8.
- Stacey, R. (1988) 'Improved transparent boundary formulations for the elastic-wave equation.' Bulletin of the Seismological Society of America, Vol. 78, No. 6 pp. 2089-2097.
- Stupazzini M., Paolucci R. and H. Igel (2009). Near-fault earthquake ground motion simulation in the Grenoble Valley by a high-performance spectral element code. Bulletin of the Seismological Society of America, 99: 286-301.
- Toscani, G., Burrato, P., Di Bucci, D., Seno, S., Valensise, G. (2009). Plio-Quaternary tectonic evolution of the Northern Apennines thrust fronts (Bologna-Ferrara section, Italy): Seismotectonic implications. Bollettino della Società Geologica Italiana 128 (2), pp. 605-613.
- Vuan A., Klin P., Laurenzano G., Priolo E. (2011) Far-Source Long-Period Displacement Response Spectra in the Po and Venetian Plains (Italy) from 3D Wavefield Simulations, Bulletin of the Seismological Society of America, 101(3): 1055-1072
- Wells D.L. and Coppersmith K.J (1994) New empirical relationships among magnitude, rupture length, rupture width, rupture area, and surface displacement Bulletin of the Seismological Society of America, 84: 974-1002.

Comments and Questions
Regarding the Report titled:
“Ground Shaking Scenarios in the Po Plain with Special Emphasis on the Area Affected
by the earthquake Sequence of May 2012”

Aybars Gürpınar

1. The general objective of the report is very worthwhile and relevant to SIGMA. This mainly because most PSHA studies for NPPs have demonstrated that the hazard is principally dominated by nearby earthquakes. For these events the ergodic assumption for the GMPEs has weaker grounds. For sites where seismicity data is lacking some fault simulation approach (possibly a hybrid approach) seems to be a rational alternative.
2. The authors have a sound basis in that they have the opportunity to utilize very good seismic data from recent events as well as reasonably good geophysical data from which fault parameters can be estimated. Therefore it is possible that the simulation can be checked with the seismic data and parameters can be thus adjusted and fine tuned.
3. As with some of the fault simulation approaches the major issue with the present simulation is the frequency limitation (1.5 Hz upper bound in this case). Although the limitation is recognized in the Report, the implications of this limitation and ways to alleviate this are not explored and discussed to a sufficient extent.
4. The goodness of fit tests do not yield results that are convincing even for the limited frequency band (up to 1.5 Hz). Several parameters are investigated separately in order to understand the sensitivity. These are the nucleation point, fault location, rake angle and rupture velocity. Figure 4.15 shows GoF scores for two hypocenters. This figure does not indicate a better fit for either of the hypocenter location. Depending on the station one or the other hypocenter looks better than the other.
5. The authors have made an effort to complement the low frequency simulation in a section titled “Generation of Broadband Accelerograms”. For the high frequency part they adopt the non-stationary synthetic accelerograms computed through the method of Sabetta and Pugliese (1996). The compatibility of the two methods used for the low and high frequency is not sufficiently discussed. It is admitted that “...this method does not allow to account neither for the same extended kinematic fault rupture model as adopted in the LF computation nor for specific 1D site amplification functions”. The results are presented in Figure 4.23 without much commentary. This whole section is rather short and not well developed.
6. Instead of developing the method and demonstrating the validity of the results (both in LF and BB), the authors prefer to treat other topics such as 3D simulations, ground shaking map and site amplification.
7. My main recommendation would be to concentrate on the applicability of the method to higher frequencies rather than losing this focus and looking at various applications of the method. The frequency limitation (of 1.5Hz) is indicated as being a computational issue rather than inherent to the simulation. However, this

point is not explored or explained. More effort is needed to alleviate this limitation in future studies.

Review of ‘Ground shaking scenarios in the Po Plain with special emphasis on the area affected by the earthquake sequence of May 2012’ by R. Paolucci and C. Smerzini (SIGMA deliverable D2-93)

The authors present ground-motion simulations computed using a spectral element code, which they have recently developed, for the two mainshocks of the Emilia-Romagna (Italy) sequence of May 2012. The deliverable is a continuation of a previous SIGMA report (D3-54) and its results are used as input to another deliverable (D3-96), neither of which I have seen. The modelling is sophisticated and uses a detailed geological model that incorporates recent measurements and finite-fault inversions of these two earthquakes. The report is also well-written and clearly presented. Generally, I think that the authors have done a very good job of their analysis and they present some interesting results. Nevertheless I have some minor comments, both on technical and editorial aspects, which are listed below in the order that they occur in the text. I recommend that the editorial aspects are addressed when producing the final version of this report and the technical remarks are considered when undertaking the next step of this task.

Technical remarks and questions:

1. P. 3 (and elsewhere): The numerical models were created to allow wave propagation up to 1.5Hz (0.67s). This is quite a low frequency, particularly for nuclear applications where often frequencies above 5Hz are of interest. I realise that it is expensive and technically challenging to extend models to higher frequencies but is it planned to extend the models to account for shorter wavelengths?
2. Table 3.1, Figure 3.3: The fault lengths and widths listed in this table appear to be large for this size of earthquake (e.g. the equations of Wells & Coppersmith would predict a size of roughly 15×10 km for M_w 6 events). However, I see from Figure 3.3 that these sizes refer to the whole fault plane used for the slip inversions and that the inversions suggest that slip did not occur over all of these modelled faults. This difference should probably be noted.
3. Figure 3.4 (and elsewhere): The Parma 2008 earthquake was quite deep (~30km, I believe) and so epicentral distance is probably not the best distance measure (hypocentral distance would be better). Also as the fault geometries are known at least for the two 2012 earthquakes and there is some near-source data it would be better to use rupture distance or distance to the surface projection of the rupture rather than point-source metrics.
4. Table 3.2: Why are the soil classes for the vast majority of the stations not known? This seems to be a significant handicap when comparing observed and predicted motions.
5. Table 4.1: Are the authors sure that all the strong-motion stations are class C sites (which I guess corresponds to a V_s of roughly 300m/s)? If not, then this near-surface model may not be appropriate for some stations and could be contributing to the misfit.
6. P. 25, ‘ground response close to the fault, such as at MRN station, is predominantly affected by the features of the kinematic source models’ (and elsewhere): Has there been only one kinematic source model published to date? What are the uncertainties of this model?
7. P. 30: Why was the effect of the fault dip not considered? Because of the position of MRN over the edge of the fault, the dip could have a large impact on the directivity effects. The dip is probably as uncertain as the rake and its impact on the ground motions could be larger.
8. Figure 4.9: As noted by the authors, the polarity of the EW component strongly suggests a hypocentre to the west (perhaps even as far as number 7). Are they sure that the polarity of the observed EW component (and the other components) is correct? Problems with polarities of strong-motion instruments are not unknown so it could be worth checking with the network operator.

9. Figures 4.11 and 4.12: What could be the cause of the large underprediction over a wide frequency range on the Fourier amplitude spectrum of the NS component? None of the variants considered comes close to matching this spectrum. Could varying the rise time (or dip) lead to a better match?
10. Figure 4.16 and Figure 4.20: It would be useful to add a comparison with a shakemap derived using the observed records via kriging or another spatial interpolation technique (e.g. Douglas, Bulletin of Earthquake Engineering, 5, 363–376, 2007). In general, what are the advantages of using simulations to generate shakemaps over interpolation of the recorded motions given that the strong-motion network was dense for the 29 May earthquake?
11. P. 38: Is modelling of non-linear soil response justified in this example? From Table 3.2 it appears that even the (linear) site class of the majority of stations is not known so modelling their nonlinear response seems to be a step too far. Also given the low frequencies modelled, for which nonlinear effects are generally thought to be minimal, it is not surprising that the impact of nonlinearity is small.
12. P. 41: The authors write that ‘the simulated shaking map [is] clearly different from the isotropic pattern that could be obtained using Ground Motion Prediction Equations (GMPEs)’. The most sophisticated models (e.g. NGA West 1 and 2) include terms (sediment depth, directivity and nonlinear soil response) that, if applied correctly, would lead to a non-isotropic pattern. It could be interesting to compare the shakemap derived using complex GMPEs and the simulations.
13. P. 44, ‘mainly due to computational limitations’: The frequency limit is also due to insufficient resolution in knowledge of the geological and source models.
14. P. 44, ‘masonry low rising [sic, should be ‘rise’] (2-3 storeys) buildings’: Do we really need ground-motion simulations to assess the response of masonry structures? I would suggest that natural accelerograms and/or response spectra are sufficient. Simulations are potentially useful for high-value infrastructure and for sites with specific and well-known geological or source characteristics. Nevertheless, I agree that we need to be able to simulate broadband records.
15. P. 45: The technique of Sabetta and Pugliese (1996) has been updated by Pousse et al. (Bulletin of the Seismological Society of America, 2006) and more recently by Aurore Laurendeau (ISTerre). I would recommend using the updated technique or one of the other recent stochastic methods (e.g. that by Jack Baker).
16. P. 45, ‘to make the Fourier spectrum of the BB signal more realistic’: In what way more realistic?
17. P. 45: Matching of the stochastic and SPEED signals between 0.5 to 0.7Hz means that most of the period range of engineering interest (generally <2s) is from the stochastic method. Because of the importance of simulating broadband records I suggest that this part of the procedure is developed further so that the frequency for the change over from stochastic to SPEED is increased. This may improve the match to the observations. Perhaps there is a better way of combining the two signals than basing it on the Arias intensities.
18. Table 5.1: How were the parameters for these scenarios chosen? Specifically, the rise time, rake and rupture velocity?
19. Conclusions: How can the results be used to improve seismic hazard assessments for the Po Plain, which I assume will be probabilistic?

Minor editorial remarks:

1. P. 3: ‘the 2 and 20 May 2012 earthquakes’ should be ‘the 20 and 29 May 2012 earthquakes’.
2. P. 5: ‘jointly developed at the Department’ should be ‘jointly developed at the Departments’.


3. Figures 2.2 and 2.3: The captions of these figures should be on the same page as the diagrams.
4. Table 2.2: Add the units of Δt (s, I assume).
5. P. 9, 'against the ideal behaviour': What does 'ideal' mean here? How is it calculated? I suppose that it is to do with the ideal parallelisation of the code. A brief explanation would be useful for the non-specialist.
6. P. 13: 'to 13 June 2012 with magnitude larger' 'magnitude' should probably be plural.
7. P. 13: I suggest deleting 'post-' from 'post-processing'.
8. Figure 3.3: It would be useful to add a legend explaining the different colours (fault slip).
9. P. 16: 'Note that much more' should be 'Note that many more'.
10. Figures 3.5 and 3.6: The underlying map interferes a bit with the plotted time-histories; I suggest that a white background is used. It would be useful to indicate (using a different colour, for example) which stations were operating during each of the two earthquakes. The vertical scale of the second plot is a little too large so the high amplitudes are not easier to distinguish.
11. Table 3.3: The units of R_h are km (not cm/s/s). It could be better to use the *de facto* standards of R_{hyp} and R_{epi} for hypocentral and epicentral distance. It would be better to write cm/s² not cm/s/s. I suggest only giving the distances to the nearest integer given the uncertainties on the hypocentral location. The number of decimal places for the strong-motion parameters should always be two (some values are only given to a single place).
12. P. 21: Where did the values for τ (rise time) and V_R (rupture speed) come from? The kinematic inversion of Atzori et al. (2012)?
13. P. 21, 'the subsoil model is in reasonable agreement with the results recently published by Milana et al. (2013)': It would be useful to add a plot confirming this.
14. P. 24, 'waveforms at 12 representative strong motion stations': How were these stations chosen? Geographical distribution?
15. P. 30: 'the slip patter' should be 'the slip pattern'.
16. P. 30: Should the rise time given here ($\tau=0.6s$) be 0.7s in agreement with the previously quoted value (p. 21)?
17. P. 30: 'hypocenters 1, 4, 7' should have an 'and' between '4' and '7'.
18. P. 30: 'Hypos' should be 'Hypocenters'.
19. P. 32, rake angle: What rake angle is reported by INGV (or Global CMT, for example) for this earthquake? Did Atzori et al. (2012) invert for this parameter?
20. P. 33: 'scarce' should be 'minimal'.
21. Figure 4.12: The caption of this figure should be on the same page as the graphs.
22. P. 35: 'the sequel' should be 'the following'.
23. P. 44, '0.1 to 25Hz': I would suggest that engineering applications require simulations up to 100Hz (PGA) rather than just 25Hz.
24. P. 45: 'limited amount' should 'limited number'.
25. P. 45: 'does not allow to account neither' should be 'does not allow accounting'.
26. P. 45, equation 4: HF should be a subscript not a superscript.
27. Figure 4.23: This figure is a little difficult to read. I suggest removing the NS and EW observed spectra (keeping only the geometric mean).
28. P. 47, ' $\tau=0.8s$ ': Do you mean ' $\tau=0.7s$ ' like for the 29 May simulations?
29. P. 48: 'is much limited' should be 'is much more limited'.
30. P. 48: Delete ', filtered between 0.1 and 1.5Hz'.
31. Figure 4.26: I recommend indicating those stations that recorded this earthquake.
32. P. 51: Space missing between 'D3-96' and "'Approches to...'".
33. P. 51: 'and will not' should be 'and they will not'.

34. P. 51: 'by different magnitude' should be 'by different magnitudes'.
35. P. 51 (and elsewhere): A different date format (e.g. 20.05.2012) is used here than elsewhere (e.g. 20 May 2012). I recommend being consistent.
36. P. 52: I recommend deleting the 'made' in the phrase ' $V_s=800\text{m/s}$ made outcropping'.
37. P. 57: 'same position of the soil site itself' should be 'same position as the soil site'.
38. P. 58: 'MIR1 and MIR8, located on a NS alignment approximately' should be 'MIR1 and MIR8, roughly located on an NS alignment'.
39. P. 58: 'as getting further' should be 'as we move further'.
40. P. 58: 'sediment increases of about 400m' should be either 'sediment increases by about 400m' or 'sediment increases to about 400m'.
41. P. 58: Delete 'by' in the phrase 'rupture scenarios breaking by the two faults'.
42. P. 58: Make 'distance' plural in 'located at large distance from'.

John Douglas

BRGM, Orléans.

18th October 2013


	<p>Research and Development Programme on Seismic Ground Motion</p> <p>CONFIDENTIAL</p> <p><i>Restricted to SIGMA scientific partners and members of the consortium, please do not pass around</i></p>	<p>Ref : SIGMA-2013-D2-93 Version : 01</p> <p>Date : Page :</p>
--	---	---



GROUND SHAKING SCENARIOS IN THE PO PLAIN WITH SPECIAL EMPHASIS ON THE AREA AFFECTED BY THE EARTHQUAKE SEQUENCE OF MAY 2012

(Deliverable D2-93)

Response to Reviewer's Remarks

	<p>Research and Development Programme on Seismic Ground Motion</p> <p>CONFIDENTIAL</p> <p><i>Restricted to SIGMA scientific partners and members of the consortium, please do not pass around</i></p>	<p>Ref : SIGMA-2013-D2-93 Version : 01</p> <p>Date : Page :</p>
--	---	---

1. J. Douglas

Technical remarks and questions

1. The reviewer is right. The frequency limit of the numerical simulations may be critical for some engineering applications such as the ones related to nuclear power plants, where frequencies above 5 Hz may be of interest. For this reason, referring to the 29 May 2012 earthquake, we have shown in Section 4.1.7 an application of a hybrid method (SPEED+SP96) to generate broadband (BB) accelerograms, usable in a large frequency range, say 0-25 Hz. To strengthen this point, a comment has been added in the introduction. This method has been successfully applied also for the computation of broadband shaking maps in the framework of a research collaboration contract between Politecnico di Milano and Munich RE (see Paolucci et al., 2013¹). To further develop the discussion in Section 1.4.7, BB ground shaking maps, in terms of PGV and PGA, are presented in the revised version of the Deliverable.
2. As noted appropriately by the reviewer, the sizes of the two fault solutions by Atzori (2012), which are well above the range predicted by the scaling laws of WC1994 (Wells & Coppersmith 1994), refer to the whole fault plane rather than to the fault area that did slip indeed. A specific remark has been introduced in the text (pg. 13, , second paragraph).
3. Figure 3.4 has been changed: it displays now the M_W - R_{hy} (hypocentral distance) distribution of Po Plain strong motion data. Table 3.3 already includes the hypocentral distance besides the epicentral one.
4. As far as the authors know, no specific measures of V_{S30} are available for most of the stations listed in Table 3.2. Assignment of soil class is done for those stations

¹ Paolucci R., Stupazzini M., Smolka A., Antonietti P.F., Guidotti R., Mazzieri I., Smerzini C., and Beretta M. (2013) Deterministic seismic scenarios from 3D numerical simulations, *Vienna Congress on Recent Advances in Earthquake Engineering and Structural Dynamics 2013 (VEESD 2013)*, C. Adam, R. Heuer, W. Lenhardt & C. Schranz (eds), 28-30 August 2013, Vienna, Austria, Paper No. 255

(e.g. Mirandola, Casaglia) where in-situ geophysical and geotechnical investigations are available.

- For simplicity, a simplified homogeneous model has been assumed for the Po Plain sediments, as shown in Table 4.1, regardless of the specific differences from one station to another. This has been calibrated by considering the quantitative information available mainly for the Mirandola (MRN) e Casaglia (T821) stations (see figure below). This figure shows that roughly the average shear wave velocity in the top 100-120 m is about 300 m/s. The discussion regarding the calibration of the subsoil model has been improved (pg. .

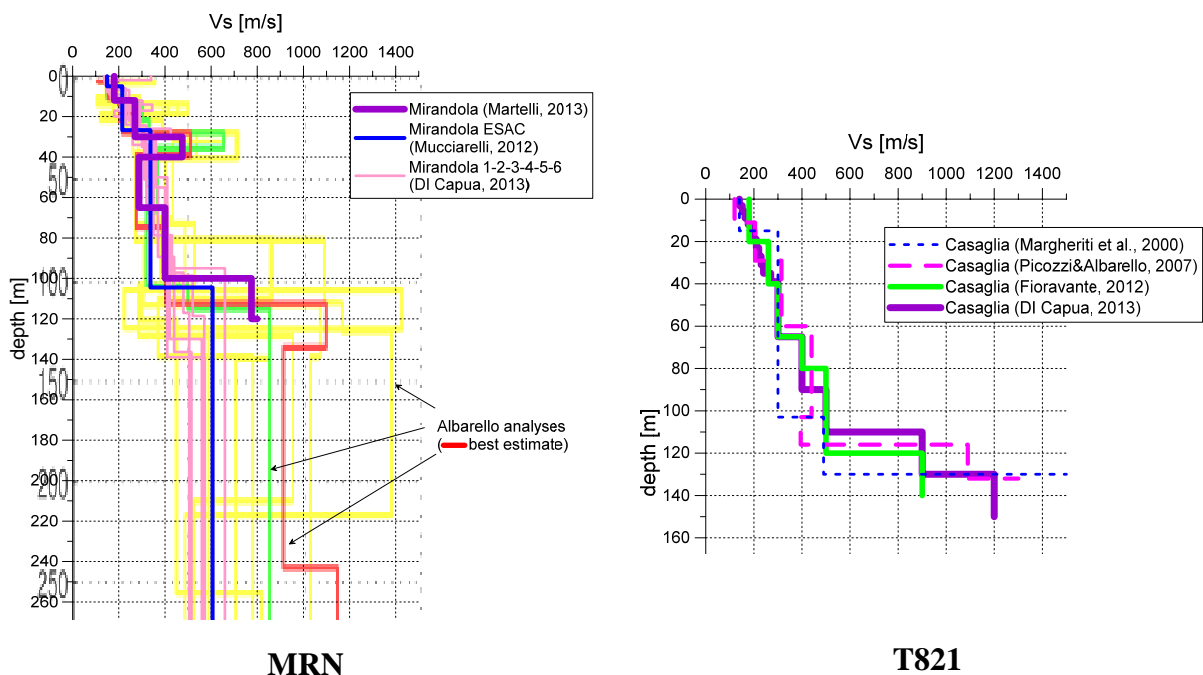



Figure 1 V_s profile at MRN (left) and T821 (right) stations as obtained from the studies available in the literature.

- We remark that the uncertainties of the finite fault solutions by Atzori et al. (2012) are rather large since they are only based on SAR data and not on strong motion data. In particular, as far as the authors know, results based on geodetic data may lead to smooth slip distributions and large fault sizes. As stressed in the Deliverable (see pg. 13, second paragraph), the uncertainties related to the seismic source for

	<p>Research and Development Programme on Seismic Ground Motion</p> <p>CONFIDENTIAL</p> <p><i>Restricted to SIGMA scientific partners and members of the consortium, please do not pass around</i></p>	<p>Ref : SIGMA-2013-D2-93 Version : 01</p> <p>Date : Page :</p>
--	---	---

the 20.05.2012 earthquake are even larger, due to the lack of data in the epicentral region. However, when we built the numerical model (soon after the earthquake itself), other fault solutions were not available. It was only recently that we got acquainted with some new studies, see e.g. Cesca et al. (2013)², Piccinini et al. (2012)³. Nevertheless, these studies provide further constraints only on finite fault parameters, such as plane orientation, rupture size and directivity, whereas details on the slip pattern cannot be found. Furthermore, the two aforementioned papers are not in agreement as regards some points, such as the rupture directivity for the 20 May earthquake. In fact, according to Cesca et al. (2013), rupture originated on a NW patch and propagated towards SE - similarly to our model -, whereas for Piccinini et al. (2012) rupture directivity exhibited towards WSW. To improve our study, the main outcomes of these studies could be incorporated in a new numerical model but this is out of the scope of this deliverable.

7. The fault dip was not considered in the preliminary analyses performed through the Hisada's code because we decided to keep constant the geometry of the seismic source model. . This is related to the fact that the SE model is constructed honouring the geometry of the fault. Therefore, any change regarding the geometric features of the fault, such as strike, dip and position in space, would have implied the construction of a new numerical model. It is relevant to underline that Cesca et al. (2013) found values of dip angles for both earthquakes of about 25-27°, in apparent disagreement with our model (40°). It would be interesting to include these findings in our simulations but, as stated above, this would be very time consuming as it requires the reconstruction of two new meshes. New comments regarding the dip angle have been introduced at pg. 30 (last paragraph before subsection entitled "nucleation point").
8. The issue related to the polarity of the strong motion instrument installed in the Po Plain was deeply discussed with the INGV and DPC staff at the very beginning of this work. As a matter of fact, this led us to consider the correct polarity of strong

² Cesca S., Braun T., Maccaferri F., Passarelli L., Rivalta Eleonora, Dahm T.(2013) Source modelling of the M5-6 Emilia-Romagna, Italy, earthquakes (2012 May 20-29), *Geophys. J. Int.*, 193, 1658-1672.

³ Piccinini D., Pino N.A., Saccorotti G. (2012), Source complexity of the May 20, 2012, Mw 5.9, Ferrara (Italy) event, *Annals of Geophysics*, 55 (4), doi: 10.4401/ag-6111.

ground motion data for some of the selected stations (opposite polarity for both MRN and NVL stations in terms of three components).

- The parametric analyses shown in Figures 4.11 and 4.12 refer to the case “hypo INGV”. As shown in Figure 4.9, the relative position of the hypocenter with respect to the slip asperity plays a major role, yielding a strong underestimation of ground motion amplitude over a wide range of frequency especially for the NS component. Even if not reported in this Deliverable, variations of rise time were investigated as well (see Figure 2). However, it turned out that they play a significant role in the relatively high frequency range ($f > \sim 1/\tau$, where τ is the rise time, see Herrero and Bernard, 1994⁴) and, therefore, they cannot explain the consistent underestimation observed in the whole frequency range ($\sim 0-2$ Hz).

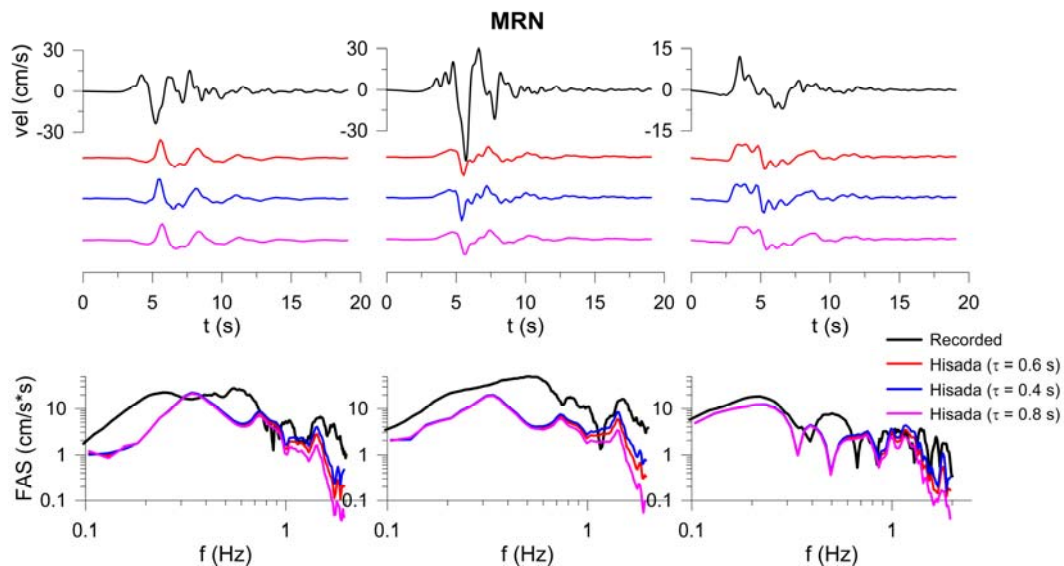



Figure 2 Effect of rise time at MRN station: comparison between observed (black) and simulated waveforms for three different values of rise time, i.e., $\tau=0.4$ s, 0.6 s, and 0.8 s.


- This is an interesting point. We have included a new paragraph in Section 4.1.6, at pg. 41 and 45, presenting the comparison between the ground shaking map computed through 3D physics-based numerical simulations and the ShakeMaps produced by the INGV (<http://shakemap.rm.ingv.it/shake/index.html>). The latter are

⁴ Herrero, A., and P. Bernard (1994). A kinematic self-similar rupture process for earthquakes, Bull. Seismol. Soc. Am. 84, 1216–1228.

	<p>Research and Development Programme on Seismic Ground Motion</p> <p>CONFIDENTIAL</p> <p><i>Restricted to SIGMA scientific partners and members of the consortium, please do not pass around</i></p>	<p>Ref : SIGMA-2013-D2-93 Version : 01</p> <p>Date : Page :</p>
--	---	---

produced by merging the observed strong motion data with the information derived by the GMPEs and local site amplification functions. The comparison is shown in terms of *PGV* and *PSA* at 3 s (Figure 4.22). This example highlights that, provided a sufficiently detailed knowledge on the geologic model and the seismic source, the major advantage of using physics-based numerical simulations is related to their ability to estimate the spatial variability of ground motion over an extended territory with a resolution that cannot be given by observed data even when strong motion networks are relatively dense, as in the case of the 29.05 earthquake (that is, however, an exceptional case in terms of coverage of strong motion stations). Furthermore, strong motion data in near-field conditions are still very scarce even worldwide and, hence, these numerical simulations offer an interesting tool to study ground motion spatial variability as well as to investigate its dependence on the features of the kinematic source model (slip distribution, location of nucleation point, fault location, etc).

11. In spite of the lack of information regarding the soil profile for the majority of stations listed in Table 3.2 and of the frequency limit of numerical simulations, we decided to perform these analyses to account for small to moderate non-linear effects that may arise for events characterized by these magnitude levels even at relatively low strain levels. Obviously the study of NL effects is limited to the long period range (> 0.67 s). We agree with the reviewer on the fact the effect of the non-linear elastic soil model is not surprisingly small. The comment in the text on pg. 38 (end of Section 4.1.5) has been rephrased accordingly.
12. The sentence at pg. 41 (second paragraph) has been changed. We refer to point 10 and the related text in the Deliverable for a discussion on the comparison between numerically- and observationally-based/empirical ground shaking maps.
13. We do agree with the reviewer, the sentence on pg 46 has been modified.
14. We do agree with the reviewer, physics-based numerical simulations are particularly useful for areas where suitable seismo-tectonic, geologic and source information are available. This has become more and more feasible in recent years- However, in urban contexts where historical the construction stock is dominated by low-rise buildings, broadband synthesis becomes fundamental. Furthermore, it is recognized that the seismic response of masonry structures is strongly affected by the features of seismic input. Therefore, the use of parametric numerical simulations with varying source parameters gives insights into the issue related to

	<p>Research and Development Programme on Seismic Ground Motion</p> <p>CONFIDENTIAL</p> <p><i>Restricted to SIGMA scientific partners and members of the consortium, please do not pass around</i></p>	<p>Ref : SIGMA-2013-D2-93 Version : 01</p> <p>Date : Page :</p>
--	---	---

the variability of the seismic response of masonry structures as a function of seismic input. It is clear that large scale 3D numerical simulations are of major interest for the evaluation of the spatial variability of earthquake ground motion over extended urban areas.

15. We thank the reviewer for this useful reference. As commented in the deliverable (pg. 47, 2nd paragraph) future work will involve the improvement of the tool for the generation of broadband accelerograms by using the method of Pousse et al. (2006), instead of SP96, for the HF synthetics. This method introduces three main improvements related to the following issues: (a) the deficit of energy in the low frequency part of the Fourier Spectrum of synthetic accelerograms is overcome (this is less interesting for our purposes since we use only the high-frequency part); (b) the envelope time function is modified to take into account the arrival time, energy, phases for P-, S- and coda waves; (c) a better description of ground motion variability is achieved by means of a Monte Carlo exploration of difference strong motion indicators, source parameters and envelope functional forms. For our purposes, the most interesting feature of this new method regards the point (c), i.e., its capability to model the ground motion variability observed in real data, that is substantially lacking in the original method of Sabetta & Pugliese (1996). In the latter, in fact, variability of simulated ground motion is due only to the random phase, while in the method of Pousse et al. (2006) uncertainty of model parameters is taken into account.
16. The sentence has been rephrased by introducing specific comments in the text (see pg. 47-48). We remark herein that the cross-over frequency band was calibrated in such a way to avoid the presence of unphysical spectral holes in the BB Fourier Spectra and, hence, to make it more realistic.
17. We agree with the reviewer, the major limit of this application in terms of broadband synthesis is the limited range of periods where ground motion comes from physics-based 3D numerical simulation. However, this drawback does not depend on intrinsic limits of the method itself, rather it is related to the strong differences between the spectral ordinates coming from the two methods (see example in Figure 3). It should be underlined that in the preliminary phase of this

work also the EXSIM code (Motazedian and Atkinson, 2005⁵) was considered, in place of SP96, for the generation of the HF synthetics. Nevertheless, the comparison between the results obtained by SPEED+EXSIM (with cross-over frequency 0.5-1 Hz for MRN and 1-1.5 for NVL) and SPEED+SP96, as displayed in Figure 4, led us to prefer the latter because it allows to have spectral ordinates close to the observed ones over a wide range of periods, especially in near-field conditions (see MRN station). In conclusion, we believe that in this particular case the low cross-over frequency band is determined by the poor performances of the physics-based model in near-field conditions as discussed in the report. In that respect it is worth mentioning the work by Smerzini & Villani (2012)⁶, where the same method (SPEED+EXSIM) was applied successfully for the case of L'Aquila earthquake by using a cross-over frequency band equal to 2.5-3 Hz.

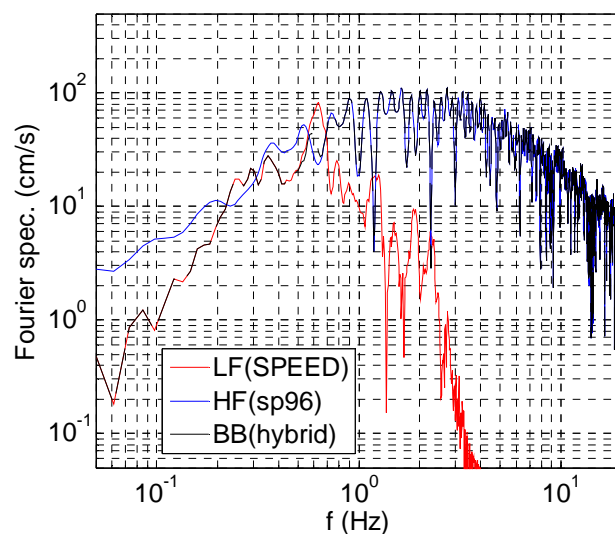


Figure 3 BB synthesis: example of application for MRN station.

⁵ Motazedian, D., and G. M. Atkinson (2005). Stochastic finite-fault modeling based on a dynamic corner frequency, *Bull. Seismol. Soc. Am.* 95, 995–1010.

⁶ Smerzini C., Villani M. (2012). Broadband numerical simulations in complex near field geological configurations: the case of the MW 6.3 2009 L'Aquila earthquake. *Bulletin of Seismological Society of America*, 102 (6), doi: 10.1785/0120120002

**BB RESULTS (speed hypo INGV)
EXSIM vs SP96**

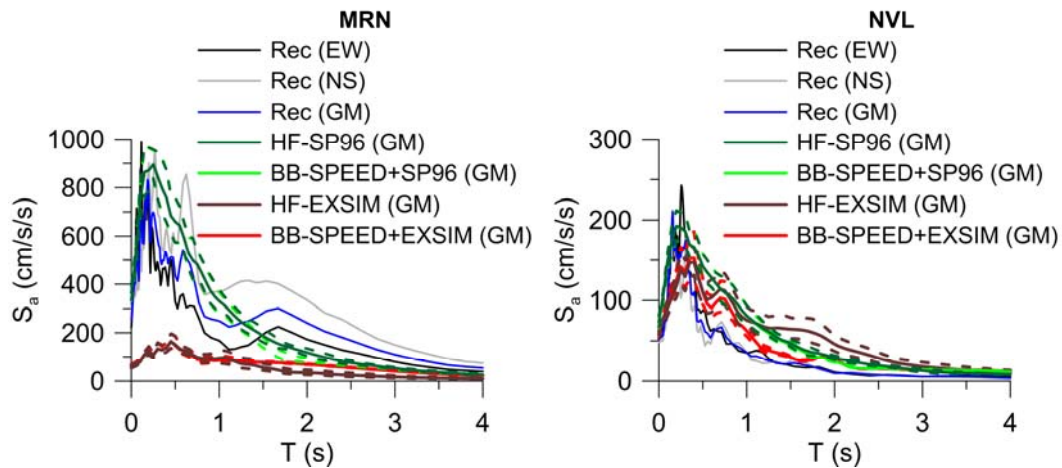



Figure 4 BB acceleration response spectra at MRN (left) and NVL (right): comparison between SPEED+SP96 (green) and SPEED+EXSIM (red)

18. The parameters were chosen by the authors, but with constraints based on scaling laws derived from observations and by studies on source dynamics. In particular, V_R was chosen in the range $0.60-0.92V_S$; the original rake angle of 90° , associated to both the Mirandola and Ferrara fault, is modified by adding some small strike-slip components (see also parametric analysis in Section 4.1.4); the rise time is chosen in the range between $0.6-0.8$ s depending on the magnitude level. As regards this point, it should be remarked that the rise time acts as a low-pass filter with cut-off frequency equal to $1/\tau$ (Herrero & Bernard, 1994), therefore the value $1/\tau$ is selected close to the maximum resolution frequency of the numerical model ($0.6-0.7$ s).
19. Considerations have been added in the Conclusion section to answer the request of the reviewer on the potential use of physics-based numerical simulations of earthquake ground motions to improve seismic hazard analyses in the Po Plain.

Minor editorial remarks

1-4: done

5: a brief explanation on the definition of parallel efficiency and speed-up is given in the text, see Eq. (1) at pg. 9.

	<p>Research and Development Programme on Seismic Ground Motion</p> <p>CONFIDENTIAL</p> <p><i>Restricted to SIGMA scientific partners and members of the consortium, please do not pass around</i></p>	<p>Ref : SIGMA-2013-D2-93 Version : 01</p> <p>Date : Page :</p>
--	---	---

6-9: done

10: it was not possible to improve the clarity of the figure without losing some of its information.

11: The standards of R_{hyp} and R_{epi} are used in the revised version of the deliverable. All other suggestions have been accepted.

12: the values of rise time and rupture velocity were chosen by the authors with constraints based on scaling laws available in the literature, in particular V_R was set equal to $\sim 0.75 \cdot V_S$, being $V_S = 3670$ m/s (see halfspace properties in Table 4.2), and $\tau = 0.7$ s, so that $1/\tau$ is close to the maximum resolution frequency of the numerical model (~ 0.67 s). See also response to point 18 of previous section.

13 A plot presenting an approximate comparison with the results published by Milana et al. (2013) is shown in Figure 4.4.

14. Yes, stations are chosen fairly uniformly based on their geographical distribution. A sentence has been introduced at the beginning of Section 4.1.2, pg. 25.

15: done

16: actually, the values of rise time of these parametric analyses are different than the ones adopted for the 3D simulations: $\tau = 0.4$ s is assumed for the parametric analyses in terms of nucleation point and location of seismic fault, while $\tau = 0.6$ s for the ones concerning rupture velocity and rake angle. Note that these differences are due to the fact the such analyses were performed in different phases of the work. However, these values are kept constant for these parametric studies and, furthermore, it has been verified that rise time variations have minor effect in this frequency range.


17-18: done

19: Atzori et al. (2012) did not invert for this parameter. Recent works (see Cesca et al., 2013) found a rake angle equal to 87° and 90° degrees for the 20 and 29 May earthquakes, respectively, in good agreement with the solutions adopted in our study.

20-27: done

28: No, in this case we assumed $\tau = 0.8$ s.

29-42: done

	<p style="text-align: center;">Research and Development Programme on Seismic Ground Motion</p> <p style="text-align: center;">CONFIDENTIAL</p> <p style="text-align: center;"><i>Restricted to SIGMA scientific partners and members of the consortium, please do not pass around</i></p>	<p>Ref : SIGMA-2013-D2-93 Version : 01</p> <p>Date : Page :</p>
--	---	---

1. A. Gürpınar

Points 2

Physics-based numerical simulations have gained increasing interest within innovative approaches for seismic hazard and risk assessment, such as in the CyberShake project (e.g., Graves et al., 2010⁷) and in the Great Southern California ShakeOut Exercise (www.shakeout.org; Jones et al., 2008⁸). They are particularly useful for those areas where appropriate seismo-tectonic, geologic and source information are available. The parametric analysis presented in Section 4.1.4 points out that the inclusion into the numerical model of appropriate kinematic model turns out to play a primary role to produce realistic ground motion predictions. Therefore, the availability of corroborated and well-constrained geologic and seismic source models would allow us to improve significantly our numerical simulations. We remark herein that the execution of parametric analyses by SPEED is not straightforward as it is a very time-consuming process. As a matter of fact, since the SE model is built by honouring the geometry of the seismic fault, any change regarding its geometric features, such as strike, dip and location, would imply the construction of a new numerical model.


Points 3-5-7

We do agree with the reviewer: the issue related to the generation of broadband ground motions, apt for use within a wide range of vibration periods of interest for engineering applications, is relevant and deserves particular attention. Therefore, we have tried to explore further this issue by extending the Section 4.1.7 of the Deliverable (from pg. 45-50).

The following topics are discussed in more detail in the revised version of the Deliverable.

⁷ Graves RW, Jordan T, Callaghan S, Deelman E, Field E, Juve G, Kesselman C, Maechling P, Mehta G, Milner K, Okaya D, Small P, Vahi K. (2010), CyberShake: a physics-based seismic hazard model for Southern California. *Pure and Applied Geophysics*, 168(3–4), 367–381

⁸ Jones L M, Bernknopf R, Cox D, Goltz J, Hudnut K, Mileti D, Perry S, Ponti D, Porter K, Reichle M, Seligson H, Shoaf K, Treiman J, Wein A (2008). The ShakeOut scenario. Technical Report USGS-R1150, U.S. Geological Survey and California Geological Survey.

	<p>Research and Development Programme on Seismic Ground Motion</p> <p>CONFIDENTIAL</p> <p><i>Restricted to SIGMA scientific partners and members of the consortium, please do not pass around</i></p>	<p>Ref : SIGMA-2013-D2-93 Version : 01</p> <p>Date : Page :</p>
--	---	---

- the 3D numerical results are still restricted to relatively low frequencies, up to about 1.5 Hz, mainly due to computational limitations as well as insufficient resolution in our knowledge on the geologic and source model. However, it should be considered that this represents a major achievement in the field of computation seismology, as highlighted by the literature overview presented in Table 1. Although this overview is not exhaustive, it shows that for the majority of complex 3D numerical models the frequency resolution is typically up to about 0.5 Hz. Furthermore, the relatively low frequency limit of our models is due to the fact the mesh has to be designed to account for low velocity sediments (consider that the maximum SE size should be at least $\sim V_S/f_{max}$ for spectral degree = 4) that, in the case of the Po plain, can reach thicknesses of the order of thousands of meters, leading, therefore, to an increase of computational burden.
- As commented in the deliverable (pg. 47, 2nd paragraph), future work will involve the improvement of the procedure for the generation of BB accelerograms by implementing the method proposed by Pousse et al. (2006) for the HF synthetics, instead of SP96. As a matter of fact, the method introduces three main improvements in terms of: (a) frequency content of ground motion following the ω -square model; (b) envelope time function for P-, S- and coda waves; (c) ground motion variability. Especially feature (c), i.e., the capability to model the natural ground motion variability as observed in real data, that is substantially lacking in SP96, would represent a relevant achievement.
- Specific remarks have been introduced to underline that other methods could be used in conjunction with SPEED to generate BB signals. In particular, we mention herein the stochastic method implemented in the EXSIM code (Motazedian and Atkinson, 2005). This method can be used in place of SP96 for the generation of HF signals as commented in the text (end of pg. 46). In the preliminary phase of our work, the generation of BB accelerograms by combining SPEED with EXSIM was explored too. Nevertheless, the comparison between the results obtained by SPEED+EXSIM (with cross-over frequency 0.5-1 Hz for MRN and 1-1.5 for NVL) and SPEED+SP96, as displayed in Figure 4, led us to prefer the latter because the agreement with the observed spectral ordinates is much better over a wide range of periods, especially in near-field conditions (see MRN station).


- To further explore the potentialities of the method for BB synthesis, the issue related to the generation of BB shaking maps is reported and discussed (see pg. 48). In particular, we show in Figure 4.25 BB ground shaking maps in terms of PGV (left) and PGA (right).

Table 1 Literature overview on recent studies on 3D numerical deterministic simulations of earthquake ground motion in presence of complex geomorphological structures and including a proper modeling of the seismic source as well (K=Kinematic, D=Dynamic, ES=extended source, PS=pointsource). The maximum frequency of numerical simulations is highlighted.

Reference	Study area	Numerical method	Model size (LxWxH in km ³)	<i>f_{max}</i>	Num. of grid points (10 ⁶)	Num. of simulations	Seismic source
Olsen and Archuleta (1996)	Los Angeles, US	FD	155 x 134 x 34	0.4	11	3	K-ES
Graves (1998)	Los Angeles, US	FD	228 x 140 x 44	0.4	22	7	K-ES
Pitarka et al. (1998)	Kobe, Japan	FD	60 x 10 x 22	0.8	N/A	1	K-ES
Kim et al. (2003)	Los Angeles, US	FE	80 x 80 x 30	1	100	1	K-ES
Aochi and Madariaga (2003)	Izmit, Turkey	BE-FD	N/A	1	N/A	5	D-ES
Aagaard et al. (2004)	Taiwan	FE	160 x 80 x 40	0.5	N/A	10	K-ES
Graves and Wald (2004)	San Bernardino, US	FD	116 x 162 x 50	0.6	N/A	3	K-ES
Komatitsch et al. (2004)	Los Angeles, US	SE	516 x 507 x 60	0.5	45.4	2	K-PS
Ewald et al. (2006)	Lower Rhine Embayment, Germany	FD	140 x 140 x 30	1	417	4	K-ES
Olsen et al. (2006)	Southern California, US	FD	600 x 300 x 80	0.5	1800	3	K-ES
Olsen et al. (2008)	Southern California, US	FD	600 x 300 x 80	0.5	1800	3	D-ES
Furumura and Hayakawa (2007)	Kanto basin, Japan	FD	440 x 250 x 160	1	N/A	1	K-ES
Day et al. (2008)	Southern California, US	FD-FE	100 x 100 x 30	0.5	N/A	60	K-ES
Wang et al. (2008)	Los Angeles, US	FD	96 x 87 x 25.5	0.56	N/A	24	K-ES
Bielak et al. (2010)	Southern California, US	FE	600 x 300 x 84	0.5	83.8	3	K-ES
Graves et al. (2008)	Southern California, US	FD	N/A	1	N/A	3	K-ES
Olsen et al. (2009)	Southern California, US	FD	N/A	0.5	N/A	7	D-ES
Stupazzini et al. (2009)	Grenoble, France	SE	40.7 x 50 x 8	2	5.7	18	K-ES
Gallovic et al. (2010)	Parkfield, US	FV/ADER-DG	100 x 60 x 28	1	N/A	6	K-ES
Graves et al. (2010)	Southern California, US	FD	N/A	0.5	1500	840000	K-ES
Smerzini et al. (2011)	Gubbio, Italy	SE	62 x 85 x 10	2.5	23.5	3	K-ES
Smerzini & Villani (2012)	L'Aquila, Italy	SE	62 x 63 x 17.7	2.5	10.5	32	K-ES

Point 6

In connection with other WPs of the SIGMA project (see e.g. Deliverable D3-96 “Approaches to account for site effects in the PSHA of selected sites in the Po area”), where our research group has been deeply involved, the numerical study presented in this Deliverable aimed at: (a) providing a better understanding of the seismic response at deep alluvial sites in the Po plain; (b) developing seismic ground shaking scenarios; (c) assessing the variability of site amplification with respect to source-to-site

	<p>Research and Development Programme on Seismic Ground Motion</p> <p>CONFIDENTIAL</p> <p><i>Restricted to SIGMA scientific partners and members of the consortium, please do not pass around</i></p>	<p>Ref : SIGMA-2013-D2-93 Version : 01</p> <p>Date : Page :</p>
--	---	---

propagation path, directivity effects coupled with complex site effects. Therefore, this work has focused predominantly on the verification and validation of the numerical models by using the available recordings, as discussed in Chapters 2, 3 and 4, while minor emphasis is given to the application of the numerical simulations in terms of site amplification and evaluation of ground motion variability.